A Four Physics Approach to Modeling Moisture Diffusion, Structural Mechanics, and Heat Conduction Coupled with Physical Aging for a Glassy Thermoplastic

by

Mojtaba Haghighi Yazdi

A thesis
presented to the University of Waterloo
in fulfillment of the
thesis requirement for the degree of
Doctor of Philosophy
in
Mechanical Engineering

Waterloo, Ontario, Canada, 2011

AUTHOR'S DECLARATION

I hereby declare that I am the sole author of this thesis. This is a true copy of the thesis, including any required final revisions, as accepted by my examiners.

I understand that my thesis may be made electronically available to the public.

Abstract

The performance of some polymeric materials is profoundly affected by long-term exposure to moisture during service. This poses problems for high precision and/or load bearing components in engineering applications where moisture-induced changes in mechanical properties and dimensional stability could compromise the reliability of the device or structure. In addition to external factors such as moisture, the material properties are also evolving due to inherent structural relaxation within the polymeric material through a process known as physical aging. Based on the current knowledge of both mechanisms, they have opposite effects on material properties.

The common approach to studying the effects of moisture is to expose the polymeric material to combined moisture and heat, also referred to as hygrothermal conditions. The application of heat not only increases the rate of moisture diffusion but also accelerates physical aging processes which would otherwise be very slow. In spite of this coupled response, nearly all hygrothermal studies ignore physical aging in their investigations due to the complexity of the coupled problem.

The goal of this work is to develop a numerical model for simulating the interactive effects of moisture diffusion and physical aging in a glassy polymer. The intent is to develop a capability that would also allow one to model these effects under various mechanical loading and heat transfer conditions. The study has chosen to model the response of polycarbonate/acrylonitrile-butadiene-styrene (PC/ABS), which is a glassy polymer blend that has very similar behaviour to polycarbonate.

In this study, a comprehensive approach which considers four physical mechanisms – structural mechanics, moisture diffusion, heat conduction, and physical aging – has been applied. The most current analytical models in the literature usually attempt to model two or three coupled physical phenomena. To develop the four coupled phenomena model, the current work has undertaken an extensive scope of work involving experimental characterization and finite element modeling.

In the experimental part of this work, seven sets of different tests were conducted to characterize the behaviour of PC/ABS exposed to moisture diffusion and accelerated physical aging. These experiments provided a comparative study between the effects of physical aging and moisture diffusion on the material's behaviour; and at the same time, provided data for the numerical modeling. The dual glass transition temperatures (T_g) of the material were determined using two techniques: dynamic mechanical analysis (DMA) and thermo-mechanical analysis (TMA). The DMA tests provided data for studying the effects of hygrothermal aging on the T_g's of the material and were

also useful for mechanical tests such as creep and stress relaxation performed using the DMA. The T_g's obtained using the TMA were also required for physical aging experiments using the dilatometry mode of TMA. Structural relaxation of the blend was studied by aging the material at 80 °C for 7 aging times in the TMA. These experiments gave an insight into the volume relaxation behaviour of the blend at a constant temperature. Specific heat capacity of the PC/ABS blend was also measured using another thermal analysis technique; *i.e.*, differential scanning calorimeter (DSC), before and after test specimens were exposed to hygrothermal aging for 168 hours.

The interactive effects of physical aging and moisture diffusion on the moisture uptake of the material were studied using gravimetric experiments performed at 5 different hygrothermal conditions. The experimental results were used to determine the coefficient of diffusion as well as the equilibrium moisture uptake of the samples. Furthermore, the effects of both moisture diffusion and physical aging on the mechanical behaviour of the polymer blend were investigated using stress relaxation tests. The comparison of the results of the tests performed on un-aged specimens with those of thermally and hygrothermally aged samples showed how physical aging effects competed with moisture diffusion. Also, the coefficient of hygroscopic expansion of the PC/ABS blend was determined using a so-called TMA/TGA technique.

The numerical modeling of the four-coupled physics was achieved using the governing equations in the form of partial differential equations. Modeling was performed using the commercial finite element software package, COMSOL Multiphysics®. First, the uncoupled physical mechanisms of structural mechanics, moisture diffusion, and heat conduction were modeled separately to investigate the validity of the PDEs for each individual phenomenon. The modeling of the coupled physics was undertaken in two parts. The three coupled physics of structural mechanics, moisture diffusion, and heat conduction was first simulated for a gas pipe having a linear elastic behaviour. The comparison of the results with similar analysis available in the literature showed the capability of the developed model for the analysis of the triple coupled mechanisms. The second part modeled the four coupled phenomena by incorporating the experimentally determined coupling coefficients. In the developed numerical model, the material behaviour was considered to be linear viscoelastic, which complicated the model further but provided more realistic results for the behaviour of the polymer blend. Moreover, an approximation method was proposed for estimating the coupling coefficients that exist between different coupled physics in this study. It was also suggested that the anomalous moisture diffusion in the material can be modeled using a time varying boundary condition. Finally, the model

was successfully verified and demonstrated using test case studies with thin thermoplastic plates. The proposed four-coupled physics model was able to predict with good accuracy the deflection of thin thermoplastic plates under bending for a set of hygorthermal test condition.

Acknowledgements

I would like to express my profound gratitude to my supervisor, Professor Pearl Sullivan for her support, guidance, encouragement, and patience during my PhD program.

Funding from Research in Motion (RIM), Waterloo, Ontario and the Natural Science and Engineering Research Council of Canada (NSERC) Research and Development Collaborative Research Grant program for this work is gratefully acknowledged. The early stages of this work were supported by the Ontario Centre of Excellence Research and Development Collaborative Program. I also would like to thank the Materials Laboratory at RIM for providing materials and technical support over the course of this project. The sincere cooperation of the members of the Materials Laboratory at RIM and specially the assistance of Dr. Bev Christian, Dr. Dwayne Wasylyshyn, Julie Liu, and Deepchand Ramjattan are gratefully acknowledged.

I would also like to express my appreciation towards Professor Mahmood Shokrieh for his guidance and encouragement during my MSc program at Iran University of Science and Technology.

Special thanks to our research group in the *Composites and Adhesives Laboratory* at the University of Waterloo. In particular, Dr. Donna Dykeman, Dr. Prasad Dasappa, Jacky Tang, Allan Rogalsky, and Nasim Paryab are gratefully appreciated. I would also like to thank one of my best friends, Yaser Shanjani, who provided me with invaluable source of inspiration and motivation.

I would also like to express my profound gratitude to my beloved ones for their support and encouragement throughout my life. Specifically, I am indebted to my lovely mother and my dear wife.

Dedication

I wish to dedicate this dissertation

to my beloved wife,

to my lovely mother,

and to the enduring memory of my father.

Table of Contents

List of Figures

List of Tables

Nomenclature

1D	1 dimensional
2D	2 dimensional
3D	3 dimensional
a	Solvent activity
A, B, t_o	Fitting parameters
ABS	Acrylonitrile-Butadiene-Styrene
a_H	Hygrothermal horizontal shift factor
A_j	Dual variable related to the internal variable
ANCOVA	Analysis of Covariance
ANOVA	Analysis of Variance
a_{ta}	Horizontal shift factor
a_v	Vertical shift factor
C	Concentration of the diffusion species
C_∞	Equilibrium concentration
C_i	Initial concentration
coeff1, coeff2, coeff3	New coupling coefficients (functions of K_μ, $C_{T\mu}$, and C_{ST})
c_p	Specific heat capacity at const. pressure
Δc_p	Difference in c_p between glassy & rubbery state
C_{ST}	Coupling coefficient related to the interaction of viscoelastic component of structural mechanics and heat conduction
$C_{S\mu}$	Coupling coefficient associated with the interaction of viscoelastic component of structural mechanics and moisture diffusion
CTE	Coefficient of Thermal Expansion
C_{TY}	Coupling coefficient linked with the effect of temperature (concentration) variation on chemical potential (entropy)
$C_{T\mu}$	Coupling coefficient related to the temperature (chemical potential) gradient effect on the mass (entropy) flux
D	Coefficient of diffusion
D	Compliance

D_c	Corrected coefficient of diffusion
DMA	Dynamic Mechanical Analyzer
DSC	Differential Scanning Calorimeter (Calorimetry)
E	Modulus of elasticity
E''	Loss modulus
E_o	Initial modulus
E_{ref}	Reference modulus
ERV	Elementary Representative Volume
f	Body force per unit of mass
F	Force
FEM	Finite Element Method
FTIR	Fourier Transform Infrared
G	Shear modulus
GPC	Gel Permeation Chromatography
h	Length of the plate
h_c	Convective heat transfer coefficient
h_o	Thickness of the dried out sample
h_{sat}	Thickness of the saturated sample
h_{xo}	Length of the square sample
h_{yo}	Width of the square sample
h_{zo}	Thickness of the square sample
I	Second moment of area
J	Flux of the diffusing species
J_s	Entropy flux
k	Constant
K_a	Apparent bulk modulus
K^{an}	Anelastic bulk modulus
K^e	Elastic bulk modulus
K_{gl}	Bulk modulus at the glassy state
K^o_{gl}	Bulk modulus at the dry state
K_s, K_T, C_{SAj}, C_{TAj}, K_{Aj}	Onsager coefficients
KWW	Kohlrausch-Williams-Watts

K_μ	Coefficient associated with the effect of chemical potential gradient on the diffusant mass flux
l	Plate thickness
L	Length of the beam
L_c	Characteristic dimension
m, n	Multiplicative factors
M_∞	Mass uptake at equilibrium
m_∞	Sample mass at saturation
M_d	Relative flux of the diffusing substance
M_{dry}	Mass of the dry sample
MDSC	Modulated Differential Scanning Calorimeter
M_o	Mass of the dried out sample
m_o	Mass of the dry sample
M_p	Relative flux of polymer
m_{ref}	Reference mass uptake
M_s	Solvent molecular weight
M_{sat}	Mass of the saturated sample
M_t	Mass uptake at time t
m_t	Mass at time t
M_w	Weight average molecular weight
m_w	Mass of the wet sample
n	Factor specifying the type of diffusion
Nu	Nusselt number
PC	Polycarbonate
PDE	Partial Differential Equation
Pr	Prandtl number
PVDF	Polyvinulidene fluoride
Q	Heat flux
q_1	Heating rate
q_2	Cooling rate
Q_{Ta}	Extent of relaxation toward equilibrium at T_a
R	External heat supply per volume

R	Ideal gas constant
Re	Reynolds number
RH	Relative Humidity
RSD	Relative Standard Deviation
S	Specific entropy
SD	Standard Deviation
S_e	Entropy due to external exchanges
s_g	Solubility coefficient
S_i	Entropy due to internal exchanges
T	Temperature
t,t',t''	Time
t_∞	Equilibrium time
T_a	Aging temperature
t_a	Aging time
$tan\ \delta$	Loss tangent
t_a^o	Aging time before stress relaxation
t_{aref}	Reference aging time
T_g	Glass transition temperature
ΔT_g	Temperature shift
$T_{g,ABS}$	T_g associated with the ABS component of the PC/ABS blend
$T_{g,PC}$	T_g related to the PC component of the PC/ABS blend
TGA	Thermo-Gravimetric Analyzer
T_{gm}	T_g of polymer-solvent system
TMA	Thermo-Mechanical Analyzer (Analysis)
T_o	Constant
U	Specific internal energy
u	Dependant variable
UEL	User-defined Element
V	Volume
v	Fluid velocity
v_s	Solvent molar volume
v_∞	Volume at equilibrium

v_o	Initial volume
w	Width of the plate
x	x-coordinate
Y_d	Mass fraction of the diffusing substance
Y_p	Mass fraction of polymer
Φ	Volume dissipation
Φ_v	Volume fraction
Φ_1	Volume dissipation due to inelastic straining
Φ_2	Thermal volume dissipation
Φ_3	Diffusive volume dissipation
Φ_g	Φ_p at which glass transition takes place
Φ_p	Polymer volume fraction
Φ_s	Solvent volume fraction
Ψ	Specific free energy
α_d^{an}	Anelastic coefficient of hygroscopic expansion
α_d^{e}	Elastic coefficient of hygroscopic expansion
α_g	CTE in glassy region
α_r	CTE in rubbery region
α_T^{an}	Anelastic coefficient of thermal expansion
α_T^{e}	Elastic coefficients of thermal expansion
β	Shape parameter
β'	Exponent from stretched exponential
χ	Flory-Huggins interaction parameter
δ_v	Vertical deflection
δ^*	Dissipative pseudo potential
ε	Infinitesimal strain
ε^{an}	Anelastic strain
ε^{e}	Elastic strain
ε^{in}	Inelastic strain
ε^{v}	Viscoelastic strain

η	Viscosity
λ, μ	Lamé's coefficients
λ_t	Effective time
λ_T	Heat conductivity
μ_d	Mass chemical potential of diffusing substance
μ_p	Mass chemical potential of polymer
μ_{ta}	Aging shift rate
ν_f	Fluid kinematic viscosity
ν	Poisson's ratio
ρ	Density of ERV
σ	Cauchy stress
σ^{an}	Anelastic stress linked with the spring in the Kelvin-Voigt (Maxwell) element
σ^{v}	Viscoelastic stress related to the dashpot in the Kelvin-Voigt (Maxwell) element
τ	Relaxation time constant
τ_c	Characteristic time
τ_o	Constant
ω_p	Polymer mass fraction
ξ_j	Internal variable

Chapter 1
Introduction

1.1 Hygrothermal Aging in Glassy Polymers

The continuous exposure of polymers to combined moisture and temperature (hygrothermal) is widely known to be highly undesirable due to the profound effects of these conditions on the thermophysical and mechanical properties of the polymeric materials and their composites. Each condition adversely affects the polymer properties and dimensional stability but the mechanisms responsible for these changes are different. In the case of moisture exposure, the rate of moisture movement from the atmosphere into the material is proportional to the concentration gradient. In the absence of heat, the direct effect of absorbed moisture in polymeric materials due to humidity includes plasticization [1, 2], hydrolysis [3-8], swelling of the material [9], and reduction in the glass transition temperature as well as storage modulus [10]. In the presence of heat, these deleterious effects are exacerbated as heat accelerates the movement of moisture.

If we only consider the condition of thermal exposure, the polymer material will undergo spontaneous structural molecular relaxation, especially in glassy polymers. The structural relaxation process, known as physical aging, is due to the non-equilibrium state of polymeric structure evolving towards equilibrium. Physical aging is characterized by the inherent mechanical relaxation of the polymer chains: it occurs naturally at very long time scales but is accelerated when the polymer is heated. This is not to be confused with chemical aging which breaks secondary or even primary bonds. There is significant interest in understanding physical aging in thermoplastics where the relaxation process is more prominent in glassy polymers than in semi-crystalline polymers. The processing techniques of thermoplastics typically involve quenching from melted state to room temperature, which results in a non-equilibrium polymer structure that will evolve with time. Consequently, the properties of the final thermoplastic products change during their service lifetimes due to physical aging processes [11]. The main changes include increased stiffness and loss in toughness to molecular densification and volumetric contraction.

Therefore, under prolonged hygrothermal exposure or hygrothermal aging, two main processes are at play: moisture diffusion and physical aging. Both are distinctly different and are in fact, opposing processes. The most obvious physical difference is volumetric: moisture swells the polymer volume

while physical aging contracts it. Accordingly, the modeling of interaction of these two processes is a coupled problem that is both complex and challenging.

1.2 Motivation for the Present Work

As polymer-based materials are increasingly utilized in engineering applications, the consequences of hygrothermal exposure of these materials in service conditions are of significant industrial interest. In the electronics industry, for example, polymeric packaging materials are used widely in integrated circuit packages and plastic encapsulated microcircuits. The hygroscopic and thermal stresses induced by hot and humid conditions are important issues as they affect component reliability. Another example is the oil and gas industry, where the behaviour of polymers used as sheaths and gaskets in oil production machinery can vary during the service lifetime, causing leaks and failures. In structural applications such as aircraft, moisture absorption in structural adhesives can result in debonding, which can adversely affect the structural integrity of aged composite sandwich structures. In mobile device applications, changes in dimensional stability and properties of thin components, such as housings for cellular phones and polymer-based chip substrates, can lead to warpage.

So far, the majority of experimental studies on moisture diffusion and physical aging phenomena have been conducted independently because of the traditional materials science approach to investigating structure-property relationships. Of the two processes, there is greater body of work published on the effects of moisture diffusion and/or hygrothermal exposure on mechanical properties. A more representative approach should couple the effects of heat (especially for hygorthermal conditions) on physical aging processes although it significantly adds to the complexity to the problem.

Studies using numerical methods, on the other hand, tend to approach the problem by performing structural analysis with consideration of the effects of moisture absorption and temperature on mechanical response. The physical aging process is usually integrated by assuming its effect on the material's modulus. Again, the two phenomena are assumed not to interact, and hence uncoupled in the analysis.

While there is a relatively large volume of independent work for each phenomenon, there are very few studies on the combined effects of physical aging and moisture diffusion on mechanical properties and volume of polymer materials. Moreover, another effect, the mechanical stresses on moisture diffusion, has not been considered in most of them. From an engineering standpoint, it is

important to be able to predict the multiple coupled effects, especially in high precision or load critical applications, since they interact as well as modify the mechanical properties and dimensional stability of the polymeric material. A more comprehensive analysis will enable polymer material users to predict the long-term behavior in conditions which more closely represent the service.

Ultimately, the model for mechanical and physical (dimensional change) response of polymer-based materials subjected to long-term hygrothermal exposure should include the interactive effects of four physical phenomenon - physical aging, moisture diffusion, structural mechanics, and heat transfer - in thin thermoplastic plates. Moisture diffusion in the thermoplastic material studied here does not follow the well known Fickian behaviour and therefore requires greater consideration in the modeling. The added effect of physical aging to moisture diffusion makes the modeling even more challenging. In spite of these challenges, the author believes that the scientific knowledge for each process and computational modeling tools have advanced sufficiently to warrant more study on the four coupled effects.

1.3 Research Objectives and Scope of Work

The primary objective of this study is to develop a numerical model for simulating the mechanical and physical response of thin polymer plates subjected to two coupled phenomena – moisture diffusion and physical aging. In this approach, all four physics will be coupled in the analysis. To achieve this objective, a material model is developed by experimental characterization to obtain the material properties of a thermoplastic polymer blend. The blend used in this study is a commonly used glassy polymer blend consisting of polycarbonate and acrylonitrile-butadiene-styrene (PC/ABS). Although blend materials are generally more complex than single polymer systems, earlier work has shown that the physical aging behaviour of PC/ABS system is very similar to PC material. The current work will adopt a phenomenological approach to material characterization.

The scope of the research work, therefore, consists of the following four main steps:

1. Material characterization through experimental tests,
2. Finite element modeling of the uncoupled physical phenomena,
3. Modeling fully coupled physics by considering all possible couplings, and
4. Verification of the model through test cases.

1.4 Summary of Thesis

This thesis is presented in six chapters. Basic definitions and theories of diffusion and physical aging are briefly discussed in the background section of Chapter 2. A review of available work in literature on multi-coupled physics, and more specifically on numerical modeling of the coupled physics will follow the background section in the second chapter. Chapter 3 covers the experimental methods including the material and the techniques used for material characterization tests. The experimental results and the discussion of the results are presented in Chapter 4. The numerical modeling of both uncoupled and coupled physics is discussed in Chapter 5 and finally, Chapter 6 outlines a summary and conclusion of the current work as well as the suggestions for the future work.

Chapter 2
Background and Literature Review

2.1 Background

Basic definitions and theories on diffusion and physical aging of polymers are briefly discussed in this section. First, the governing equations of diffusion in their simplest forms are introduced and then, different types of diffusion are explained. This is followed by the definition of physical aging and its effect on material response of polymers.

2.1.1 Diffusion

The first and the most well-known theory for diffusion was presented by Fick in 1855, based on an analogy between diffusion and heat flow, as follows [12]:

$$J = -D\frac{dC}{dx} \tag{2-1}$$

where J and C are the flux and concentration of the diffusion species, respectively; and D is known as the coefficient of diffusion. The above equation expresses a steady state diffusion in a one-dimensional system (direction x) and is referred to as Fick's first law of diffusion.

Fick's second law of diffusion introduces a relation for non-steady state diffusion, as follows [12]:

$$\frac{\partial C}{\partial t} = \frac{\partial}{\partial x}\left(D\frac{\partial C}{\partial x}\right) \tag{2-2}$$

There are three classes of diffusion in matrix polymers, which are defined based on the relative rate of mobility of the diffusing substance and the polymer [13]:

1. Case I or Fickian diffusion, in which the rate of the diffusion process is much smaller than that of the relaxation modes of the polymeric matrix.

2. Case II or non-Fickian diffusion, in which the rate of the diffusion process is bigger than that of the relaxation modes of the polymeric matrix.
3. Anomalous diffusion, in which both rates of the diffusion process and the relaxation modes are comparable.

In order to recognize the type of diffusion, a mathematical law is used, as follows:

$$\frac{M_t}{M_\infty} = kt^n \tag{2-3}$$

where M_t is the mass uptake of the diffusing substance at time t, and M_∞ is the mass uptake at the time when equilibrium reaches. k is a constant and n specifies the type of diffusion: n = 0.5 relates to Fickian diffusion, n = 1 indicates non-Fickian diffusion, and intermediate values of n suggest a combination of these two categories.

As mentioned in Chapter 1, the effects of moisture diffusion in a polymeric material include hygroscopic swelling, glass transition temperature change, mechanical and electrical properties alteration, and material degradation.

2.1.2 Physical Aging

The term of physical aging, according to Hutchinson [11], refers to a process in which the change in a physical property is recorded with time at constant temperature. Figure 2-1 illustrates how physical aging occurs in a glassy polymer from a thermodynamic standpoint. When a polymer is cooled down from a temperature above its glass transition temperature (T_g) to below it (step 1, in Figure 2-1), its behaviour deviates from thermodynamic equilibrium state (step 2). Consequently, there remains an excess amount of thermodynamic quantities (such as excess specific volume or enthalpy) in the material. At constant temperature (aging temperature, T_a), the excess thermodynamic quantities will reduce as the material moves towards equilibrium state (step 3).

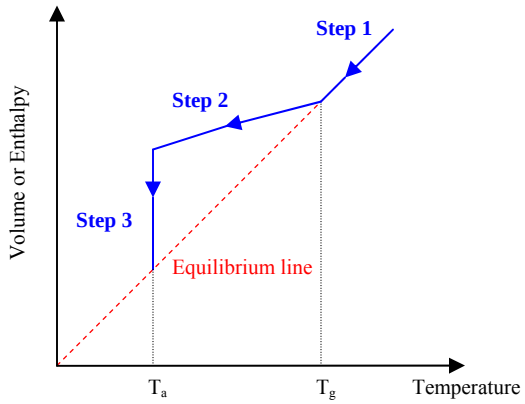

Figure 2-1 Schematic illustration of physical aging process (adopted from [11]**).**

The reductions of volume and enthalpy in step 3 of Figure 2-1 are referred to as volume and enthalpy relaxations, respectively. Volume relaxation can be experimentally investigated using dilatometry or Thermo-Mechanical Analysis (TMA), and enthalpy relaxation can be studied using Differential Scanning Calorimetry (DSC).

Some investigators have found similarities between the two volume and enthalpy relaxations. Therefore, there have been attempts to relate these two phenomena. This was achieved through introducing a term called the apparent bulk modulus, K_a, which is defined as the ratio of enthalpy change to volume change [14].

It is well known that the properties of polymers are inherently time- and temperature-dependent or viscoelastic. Since the study of viscoelasticity is already well established, research in physical aging has adopted the same methods to measure dynamic mechanical properties, creep compliance, or stress relaxation modulus. These experiments are performed using a Dynamic Mechanical Analyzer (DMA). The effect of physical aging on creep compliance (or stress relaxation modulus) appears as a shift in the timescale to longer times on isothermal annealing. This effect will be more explored in the experiments described in Chapters 3 and 4.

2.2 Literature Review

To study the coupled processes of moisture diffusion and physical aging, two more physical mechanisms need to be considered: structural mechanics and heat transfer. The various combinations of the coupling of the four mentioned physics have been studied for polymeric materials. Figure 2-2

shows the four mentioned physical concepts and the combination of them, which are dual, triple, and quadruple coupled physics.

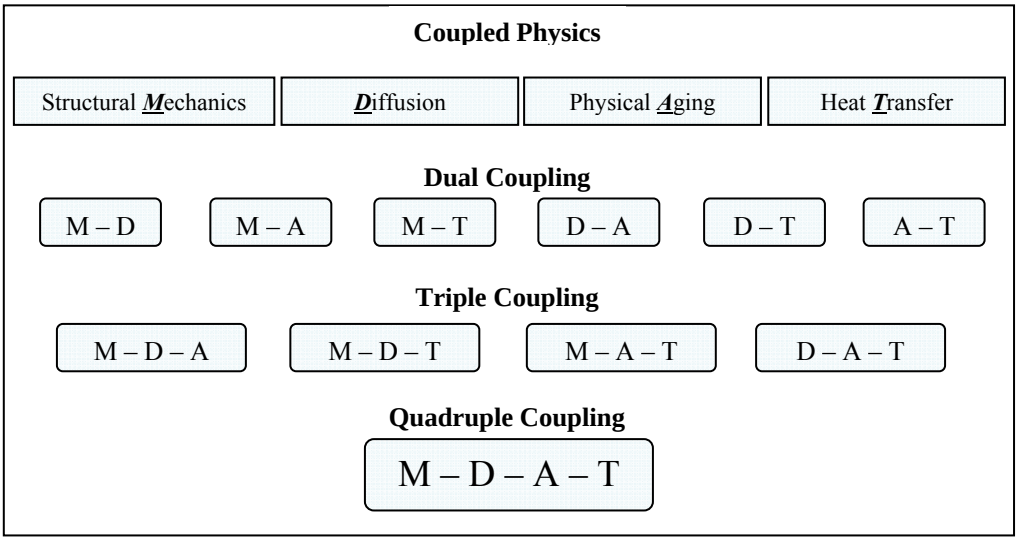

Figure 2-2 Schematic of the dual, triple, and quadruple coupled physics (M: Structural Mechanics, D: Diffusion, A: Physical Aging, T: Heat Transfer).

Table 2-1 presents a summary of the various studies published in the open literature which the author considers to be coupled physical approaches. Earlier works dealt with theoretical studies (*e.g.* [15-20]), whose results were used to develop mathematical models (*e.g.* [21, 22]) and became the basis for subsequent works. Experimental approaches were used in the majority of works studying the coupled physics (*e.g.* [23-28]). More than a third of the published work is experimental. In these works, the effects of diffusion and physical aging on mechanical response of polymers and polymer composites, and vice versa have been experimentally investigated. Several authors have also worked on the analytical (*e.g.* [29, 30]) as well as numerical (*e.g.* [31]) solutions for governing equations of the coupled physics. Among the numerical solutions considered for these physics, many authors have used finite element analysis. The third largest body of work is related to finite element analysis. Since the present work is focused on this approach, a brief review of the literature in this area is presented in the following section.

Table 2-1 Number of published studies on coupled physics.

		Type of Study		
Coupling	**Physics***	**Experimental**	**Theoretical**	**FEM**
Dual	M – D	9	20	7
	M – A	17	6	-
	D – T	6	-	3
	D – A	1	-	-
Triple	M – D – T	1	6	16
	M – D – A	-	1	-
	M – A – T	2	-	1
Quadruple	M – D – A – T	1	-	3
Total		37	33	30
Percentage		37 %	33 %	30 %

* M: Structural Mechanics, D: Diffusion, A: Physical Aging, T: Heat Transfer

2.2.1 Dual Coupled Physics

The studies on the dual coupled physics have been performed on polymers as well as polymer composites. The first dual coupled physics studies are related to coupled mechanical and diffusion phenomena. Vijalapura and Govindjee [32] presented a numerical simulation of a coupled diffusion-deformation phenomenon. The simulation was aimed for glassy polymers with case II diffusion. They used the balance laws to develop an initial boundary value problem in the form of nonlinear partial differential equations (PDEs). In order to solve the complicate set of nonlinear equations, they performed space and time discretizations using finite element and finite difference methods, respectively. They solved a one dimensional problem to find the formation and propagation of the sharp solvent front caused by case II diffusion. They concluded that finite element method has advantage over finite difference in global mass conservation.

There are also a few other works on polymers, which were used in electronic packaging industry [9, 33, 34]. Holalkere *et al.* [33] in their study of plastic package delamination, used finite element stress analysis together with fracture mechanics to evaluate moisture sensitivity of plastic encapsulated microcircuits. In the procedure they employed, moisture diffusion and hygrothermal stress analyses were numerically performed, which led to the prediction of new package delamination before prototyping and reliability testing. Hygroscopic modeling of plastic ball grid array (PBGA) packages has been the subject of the work of Wong *et al.* [9]. Hygrothermal stresses were found using finite element analysis with the similarity between hygroscopic swelling and thermal expansion. It

was found that hygroscopic stresses are significant compared to thermal stresses during solder reflow. Moisture induced failure of adhesive flip chip was investigated by Teh *et al.* [34]. In that work, finite element analysis was used to study the effect of the coefficient of moisture expansion mismatch on hygroscopic swelling stress induced in the package. The finite element analysis showed that the hygroscopic stress has the largest value in the center of the package, suggesting that the failure initiates in the middle of the package. There was fairly good agreement between the presented modeling and the experimental observations.

A number of works were devoted to the coupled behaviour of structural mechanics and diffusion in polymer composites. Moisture diffusion in adhesively bonded carbon fibre composite joints was investigated by Abdel Wahab *et al.* [35]. First, a nonlinear transient moisture analysis was performed using finite element analysis. Then, moisture dependent mechanical properties were incorporated in the finite element model using the calculated moisture concentrations as input data in the subsequent stress analysis. The comparison between the obtained results and those resulted from analytical solutions showed that the thinner the adhesive layer is, the closer the finite element results are to analytical solutions. In order to fit both results, a correction factor was proposed for the results of finite element analysis. This sequential application of moisture diffusion and stress analyses was used in another study by Abdel Wahab *et al.* [36]. They studied the durability of single lap joints and butt joints by applying a transient moisture diffusion followed by a nonlinear stress analysis. The swelling strains were also incorporated into the stress analysis according to the moisture distribution at a particular time. The results of the simulation were then used to explain the effect of moisture on joint strength.

The work of Wong *et al.* [37] was associated to the coupled diffusion and thermal processes. They discussed the implementation of modeling moisture diffusion in electronic multi-material packages using finite element analysis technique. The boundary conditions consisting of temperature and humidity were taken to be dynamic. Based on experimental and simulation results, suggestions have been made on the application of finite element analysis for modeling moisture diffusion in integrated circuit (IC) packages with dynamic temperature and humidity conditions. Yu and Pochiraju [38] presented a three-dimensional Glaerkin finite element methodology for modeling the coupled moisture diffusion and thermal processes in polymer composite materials. The modeling approach considered anisotropic as well as temperature-dependent diffusion coefficients. Several numerical examples were used to illustrate the modeling of the coupled phenomena. Finite element analysis was

also used by Shirangi *et al.* [39] to investigate moisture diffusion and temperature-dependent residual moisture content in molding compounds and IC packages. The anomalous dual-stage moisture diffusion was successfully modeled using finite element analysis and the results showed very good agreement with the experimental data.

2.2.2 Triple Coupled Physics

Similar to the dual coupling studies, the works on triple coupled physics have also been reviewed for both polymers and polymer composites. Starting from the coupled mechanical-diffusion-thermal physics, there are several works on polymers used for electronic packaging [40-45]. Lin and Tay [40] studied the mechanics of interfacial delamination in moisture-sensitive plastic IC packages. They presented a methodology of computing the resultant total stress intensity factor due to the effects of hygroscopic and thermal stresses. Therefore, the only coupling considered was the effect of moisture diffusion and temperature change on developing stress in the material. The onset of delamination propagation was predicted using finite element analysis. Finite element analysis was also used by Yi and Sze [41] to study moisture absorption and residual stresses in plastic encapsulated IC packages. The effects of moisture concentration and temperature distribution in the material were incorporated in the model in the form of hygrothermal stresses and were combined with viscoelastic stress. Fickian moisture diffusion was also analyzed with finite element method to obtain the moisture concentration distribution in the package. The effect of temperature on diffusion appeared in the coefficient of diffusion in the form of an Arrhenius relation. The results showed that both temperature and moisture content influenced the moisture distributions as well as the residual stresses in the packages. Furthermore, Chang *et al.* [42] used finite element analysis to obtain temperature distribution, moisture diffusion, and hygrothermal stress in plastic ball grid array (PBGA) packages during the solder reflow process. The only coupling considered in their study, was the effect of temperature and moisture content on hygrothermal stresses. A similar study has also been done by Lahoti *et al.* [43], in which three-dimensional finite element analysis was carried out to study the effect of temperature and moisture on flip chip ball grid array packages. Dudek *et al.* [44] also used finite element analysis to study the effect of temperature and moisture on viscoelastic behaviour of polymeric compounds in electronic packaging. Also, Fan and Zhao [45] developed a damage mechanics-based continuum theory for the coupled physics including moisture diffusion, heat conduction, and material deformation in encapsulated microelectronics devices. Using a simplified process, they solved the coupled equations sequentially using finite element analysis.

A so-called fully coupled mechanical-diffusion-thermal model was presented by Rambert *et al.* [46]. The model was developed based on the framework of classical thermodynamics and a set of coupled constitutive equations were derived for linear elastic behaviour [47]. Rambert *et al.* [46] employed finite element analysis for numerical implementation of the direct coupling and developed a user-defined element (UEL) for this purpose. They performed a qualitative study to investigate the effects of the five coupling coefficients that exist in the coupled constitutive equations.

Rambert and Grandidier [48] extended the model to include viscoelastic behaviour by considering the Kelvin-Voight's model. In a similar study, Rambert *et al.* [47] added chemical reactions to the other three couplings and developed the related constitutive equations. Rambert *et al.* [49] extended the work to include gradient-type elasticity. They studied the impact of direct couplings, especially the effect of temperature and chemical composition of the structure by finite element analysis of a simple one-dimensional case.

Using the similar modeling approach of Rambert *et al.* [46-49] and employing finite element method, Jugla *et al.* [50] analyzed the couplings between chemistry, thermal behaviour, and mechanics for cure simulation of a thermosetting matrix. They compared the results of the analysis with experimental data for the cure. Using the encouraging results of the comparison, they suggested that their approach can be applied to provide local information during the cure.

Valançon *et al.* [51] also used the fundamental principles of continuum mechanics and thermodynamics of irreversible processes to derive the governing equations for a thermo-diffuso-mechanical problem. They verified their model by analyzing structural relaxation after relative humidity jumps and compared their results with experimental results available in literature. The comparison was fairly good but other simulations were necessary to fully validate the model.

There are also several works on the mechanical-diffusion-thermal coupling [52-56] that have been performed on polymer composite materials. Roy and Reddy [52] modeled viscoelastic response of the adhesive layer of a bonded joint. Schapery's nonlinear single integral constitutive law [57] was used and nonlinear shift factor was also employed to include the effect of temperature and stress level. Nonlinear Fickian diffusion was also modeled to consider the effect of moisture concentration. A comparison of the results with available numerical and analytical data in literature was used for validation. However, their model was not able to model stress-driven diffusion [51]. Roy [53] also derived governing equations for diffusion in polymers and polymer matrix composites. The equations were capable of modeling the effect of coupling between stress, temperature, and moisture histories

on the diffusion process. Finite element analysis was employed to solve the weak form of the governing equations for a special case of unstressed isothermal diffusion. The results were compared with the experimental data available in literature and it was seen that the model over-predicts the moisture uptake for the considered dual-stage diffusion. A three-dimensional finite element analysis was employed by Marques and Creus [54] to analyze the behaviour of polymeric matrix laminated composites under combined viscoelastic and hygrothermal loads. The effects of temperature and moisture content appeared in dependency of creep function and coefficients of thermal and hygroscopic expansion on these variables. Numerical examples concerning the time-dependent response of plates and shells were modeled and the results showed good agreement with the results available in literature. Using the so-called "semi-coupled" mechanical-diffusion finite element analysis, Ashcroft *et al.* [55] investigated the environmental degradation of adhesively bonded composite joints. Their predictive model was capable of modeling mechanical-environmental coupling but was limited when solving complex problems. Their methodology provided modeling of the effect of moisture concentration on mechanical response. In another study, Loh *et al.* [56] determined the moisture-dependent swelling coefficient of a rubber toughened epoxy adhesive using the semi-coupled mechanical-diffusion finite element analysis. First, they modeled the dual stage uptake behaviour of the adhesive using a transient diffusion analysis and then used the results as predefined field variables for subsequent mechanical analysis. In the mechanical analysis, they considered moisture-dependent mechanical properties and employed an iterative method to obtain the swelling coefficient. They also modeled the deflection of a bi-material curved beam exposed to temperature and moisture diffusion. The beam was built by curing a layer of adhesive on a thin steel sheet. The deflection due to moisture diffusion was obtained using the same method as used for swelling coefficient determination. This was while the deflection due to temperature change was calculated using a separate thermal analysis. The total deflection was determined by summing the deflections due to moisture and temperature variations. A comparison of the modeling results with the experimental data was also made; but except for the beginning of the process, there was no good agreement.

The work of Lai and Bakker [58] was related to the mechanical-aging-thermal coupling. They developed a three-dimensional constitutive model for isotropic non-linear viscoelastic materials with the effects of temperature and physical aging. They established their constitutive modeling on the basis of one-dimensional Schapery representation [57] for non-linear viscoelasticity and incorporated

the effects of physical aging and temperature through the reduced time. Finite element analysis of some numerical examples agreed well with the experimental data for PMMA.

2.2.3 Quadruple Coupled Physics

To the best of the author's knowledge, there is no work in open literature that includes the finite element modeling of quadruple mechanical-diffusion-aging-thermal coupled phenomena. Two studies by Oliveira *et al.* [59, 60] focused on the physics of structural mechanics while the effects of temperature and moisture on this physics were incorporated. Also, the effect of physical aging was only considered on the modulus of the material. Using geometrically nonlinear finite element analysis, Oliveira *et al.* [59] modeled failure behaviour of composite plates and shells. They included thermal, hygroscopic, and viscoelastic effects in their material behaviour modeling. Several examples were also employed to compare the modeling results with those of closed solutions, and hence, provided an illustration of advantages and limitations of the modeling. In another study [60], they presented a numerical framework for analysis of composite structures. The formulation for aging processes including viscoelasticity and hygrothermal effects was given and tested for several examples having large displacements.

2.3 Concluding Remarks

About 100 published studies were reviewed on the coupled physics dealing with moisture diffusion and physical aging. Among these studies, those related to finite element analysis were focused on and discussed. Studying the dual, triple, and quadruple coupled physics on polymers and polymer composites revealed two main general approaches in finite element analysis: i) semi-coupled or sequential analysis, and ii) fully-coupled analysis.

It was found that most of these works did not consider the complete coupling between the studied physics. It is, therefore, concluded that there is no work in the open literature to date on the finite element analysis of the coupling of the four coupled physics, which are structural mechanics, moisture diffusion, physical aging, and heat transfer. The work of Rambert *et al.* [46-49], first published in 2003, can be a good starting point for our modeling for the following reasons:

1. It models all the direct couplings based on the laws of classical thermodynamics. Similar procedure has also been employed by other investigators (*e.g.* [51, 61]) and their comparisons of the modeling results with experimental data have shown the validity of this type of approach towards modeling.

2. The five coupling coefficients, which have been used in this work, have physical meanings. They can be related to famous factors such as Soret effect factor or pressure stress factor. In the parametric study of Rambert *et al.* [46-49], the physical aspects of each coupling coefficient and the consequence of changing the value of each of them on a real structure are explained.

3. Jugla *et al.* [50] have used the same modeling approach in the cure simulation of a thermosetting matrix and the comparison of the results of finite element analysis with experimental data has shown the capability of the method in modeling of coupled physics.

Chapter 3
Material and Experimental Methods

3.1 Material

The material used in this study is the PC/ABS polymer blend, which constitutes of two polymer materials, Polycarbonate (PC) and Acrylonitrile-Butadiene-Styrene (ABS). Each of the two components of the PC/ABS polymer blend has some advantages and drawbacks. PC is well-known for its high impact resistance and ductility, low water absorption, and dimensional stability but it possesses poor chemical resistance [12]. PC has industrial applications such as in safety equipment. ABS, on the other hand, has also some advantages including outstanding strength and toughness, resistance to heat distortion, and good electrical properties but it is flammable and is soluble in some organic solvents [12]. ABS has also numerous applications such as in automotive components and electrical and electronic assemblies.

PC/ABS blends are increasingly replacing polycarbonate because they offer better thermal and mechanical properties, improved physical aging properties, easier processability, and are more cost-effective [62, 63]. In this study, a commercial grade of 75:25 PC/ABS from SABIC Innovative Plastics™ (formerly, GE Plastics), designated as Cycoloy C6600, has been used. It is a widely used PC/ABS ratio with a melt flow rate of 21.5 *g*/10 *min* at 260°C with 2.16 *kgf* in accordance to the ASTM standard [64]. The weight average molecular weight (M_w) of the blend was found to be 45,000 by Jordi FLP using gel permeation chromatography with RI (GPC-RI) and GPC-FTIR techniques. The size of the molecules in solution was found to be the same and could not be resolved using GPC. Moreover, GPC-FTIR confirmed that they were eluting at the same time.

3.2 Polymer Characterization Techniques

The experiments performed for characterization of the PC/ABS polymer blend in this study are conducted using thermal analysis techniques with the following machines: i) Dynamic Mechanical Analyzer (DMA), ii) Thermo-Mechanical Analyzer (TMA), iii) Differential Scanning Calorimeter (DSC), and iv) Thermo-Gravimetric Analyzer (TGA). These techniques are briefly introduced in this section. More explanations on these instruments including usages, calibrations, and testing procedures can be found elsewhere [65].

Dynamic Mechanical Analyzer or DMA is famous for the periodic loading regime it applies and therefore is particularly suitable for evaluation of viscoelastic materials. For example, it can be used for determination of the glass transition region of a polymeric material by applying a sinusoidal load. DMA is also equipped with different clamps which provide the measurement capabilities for mechanical characterization of polymer materials in various geometries. DMA can also apply constant loads, which makes the machine useful for doing creep and stress relaxation tests. In this study, the three-point bending mode of the DMA is employed to measure the glass transition temperature of the PC/ABS blend. The machine is also used for conducting both creep and stress relaxation tests using the same three-point bending clamp.

Thermo-Mechanical Analyzer or TMA is also an important instrument today due to its capability to measure both T_g and the coefficient of thermal expansion (CTE), as well as several other physical characteristics depending on the operating mode [66]. TMA has several operational modes, namely expansion, penetration, flexure, and tension [67, 68], which give different types of thermophysical data. TMA is used in this study to measure the T_g and CTE of the PC/ABS. The machine is also used for volume relaxation investigation of the PC/ABS blend.

Differential Scanning Calorimeter, DSC, measures the heat flow into or out of a polymer sample as a function of temperature and time. The energy changes of the sample compared to a reference sample can be used to measure the transitions occurring in the sample. Enthalpy or specific heat capacity, glass transitions, melting point, crystallization temperature, and a number of other properties can be determined with a DSC. In this study, the specific heat capacity of the PC/ABS blend is investigated using the DSC.

Finally, the Thermo-Gravimetric Analyzer (TGA) is used in a wide variety of applications. In TGA, the mass change of a sample is recorded as a function of time and temperature in a controlled atmosphere. The instrument can be used to measure the mass loss or gain of the sample due to some processes such as decomposition, oxidation, and dehydration; and therefore, useful information such as the composition of the material and its thermal stability can be obtained. The TGA is used in this study to measure the mass change of the PC/ABS blend during the drying of the sample following moisture absorption in a humid environment.

3.3 Experimental Methods

In this study, several experiments are performed to characterize the PC/ABS polymer blend. These tests have been specifically designed to study the effects of coupled moisture diffusion and physical aging through exposures of the blend to hygrothermal conditions. The experimental methods of these tests are presented in this section in two categories: thermophysical properties and mechanical properties. In the thermophysical properties section, T_g of the blend is studied using two thermal analysis techniques; *i.e.*, TMA and DMA. Physical aging study will follow this section and it includes the aging experiments performed using the TMA to study the volume relaxation of the material at the aging temperature of 80 °C. Since the specific heat capacity of the material needs to be determined for numerical analysis of heat conduction, the next section deals with the experiments conducted using the DSC to study the effects of hygrothermal aging on specific heat capacity. The last part of the thermophysical properties section is related to moisture uptake study, in which mass uptake of the blend under 5 hygrothermal conditions is studied and the effects of hygrothermal aging on the coefficient of diffusion as well as equilibrium moisture uptake are investigated. The steps of the thermophysical properties section are illustrated schematically in Figure 3-1.

In the mechanical properties section, stress relaxation tests were performed on the material after the test specimens were thermally and hygrothermally aged under different conditions. These tests which have been done at two ranges of aging time; *i.e.*, short term and long term, are used to study the effects of hygrothermal aging on the modulus of the blend. These material characterization tests also provide the material parameters which are used in the modeling of the viscoelastic behaviour of the PC/ABS blend. Figure 3-2 depicts the schematic of the steps of the mechanical properties experiments.

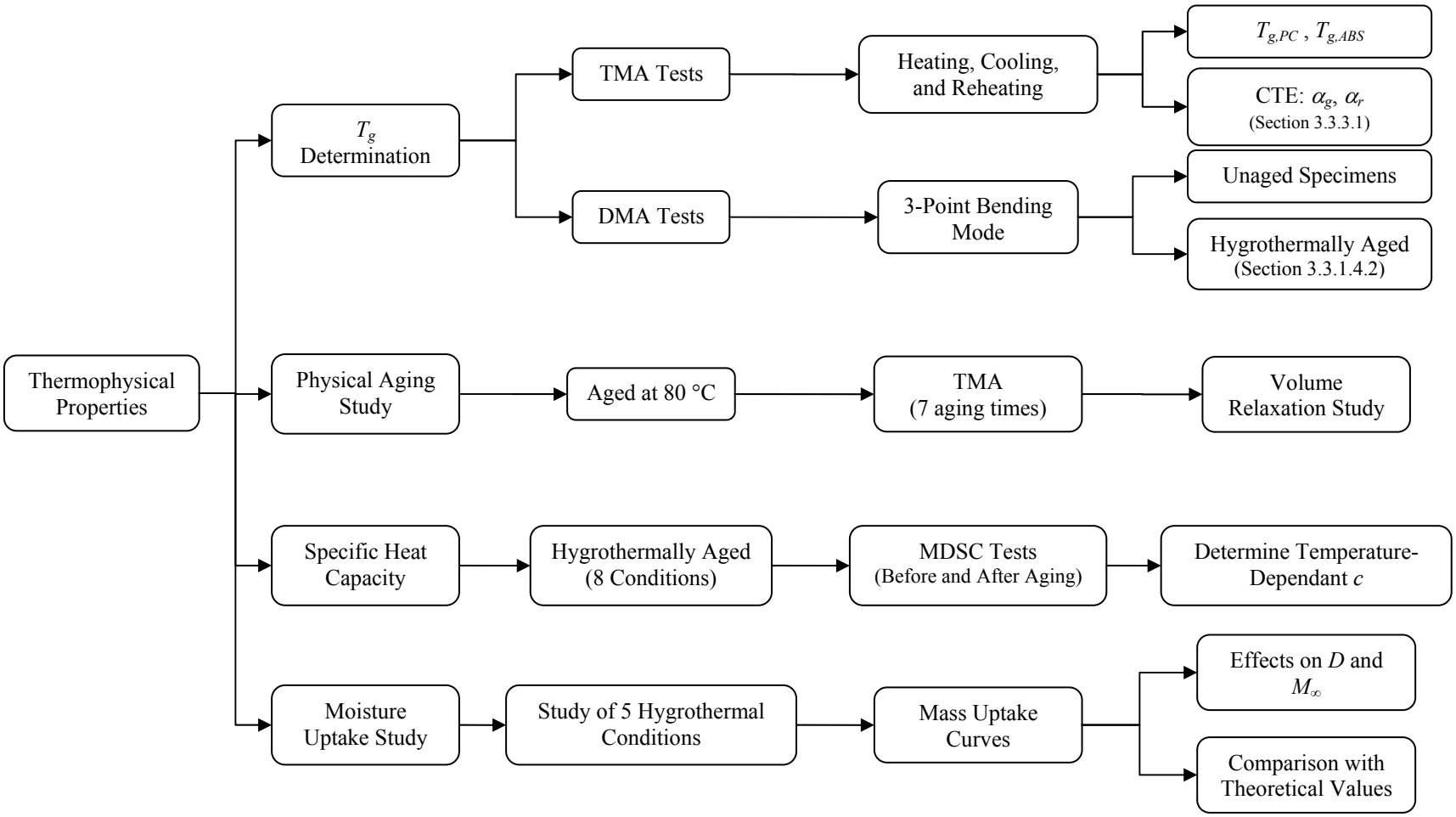

Figure 3-1 Schematic of experiments related to the thermophysical properties.

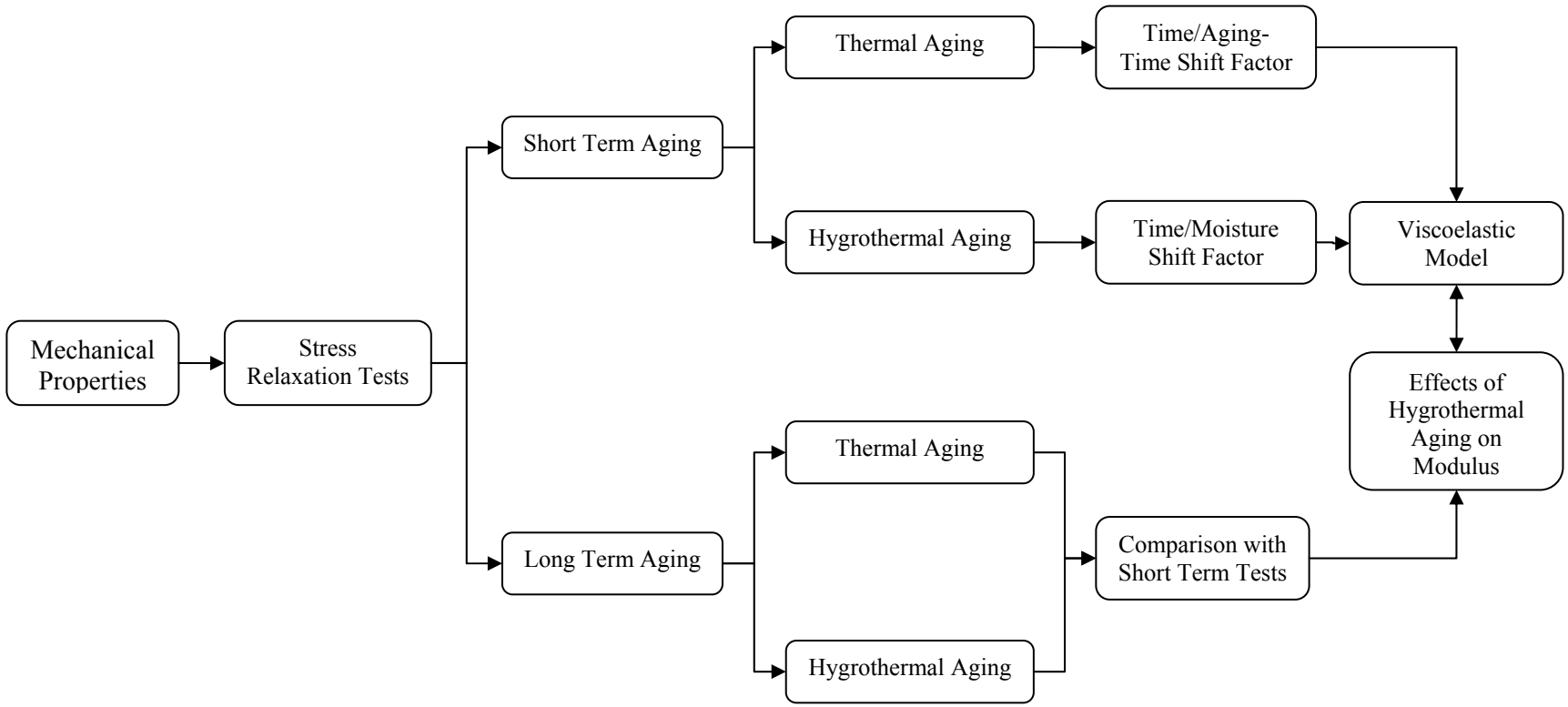

Figure 3-2 Schematic of experiments attributed to the mechanical properties.

3.3.1 Thermophysical Properties

This section includes the experiments for investigating the thermophysical properties of the PC/ABS blend.

3.3.1.1 Glass Transition Temperature Study

The glass transition temperature of polymer materials is an important characteristic of the material and its determination is crucial for material characterization. Specifically, in order to initiate the physical aging process in the PC/ABS polymer blend, test specimens need to be quenched from a temperature above glass transition temperature (T_g) of the material to below it. The purpose is to erase previous thermal history. Therefore, the T_g of the material has to be determined before conducting the aging tests.

The PC/ABS polymer blend constitutes of two components that have been found to be partially immiscible [62, 69], and hence the presence of two glass transition temperatures (T_g) are important design considerations. Thermal analysis techniques are known to be convenient means of determining the T_g of polymer blends. The presence of dual T_g's for the PC/ABS blend has already been reported using DSC and DMA [62, 63, 69, 70], but there are no studies in the open literature using the TMA method to study this blend. In this work, the T_g of the blend has been determined using two thermal analysis techniques; *i.e.*, TMA and DMA. Determination of T_g using the TMA is required for volume relaxation investigation and obtaining the T_g's of the blend using the DMA is beneficial for hygrothermal studies of the material.

3.3.1.1.1 TMA Tests

It is widely known that heating rates affect the reliability of glass transition measurements due to thermal lags. A review of the open literature going as far back as 30 years revealed a number of reports on the different heating rates used for characterizing polymers by different methods including TMA [71]. However, there are only a limited number of reports [66, 72] on the influence of different heating rates on T_g measured using TMA.

This section is focused on comparing the values between a dilatometer and expansion mode using a TMA. The secondary objective is to determine the practical heating rates for studying PC/ABS. This is particularly important for the dilatometer probe as there is a need to measure the volumetric expansion or contraction of the blend for understanding mechanisms such as structural relaxation during physical aging (described in section 3.3.1.2).

Thermo-mechanical analysis was performed on a TA Instruments 2940 TMA using two modes: 1) an expansion probe, and 2) a dilatometer. The temperature measurement reproducibility in the TMA chamber was ± 2 °C while machine sensitivity for deformation measurement was ± 100 *nm* [73]. In both of testing modes, each sample was weighed to 0.1 *mg*.

The temperature was ramped from room temperature to 135 °C under a nitrogen purge gas with flow rate of 100 *mL*/*min*. An isothermal treatment at 135°C for 10 minutes was used to remove the thermal history of the sample, followed by a cooling scan to 60°C. Subsequent to this, a second heating scan was applied to find the glass transition temperature after thermal history removal [74]. In total, seven heating (q_1) and cooling rates (q_2) were investigated, that is, $q_1 = q_2$ = 0.5, 1, 2.5, 5, 10, 15, 20 °C/min. Four samples were tested at each of the heating and cooling rates to increase the power of statistical evaluation and to maintain the statistical normality assumption. The calibrations and methodology specific to each probe are described below.

Expansion Mode

An expansion probe with a circular flat tip was used to measure the displacement change of the polymer samples under constant thermal heating and cooling rates, in accordance with the ASTM E 1545-05 [75] standard. Calibrations for temperature and length change were done according to ASTM E 2113-04 [76] and E 1363-03 [77] standards, respectively. Samples with dimensions of 5×5 *mm* were cut from a 152×305 *mm* sheet of 3 *mm* nominal thickness. The samples had an average mass of 100.5 *mg* (with standard deviation of 3.8 *mg*).

Dilatometer Mode

The dilatometer accessory kit for the TMA consisted of a dilatometer probe, sample vial, filling medium, and aluminium balls. The filling medium was used to convert the volume change of the sample inside it into displacement recorded by the dilatometer probe. The samples were in the form of small granules with average mass of 56.7 *mg* (with standard deviation of 1.8 *mg*).

Baseline and displacement calibrations were conducted before the tests. The baseline calibration consisted of a thermal scan from room temperature up to 160 °C with a heating rate of 1 °C/min and under the compression loading of 0.01 *N* [78]. This load value of 0.01 *N* was also used in testing. The displacement calibration is similar to temperature calibration in DSC, in which the melting point of a standard material (usually indium) is used for calibration. For this calibration, three aluminium balls were placed into the vial with $3/4^{th}$ of the vial filled with the filling medium. The cell constant in the

software, referred to as vial constant in TMA, was set to 1. The thermal procedure was the same as what was done for baseline calibration.

3.3.1.1.2 DMA Tests

Determination of T_g was also conducted using a TA Instruments Q800 Dynamic Mechanical Analyzer (DMA). The tests were performed in bending mode of the instrument using a 3-point bending clamp. In accordance to ASTM D 5023-07 Standard [79], sample dimensions of 64×13×3 mm were used with a 50-mm span bending clamp to achieve a span-to-depth ratio of 16:1. Samples were heated from 60 °C to 132 °C (a temperature level above $T_{g,PC}$ (~ 112 °C), which is higher than $T_{g,ABS}$ (~ 100 °C) [70]) with the heating rate and frequency of 1 °C/min and 1 Hz, respectively. Since possible residual stresses produced in the manufacturing process [28, 80] can cause variations in the T_g of the material, the T_g determination test was repeated on samples after they were rejuvenated by isothermal heat treatment at 135 °C for 10 minutes and then quenched to room temperature.

The value of strain amplitude for the T_g determination tests was specified based on a previously established method [81]. In order to find the appropriate strain amplitude for the experiments, a strain sweep test was applied to 5 different samples in 6 repeated cycles at room temperature. In each cycle, strain was swept from 10 to 50 μm at nine steps. Storage modulus at each cycle was recorded and standard deviation of storage moduli between samples and within cycles was obtained to determine the reproducibility and repeatability of the results.

3.3.1.2 Physical Aging Study

As mentioned earlier, the structural relaxation in a polymer material is manifested as enthalpy and volume relaxation in the material. The enthalpy relaxation of the PC/ABS polymer blend has already been studied [70] using the DSC. To the best of the author's knowledge, the volume relaxation of the PC/ABS blend, however, has not been studied. In this section, the experiments performed to study the volume changes during physical aging at a constant temperature are described.

The measurement of volume changes of the PC/ABS material is possible in the dilatometry mode of the TMA. To achieve this, three granules of PC/ABS weighing, on average, 54 *mg* were placed inside the vial surrounded completely by the filling medium. The sample was then exposed to a thermal procedure on the TMA stage.

According to the results of T_g determination tests performed using the TMA (will be presented in section 4.1.1.1), the heating rate of 0.5 °C/min is employed for the aging tests. Therefore, the temperature was ramped at a rate of 0.5 °C/min from 30 °C to 135 °C and then held constant for 10 minutes. The sample was then cooled down to the aging temperature, 80 °C, at the same rate of 0.5 °C/min. The temperature was kept constant at the aging temperature of 80 °C for 30 minutes. During this step, the measured volume change is an indication of the volume relaxation during physical aging period. This step was followed by decreasing the temperature at a rate of 0.5 °C/min to 30 °C. This cycle was repeated 5 times to find the number of cycles required to obtain consistent results for the aging period. The results showed that the deviation in the volume relaxation measured at each cycle is negligible after the third cycle. Therefore, for the subsequent volume relaxation experiments, the aforementioned thermal cycle was repeated 3 times and on the third cycle the material was aged for the duration of aging time, t_a. 7 periods of aging time were used: 0.5, 2, 8, 48, 96, 336, 1008 *hr*. Four replicates were tested at each of the aging time periods. Since the PC/ABS material is placed inside the filling medium, its recorded volume changes needed to be corrected for the volume changes due to the filling medium. Therefore, similar tests were performed on the vial having only the filling medium. The measured volume changes were then used to correct the corresponding values measured during physical aging of the PC/ABS material.

3.3.1.3 Specific Heat Capacity

The specific heat capacity of a material is known to affect the processes in which heat transfer is involved. For polymer materials, the values of specific heat capacity have been experimentally obtained at different temperatures and empirical relations were proposed [82-91]. For example, Gaur *et al.* [82-88] obtained heat capacity of linear macromolecules such as selenium, polyethylene, polyoxides, polypropylene, polystyrene, acrylic polymers, polyesters, and polyamides. In most of these works, calorimetric experiments such as DSC or temperature modulated DSC have been employed. A data bank, *Advanced THermal Analysis System* (ATHAS) [92], containing the results of thermal analysis of polymer materials has already been developed. While there is data for more common polymer systems, the value of the specific heat capacity of the PC/ABS polymer blend is not available in the open literature. In this section, the specific heat capacity of this polymer blend is experimentally determined. Since it is not known if the value is influenced by combined heat and humidity conditions, their effects are also investigated in this section.

A Modulated Differential Scanning Calorimeter (MDSC), TA Instruments DSC 2920, was used to conduct the tests. Samples in the form of granules with average weight of 10 *mg* were first stored inside a desiccator for 48 hours. The samples were then dried inside an oven at 80 °C for 30 minutes. Next, the samples were moved to the DSC for conducting a modulated DSC test before hygrothermal conditioning. In the DSC, thermal history of the samples was erased by an isothermal hold at 135 °C for 10 minutes. Following this step, the samples were heated from 10 °C to 135 °C at the rate of 5 °C/min with oscillation amplitude and period of 1.06 °C and 70 sec, respectively. In this step, the specific heat capacity of the material was recorded. The samples were then moved to an environmental chamber for hygrothermal aging. Before the samples were transferred to the environmental chamber, their thermal history was removed by an isothermal heating at 135 °C for 10 minutes. Hygrothermal conditioning of the samples was performed under 9 different hygrothermal conditions for 168 hours. The hygrothermal conditions included 50 °C/50% RH, 50 °C/93% RH, 50°C/fully immersed, 65 °C/50% RH, 65 °C/93% RH, 65°C/fully immersed, 80 °C/50% RH, 80 °C/75% RH, and 80°C/fully immersed. The temperature levels of the hygrothermal conditions were selected to be below the dual glass transition temperatures of the constituent components of the blend. Following the hygrothermal aging at each of the conditions, the samples were moved back to the DSC for another modulated DSC test. A similar heating scan to that performed *before* hygrothermal aging was conducted from 10 °C to 145 °C to measure the specific heat capacity of the material *after* hygrothermal aging. A comparison between the specific heat capacity *before* and *after* hygrothermal conditioning can reveal the effect of hygrothermal aging on the measured value. In these tests, 3 replicates were used for each of the hygrothermal conditions.

3.3.1.4 Moisture Uptake

Hygrothermal exposure of a polymer material is commonly associated with a form of hot-wet conditioning. Although there are actually two physical mechanisms at play – moisture absorption and structural recovery/relaxation associated with physical aging – during prolonged hygrothermal exposure, most studies have focused on the former since the effects of structural relaxation are more difficult to delineate during moisture uptake at high temperature. Our attention is now focused on the effects of hygrothermal conditions on moisture uptake behaviour in the material over a prolonged period. The objective is to explore the effects of the two opposing mechanisms, moisture diffusion and physical aging. In this part of the study, gravimetric experiments are conducted on the PC/ABS

specimens and the effects of two factors of relative humidity and aging temperature on the obtained results are investigated.

3.3.1.4.1 Moisture Uptake Measurements

According to ASTM D570-98 Standard [93], test samples were cut in the form of a bar with nominal dimensions 76.2×25.4 *mm* by the thickness of the sheet, 2.84 *mm*. Cut edges were smoothed so as to be free from cracks and were polished slowly to avoid heating the surfaces.

Samples were conditioned prior to moisture absorption and physical aging to ensure that moisture uptake measurements were taken from the same reference point. First, the specimens were stored in a desiccator for 48 hours in accordance to the ASTM D 618-08 Standard conditioning guidelines [94]. They were then placed into an oven at 135°C for 10 minutes which maintained a dry atmosphere to erase any previous thermal history [70]. Specimens were then removed from the oven, weighed to obtain the mass of dry samples, and placed directly into five conditioning environments as described below. During weighing of the specimens they were exposed to room temperature for about one minute, therefore the cooling rate was the same for all the samples. Numerical analyses of heat transfer in the material showed that the brief exposure does not cause the temperature of the samples to drop below the aging temperatures.

Samples were subjected to 5 different conditions: (i) 65°C/50% RH; (ii) 50°C/93% RH; (iii) 65°C/93% RH; (iv) 50°C/50% RH; and lastly (v) stored at room temperature fully immersed in distilled water, to investigate their effects on the coefficient of diffusion and equilibrium moisture content. Hygrothermal aging for conditions (i)-(iv) was conducted inside environmental chambers with the samples standing on one end in grooves machined into an aluminum block such that both surfaces of each sample were equally exposed to their conditioning environment. Samples fully immersed in water were rested on one end inside an enclosed container. Three of these conditions were first studied by Tang [95] and has been extended in this work for a more complete set of data. With the full data set, it was possible to conduct a statistical analysis on the effects of the humidity and aging temperature on the material response.

The ASTM D570-98 Standard [93] was adopted for the sampling frequency of moisture uptake measurements. Samples are initially weighed prior to conditioning; after 1, 3, 7, and 10 days; and then once every week thereafter until the increase in weight indicated by three consecutive readings average less than 1% of the total increase in weight or 5 mg, whichever is greater. Each condition

was replicated with 3 samples for moisture uptake monitoring. An analytical balance capable of reading 0.0001 g was used to record the mass of prepared specimens.

In order to obtain more accurate values of coefficient of diffusion, another set of specimens were conditioned at the same hygrothermal conditions and their moisture uptake was recorded every hour until the samples reached at the half of their equilibrium moisture uptake.

3.3.1.4.2 T_g Measurements

Moreover, to investigate the reversibility of changes caused by moisture absorption, T_g determination tests were conducted on hygrothermally aged samples at the four hygrothermal conditions after 7 days of moisture uptake. Test samples were in the form of bars with the same dimensions as those used for T_g determination using the DMA discussed in section 3.3.1.1.2. The procedure of the T_g determination tests were similar to those described in section 3.3.1.1.2. To investigate the effect of hygrothermal aging on T_g of the material, experimental results were compared with the T_g of un-aged specimens obtained in section 4.1.1.2.

3.3.2 Mechanical Properties

Methods of investigating the effects of physical aging on viscoelastic response, such as stress relaxation, are already well established. Struik, one of the pioneers in the field of physical aging, developed a test method [96], which provides the possibility of doing sequential creep or stress relaxation experiments on a thermally aged material at increasing physical aging times. Using superposition principles such as time/temperature and time/aging-time superposition principles, the obtained curves can be collapsed into a single master curve. Following Struik, many researchers have applied his method to investigate creep or stress relaxation behaviour of different polymer materials [80, 97-101]. For example, Guo and Bradshaw [80] characterized isothermal aging of PEEK and PPS films by creep and stress relaxation experiments using a dynamic mechanical analyzer.

The effects of moisture on the viscoelastic behaviour of polymeric materials have also been investigated by a number of researchers [102-110]. They have shown that the time/temperature superposition principle can be extended to develop the time/moisture superposition principle to produce master curves from momentary curves. When aged polymer-based materials are exposed to humid environments, the effect of moisture modifies the material properties further. One observed effect is osmotic swelling of the polymer particularly when the partial pressure of the penetrant (in

this case moisture) is increased, which in turn changes the material state from glassy to rubbery state [111].

There is, however, less knowledge on how combined heat and humidity affects viscoelastic behaviour. This part of the work has investigated the viscoelastic behaviour of PC/ABS polymer blend for a set of temperature and humidity (hygrothermal) combinations. By quantifying stiffness/modulus changes using stress relaxation tests, the relative effects of each mechanism can be followed.

Stress relaxation tests were performed using a TA Instruments 2980 Dynamic Mechanical Analyzer (DMA). The tests were performed in bending mode of the instrument. To minimize errors due to clamping effects in cantilever-type clamps, the 3-point bending clamp [112, 113] was used.

In accordance to the ASTM D 5023-07 Standard [79], sample dimensions of 64×13×3 *mm* were used with a 50-*mm* span bending clamp to achieve a span-to-depth ratio of 16:1. Samples were cut from a 150×202 *mm* sheet. Cut edges were polished slowly to produce smooth surfaces free from cracks. All test specimens were stored inside a dessicator for 48 hours before testing in accordance to the ASTM D 618-08 Standard conditioning guidelines [94].

3.3.2.1 Linearity Range Determination

In order to conduct stress relaxation experiments on physically aged specimens and apply Boltzmann's superposition principle, it is necessary that the test stress/strain levels are within the linear range of material response. Therefore, stress relaxation experiments were conducted on samples that were aged at 80 °C for the lowest aging time (26 min) and storage modulus curves were plotted versus loading time. The specimens were rejuvenated and cooled to the aging temperature and then aged again for another stress relaxation test at a higher strain level. A significant vertical shift in the curves of storage modulus in terms of loading time at increasing levels of strain indicates the onset of nonlinearity.

After selecting a strain level in the linear viscoelastic range for thermally aged samples, the method was repeated to check the linear range for hygrothermally aged samples. In this set, stress relaxation tests were conducted on three specimens that were hygrothermally aged (fully immersed) in distilled water at 80 °C for 168 hours. This condition has the highest temperature and relative humidity among all the conditions used in this study.

3.3.2.2 Short Term Aging Tests

3.3.2.2.1 Thermal Aging Test

In order to provide a common starting point for the specimens and initiate the process of physical aging in the material, the conditioned samples were isothermally heated at 135 °C for 10 minutes. This step, performed in an oven, erases the thermal history of the material. Specimens were then moved to the DMA instrument to start stress relaxation experiments. In order to reduce temperature loss in the rejuvenated specimens, the temperature of the DMA oven had already been set to the aging temperature. Each aging treatment is conducted inside the DMA and consists of the following steps: the specimen is isothermally aged at the selected aging temperature and then loaded at 0.5% strain for the duration of the relaxation test which is one-tenth of the aging time [96]. The specimen is then unloaded. The steps are repeated each time with incremental aging time duration until all the selected aging periods are completed.

The three selected aging temperatures, T_a; *i.e.*, 50 °C, 65 °C and 80 °C, are well below the T_g's of the blend's components. There were 7 different aging times, t_a, used in this part of the study as shown in Table 3-1. Each of these aging times is 1.8 times longer than the previous aging time.

Table 3-1 Levels of aging time, t_a [min], used in stress relaxation experiments on thermally aged samples.

t_{a1}	t_{a2}	t_{a3}	t_{a4}	t_{a5}	t_{a6}	t_{a7}
28.2	50.8	91.5	164.6	296.4	533.5	960.2

The selected aging times are based on the results of the moisture uptake tests conducted at two aging temperatures of 50 °C and 65 °C (the results will be presented in section 4.1.4). In those experiments, test specimens, on average, reached at 40% to 60% of their maximum moisture uptake after about 16 hours. Therefore, the highest aging time, t_{a7}, which is about 16 hours, was also used for the hygrothermal aging test described in the following section.

3.3.2.2.2 Hygrothermal Aging Test

Stress relaxation tests were applied to investigate the coupled effects of physical aging and moisture absorption on the mechanical behaviour of the PC/ABS blend. After conditioning of the

specimens inside a desiccator for 48 hours, they were treated in an oven at 135 °C to remove their thermal history. This was followed by exposure to nine different hygrothermal conditions for 16 hours: (1) 50°C/50% RH, (2) 65°C/50% RH, (3) 80°C/50% RH, (4) 50°C/93% RH, (5) 65°C/93% RH, (6) 80°C/75% RH, (7) 50°C/fully immersed, (8) 65°C/fully immersed, and (9) 80°C/fully immersed. After each aging condition, the specimens were subjected to stress relaxation tests in the DMA instrument for 96 minutes (equal to one tenth of the hygrothermal aging time ([96]). Before the stress relaxation test, the sample was equilibrated at the hygrothermal aging temperature. Each stress relaxation test consisted of applying an instantaneous strain of 0.5% (as in thermal aging) to the specimen and the decay of the material's modulus was recorded.

In order to reduce moisture evaporation from the specimens, they were coated with a thin layer of Dow Corning® high-vacuum grease [103, 110]. The effect of the coating on the viscoelastic response was verified by comparing the response of samples with and without coating. It was observed that coating had a negligible effect on the viscoelastic response of the samples.

Stress relaxation tests were also conducted on un-aged samples. Before stress relaxation tests, PC/ABS samples were dried by conditioning inside a desiccator for 48 hours and also placed in an oven at 80 °C for 30 minutes. This approach was applied to study the competitive effects of physical aging and hygrothermal aging processes on the viscoelastic response of the material by comparing the results of both thermal and hygrothermal aging tests with the results of stress relaxation tests on un-aged samples.

3.3.2.3 Long Term Aging Tests

Stress relaxation tests were conducted on samples that were aged at only one prolonged aging time; *i.e.*, 168 hours. These tests, which will be referred to as "long" term aging tests, were applied on both thermally as well as hygrothermally aged specimens. For thermally aged specimens, samples were aged for 168 hours inside an oven controlled within ± 1 °C at the three aging temperatures of 50 °C, 65 °C, and 80 °C after thermal history erasure. They were then tested in the DMA testing machine under stress relaxation loading for 16.8 hours (one tenth of aging time). In hygrothermal aging tests, specimens were aged in an environmental chamber at nine hygrothermal conditions for 168 hours and then tested in the DMA testing machine for stress relaxation loading of 16.8 hours. The procedure of stress relaxation loading was similar to the short term aging tests described in the preceding sections.

3.3.3 Coupling Coefficients — First Set

This section includes the experiments conducted to obtain the first set of coupling coefficients that exist in the coupled physics of structural mechanics, diffusion, heat conduction, and physical aging. The first set includes the elastic coefficient of thermal expansion as well as the elastic coefficient of hygroscopic expansion. Other sets of coupling coefficients will be defined and determined in Chapter 5, where the constitutive equations are presented.

3.3.3.1 Coefficient of Thermal Expansion

The experiments conducted to obtain the coefficient of thermal expansion (CTE) are exactly those performed to obtain the T_g of the PC/ABS blend described in section 3.3.1.1.1. As in the tests applied under the two modes of expansion and dilatometry, the displacement change of the material is recorded in a temperature scan, the CTE can also be determined from the experimental results. The CTE has, therefore, been determined before and after T_g of the material.

3.3.3.2 Coefficient of Hygroscopic Expansion

The second coefficient in the first set of coupling coefficients relates to the elastic coefficient of hygroscopic expansion. A review of the related work dealing with experimental determination of the coefficient of hygroscopic expansion revealed that a technique using two thermal analysis instruments has been proposed by Wong *et al.* [9, 114]. The so-called TMA/TGA technique was used later by other investigators [115-118] to determine the coefficient of hygroscopic expansion. In this technique, two identical specimens are exposed to a humid environment to absorb moisture. After saturation, one of the samples is moved to the TMA while the other one is placed inside the TGA. The moisture is then removed from the samples at constant temperature inside the TMA and TGA. The length change during moisture desorption is recorded in the TMA while the TGA measures the amount of moisture diffusing out of the sample. The ratio of length change (strain) to moisture concentration is related to the coefficient of hygroscopic expansion.

In this study, the TMA/TGA technique was employed to obtain the coefficient of hygroscopic expansion for the PC/ABS polymer blend. Test specimens were cut in the form of square bars from a PC/ABS sheet. A TA Instruments TMA Q400 and a TA Instruments TGA Q50 were used to conduct the experiments. According to Zhou [115], using samples with higher aspect ratios (the ratio of length or width to thickness) results in more accuracy in obtaining the coefficient of hygroscopic expansion. However, the sample size is limited to the size of TMA stage as well as the size of TGA sample

holder. Considering these two limitations, samples with dimension of 4×4×0.5 *mm* were cut from a large sheet of PC/ABS blend.

Zhou *et al.* [117] have studied the sources of error in determination of the coefficient of hygroscopic expansion using this technique and proposed a practical guideline in conducting the experiments. The steps of the experiment in this study were adopted based on the guidelines proposed by Zhou *et al.* [117]. Two identical specimens were stored in a desiccator for 48 hours and then dried inside an oven at 80°C for 30 minutes. The length, width, and thickness of the samples (h_{xo}, h_{yo}, h_{zo}) as well as the mass of the dry samples, M_{dry}, were measured. Next, samples were conditioned inside an environmental chamber at the specified hygrothermal conditions until saturation. Following saturation, specimens were moved to the TMA and TGA. The thickness of the sample, h_{sat}, and the mass of the sample, M_{sat}, were recorded in the TMA and TGA, respectively. Specimens were then dried out completely at the same temperature of hygrothermal condition and the thickness, h_o, and the mass, M_o, of the specimens was recorded at the end of the test.

Samples were exposed to 8 different hygrothermal conditions: 1) 50 °C/50% RH, 2) 50 °C/93% RH, 3) 50 °C/fully immersed, 4) 65 °C/93% RH, 5) 65 °C/fully immersed, 6) 80 °C/50% RH, 7) 80 °C/75% RH, and 8) 80 °C/fully immersed. Three replicates were tested at each hygrothermal condition.

3.4 Concluding Remarks

In this chapter, the experimental methods related to seven different characterization tests for a PC/ABS polymer blend were explained. These tests, which have been performed using thermal analysis techniques, were mostly designed to study the effects of moisture diffusion and physical aging on the properties of the material and therefore, enabled us to study the thermophysical and mechanical properties of the polymer used in this study. The experimental results as well as the corresponding discussion will be presented in the following chapter.

Chapter 4
Experimental Results and Discussion

The experimental methods for characterization of the PC/ABS were explained in the previous chapter. The experimental results as well as the corresponding discussion are presented in this chapter.

4.1 Thermophysical Properties

The first category of properties investigated in this study was related to the thermophysical properties, whose experimental results are explained in the following sections.

4.1.1 Glass Transition Temperature

The dual T_g's of the PC/ABS blend have been determined using two thermal analysis techniques; *i.e.*, TMA and DMA. The results of the experiments are presented and discussed in the following section.

4.1.1.1 TMA Tests

The T_g can be specified using different methods, either the onset temperature or the inflection point on the curve [119]. Since the slope of length change versus temperature shows the CTE and there is a change in CTE at T_g [120], the T_g can be defined at a point where the curve slope changes. Assigning T_g to this blend was, therefore, done using two tangent lines drawn on the curve at the points where the slope changes, as proposed by Earnest [78] for an expansion probe test. The same method is also applicable to the curves obtained from dilatometer. Figure 4-1 shows how two T_g's were typically assigned from dilatometer mode results at the heating rate of 0.5 °C/min. The first point shows the T_g of ABS in the blend at 100.30 °C and the second point assigns 127.57 °C to the T_g of PC in the blend. The same method was also used for the expansion probe analysis.

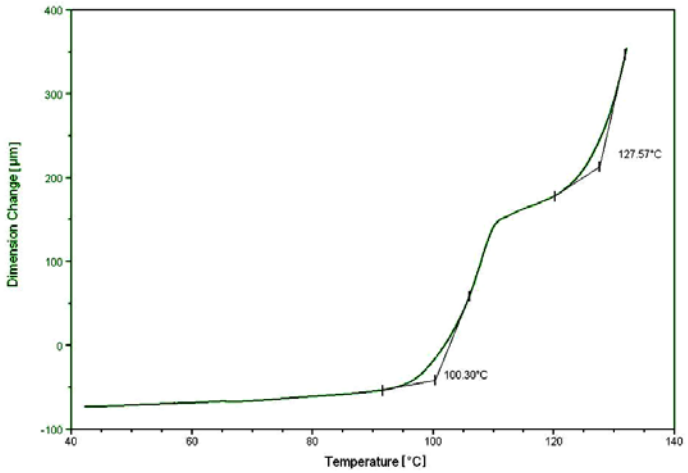

Figure 4-1 Assignment of T_g on the blend curve in dilatometer mode at heating rate of 0.5 °C/min.

Figures 4-2 and 4-3 show the typical curves obtained at different heating rates from expansion probe and dilatometer modes, respectively. The superimposed curves demonstrate that the shape of the curves was strongly dependent on applied heating rates.

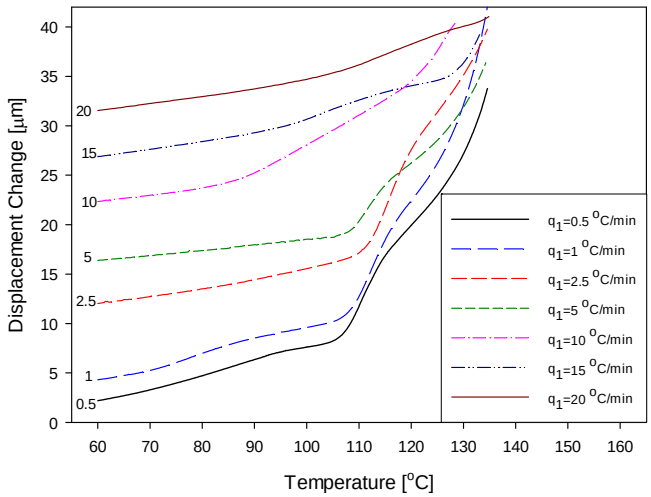

Figure 4-2 Displacement change versus temperature at different heating rates from expansion probe mode experiments.

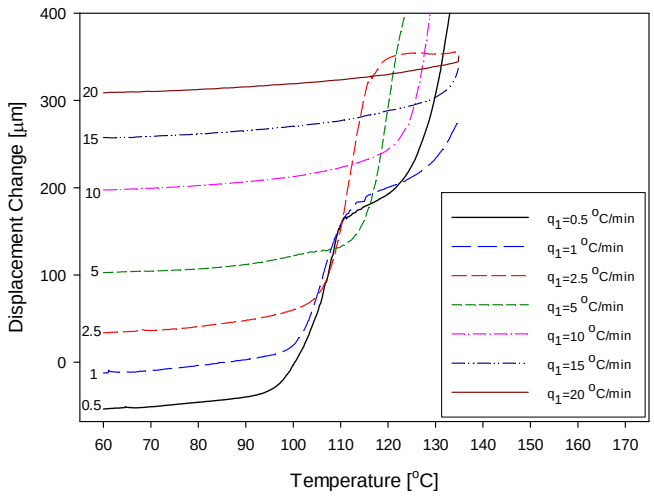

Figure 4-3 Displacement change versus temperature at different heating rates from dilatometer mode experiments.

As seen in Figures 4-2 and 4-3, the resolution of the two T_g's of the blend components and confidence in assignment accuracy become increasingly more challenging with increasing heating rates. High heating rates produce significant thermal lag errors in the results, which are well known for the TMA technique since the sample mass is relatively large [62, 121]. High heating rates cause high thermal gradients in the sample and in the furnace, from which thermal lag errors increase [66]. Lower heating rates are therefore recommended in order to avoid erroneous T_g values [119]. Our results suggest that lower heating rates ranging from 0.5 to 5 °C/min are most practical for TMA experiments at the two expansion and dilatometer modes.

Figures 4-4 and 4-5 show the T_g of PC and ABS obtained during heat-up and cool-down scans in the expansion probe and dilatometer modes, respectively. The obtained glass transition temperatures seem reasonable as they fall within the temperature range between T_g of pure PC and that of pure ABS for this partially immiscible blend. However, dilatometer and expansion probe tests failed to detect $T_{g,PC}$ on cooling scan.

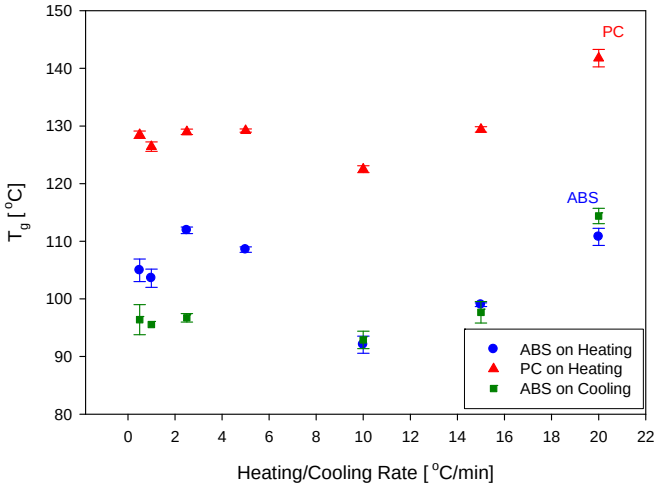

Figure 4-4 T_g's of the blend components obtained using the expansion probe for various heating and cooling rates.

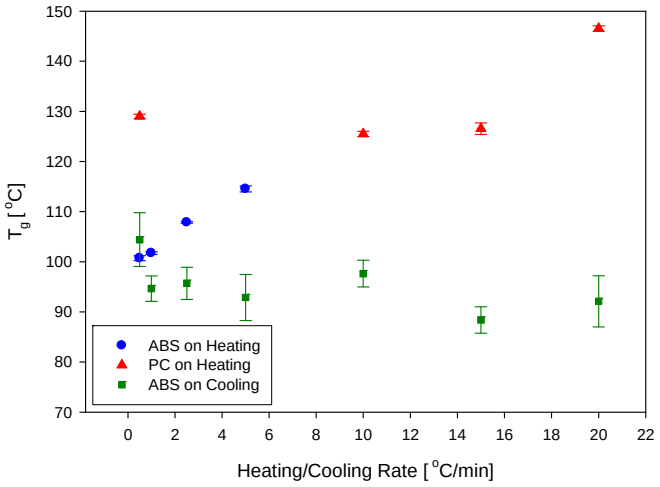

Figure 4-5 T_g's of the blend components obtained using the dilatometer probe for various heating and cooling rates.

Figures 4-4 and 4-5 show a general trend in T_g values with increasing heating rates but the effect of cooling rate is less obvious. One explanation for the latter observation is the larger error bars in the cooling rate curve for ABS which suggests that cooling rate experiments are more prone to thermal

lag errors. Another parameter that can be obtained from the curves in Figures 4-4 and 4-5 is the T_g at zero heating/cooling rate by extrapolating to zero scan rate. Table 2 shows the T_g of ABS at zero heating/cooling rate from dilatometer and expansion probe tests.

Table 4-1 T_g of ABS at zero scan rate from expansion probe and dilatometer tests measured in °C.

Mode	Heating	Cooling
Expansion probe	98 ± 2.5*	96 ± 2.1
Dilatometer	99 ± 0.9	100 ± 4.1

*95% Confidence Interval

It can be seen that the T_g's at zero rate are within the experimental error on heating and cooling scans for both expansion probe and dilatometer tests. In fact, T_g at zero rate can be considered to be the same if examined within the maximum experimental error of 3.8 %. This observation is consistent with earlier suggestion by Schwartz [72] that T_g at zero rate could be considered a material constant.

In order to check whether there is a statistical difference between the T_g's measured at various heating rates, an Analysis of Variance (ANOVA) was performed. ANOVA showed that, in general, there is a statistical significance between the results of each heating rate group with significance level of 0.05, which means that the heating rate influences the values of T_g. This was expected because the glass transition is a relaxation process and is influenced by heating rate change [122]. This is also similar to the findings of Schwartz [72], in which heating and cooling rates influenced T_g. However, there was no difference between the results of heating rate of 0.5 with 1 °C/min, and between those of 2.5 and 5 °C/min measured by the expansion probe.

It is also known that the sample mass influences the obtained T_g [74, 123]. In order to compare the data within each heating rate group the effect of sample mass should be accounted for. This was accomplished using Analysis of Covariance (ANCOVA), in which the sample mass was taken as a covariate, thus enabling us to compare the T_g obtained from both TMA modes together. The difference between masses (100.5 *mg* for the case of expansion mode and 56.7 *mg* for the dilatometer case) was considered and the results were compared. ANCOVA showed that there is no statistical significance in T_g data due to the sample mass change and therefore, the results could be compared.

In order to compare the values of T_g's between expansion probe and dilatometer results, the 95% confidence interval was calculated for each of them and checked whether the T_g of the other group falls within this interval or not. Using this method, it was found that T_g's of PC and ABS obtained from expansion probe and dilatometer are equal for heating/cooling rate of 0.5 °C/min. However, there was no agreement between the T_g's obtained from expansion probe and dilatometer modes at the other heating rates.

The second heating scan after the cool-down scan was performed to measure the T_g after thermal history removal during the isothermal step. The comparison of the curves found from the first and second heating scans, Figure 4-6, shows the effect of thermal history removal.

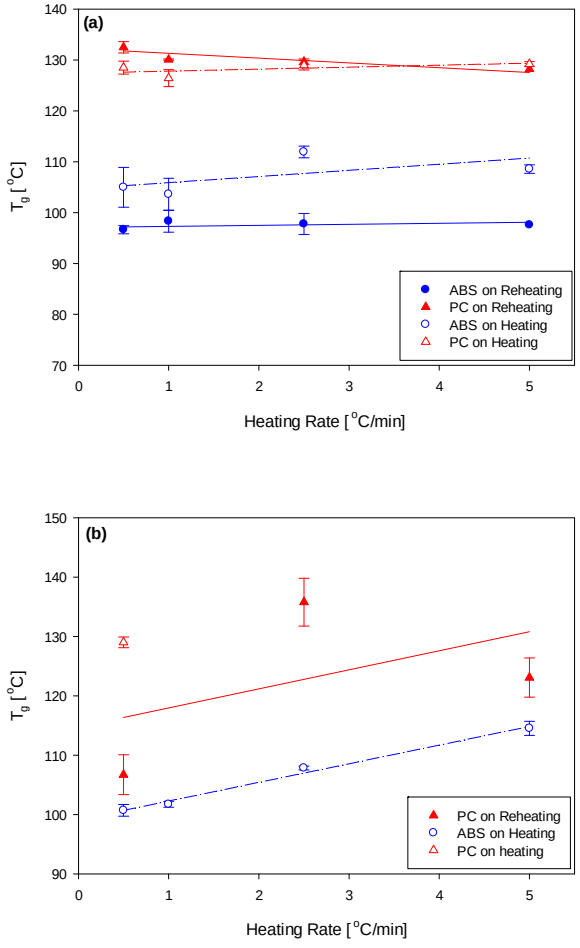

Figure 4-6 Comparison of T_g's of the blend components obtained on heating and reheating scans for (a) expansion probe mode and (b) dilatometer mode.

Figure 4-6 (a) demonstrates the difference between T_g's of both PC and ABS obtained from the expansion mode before and after thermal history removal step. It is seen that the thermal history removal had greater effect on PC than had on ABS. Figure 4-6 (b) shows that the dilatometer was able to detect the glass transition of ABS in the blend during first heat-up but not the second. This is very likely due to the low ABS content in the blend. This was also observed in DSC and DMA studies of this blend [95].

The difference in the glass transition temperatures recorded by expansion probe and dilatometer is due to the fact that displacement of the sample is recoded in one dimension by the expansion probe, whereas the dilatometer kit makes it possible to convert the volume change of the sample into displacement. Therefore, the displacement of other directions is not accounted for in the expansion mode.

It should also be pointed out that although TMA has its own advantages, particularly for measuring volume relaxation of polymers or measuring coefficient of thermal expansion, it has some disadvantages that may cause differences between the results. One of its drawbacks is that the thermocouple is not in direct contact with the sample, which results in inaccuracy in temperature measurement of the sample. This is also another cause of thermal lag errors mentioned earlier.

4.1.1.2 DMA Tests

Strain sweep tests were applied on 5 different specimens and were repeated 6 times (6 cycles) on each sample. The average of the recorded storage modulus for all of the 6 cycles was calculated at each amplitude level and is shown for a typical specimen in Table 4-2. The repeatability of the results based on the standard deviation (SD) and relative standard deviation (RSD) of the storage modulus are also reported.

Table 4-2 Storage modulus of a typical specimen in the strain sweep test.

	Storage Modulus		
Amplitude	**Average**	**SD**	**RSD**
[μm]	*[GPa]*	*[GPa]*	*[%]*
10	1.89	0.023	1.22
15	1.88	0.015	0.80
20	1.92	0.013	0.68
25	1.95	0.010	0.51
30	1.96	0.012	0.61
35	1.97	0.011	0.56
40	1.99	0.008	0.40
45	2.00	0.007	0.35
50	2.03	0.008	0.39

The reproducibility of the results was studied by obtaining the variability of the values of storage modulus between the five tested specimens. The average, standard deviation, and relative standard deviation of the values of storage modulus of the 5 specimens are calculated and presented in Table 4-3.

Table 4-3 Variability of storage modulus among the 5 tested specimens with respect to amplitude in the strain sweep test.

	Storage Modulus		
Amplitude	**Average**	**SD**	**RSD**
[μm]	*[GPa]*	*[GPa]*	*[%]*
10	1.80	0.24	13.33
15	1.83	0.14	7.65
20	1.92	0.09	4.69
25	1.96	0.06	3.06
30	2.00	0.04	2.00
35	2.02	0.03	1.49
40	2.04	0.03	1.47
45	2.05	0.03	1.46
50	2.08	0.03	1.44

Tables 4-2 and 4-3 show that the relative standard deviations decrease with strain amplitude. Therefore, higher amplitudes seem to give more repeatable data for T_g determination test. However, since the material softens as the sweep temperature approaches the glassy region; higher strain amplitudes cannot be applied. It was found that the most practical amplitude for the T_g determination test was 20 μm.

The glass transition temperature was assigned based on the peaks of the $tan\ \delta$ (ratio of storage modulus to loss modulus) signal [124]. Figure 4-7 shows the $tan\ \delta$ curve for a typical sample; the first peak corresponds to the T_g of ABS while the second is related to PC. The average values of T_g of ABS and PC over the 3 tested specimens are ~ 94 °C and 120.4 °C, respectively.

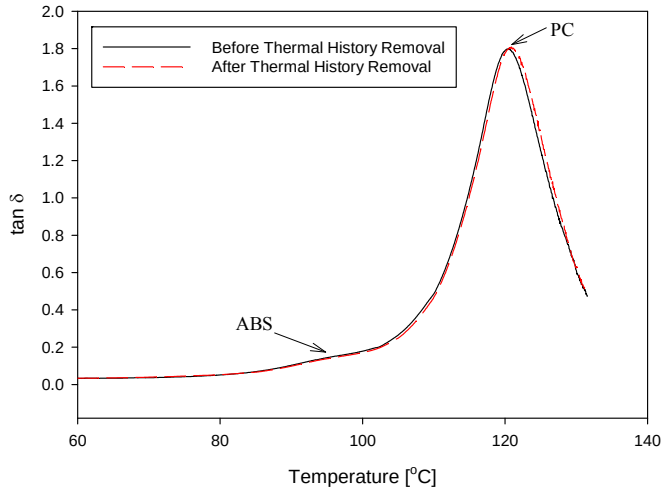

Figure 4-7 Glass transition temperature determination from *tan δ* curve before and after thermal history removal for a typical sample.

To investigate the effect of thermal history removal on the values of T_g, the samples were rejuvenated and tested for the second time. The corresponding *tan δ* curve is overlaid on the curve from the first run (before thermal history removal) in Figure 4-7. As seen in the figure, the $T_{g,ABS}$ is not affected while $T_{g,PC}$ is minimally affected (0.4 °C on average).

If the current glass transition temperature values are compared with those obtained from the TMA tests as well as those determined from DSC and DMA experiments conducted in this study and also reported by Tang and Lee-Sullivan [70], the TMA values are the highest as shown in Table 4-4. It is noted, however, that the values of DSC have been obtained using a heating rate of 10 °C/min [70] while TMA results were obtained using a heating rate of 0.5 °C/min. The values of DMA were also obtained using the single cantilever mode [70] and 3-point bending mode at a frequency of 1 Hz and a heating rate of 1 °C/min.

Table 4-4 Comparison of glass transition temperatures obtained using DSC, DMA, and TMA.

Method			$T_{g,ABS}$ (°C)	$T_{g,PC}$ (°C)
DSC [70]			92	112
DMA (single cantilever mode) [70]			100	112
DMA (3-point bending mode)			94	120
TMA	Expansion Probe	Heating	105	129
		Cooling	98	-
		Reheating	97	132
	Dilatometer	Heating	101	129
		Cooling	104	-
		Reheating	-	130

As was expected, there are differences in the T_g values since each of these methods measure a different thermal property. Specifically, the DSC measures heat capacity, the TMA measures thermal expansion (length or volume), while the DMA measures loss tangent (*tan δ*) or loss modulus (E″) as a function of temperature [125].

It is seen that T_g values obtained from DSC are lower than those obtained from DMA and they are all lower than those obtained from TMA. Therefore, the increasing trend of the methods is *DSC* → *DMA* → *TMA*, which is similar to the trend presented for butadiene rubber by Sircar *et al.* [125].

4.1.2 Physical Aging Study

The volume relaxation of the PC/ABS material was studied using physical aging tests in the dilatometry mode of the TMA at the aging temperature of 80 °C. Table 4-5 tabulates the specific volume recovered during the physical aging period for the 7 aging times. The specific volume is defined as the ratio of the volume change to the mass of each sample. These values are corrected for the volume changes due to the filling medium.

Table 4-5 The volume relaxation of the PC/ABS at the aging temperature of 80 °C.

Aging Time *[hr]*	**Specific Volume Recovered** $\times 10^{-6}$ *[m³/kg]*	**Average (± RSD%)** $\times 10^{-6}$ *[m³/kg]*
0.5	1.79 2.48 1.65 1.93	1.96 (± 18.4%)
2	1.87 1.06 1.03	1.32 (± 36.1%)
8	5.25 8.84 8.54 6.66	7.32 (± 23.0%)
48	16.92 16.11 18.13 22.43	18.40 (± 15.3%)
96	39.68 19.64 33.43 21.34	28.52 (± 33.8%)
336	28.13 61.76 49.15	46.35 (± 36.7%)
1008	87.08 58.79	72.94 (± 27.4%)

As expected, the volume recovered during physical aging at 80 °C increases with aging time. A similar trend has been seen for the enthalpy relaxation of PC/ABS blend [70]. The values of relative standard deviation (RSD) may appear high in Table 4-5 but this is usually observed in polymers.

Cowie and Ferguson [126] defined $\Phi_{Ta}(t)$ for the extent of relaxation toward equilibrium at the aging temperature, T_a, for enthalpy relaxation. Similar definition can be applied for volume relaxation, using KWW function [127] for $\Phi_{Ta}(t)$:

$$\phi_{T_a}(t) = \frac{v(t) - v_\infty}{v_o - v_\infty} = exp\left[-\left(\frac{t}{\tau}\right)^{\beta}\right] \tag{4-1}$$

Therefore, the parameter (v_o-$v(t)$), which is the measured volume change in the TMA, can be presented by:

$$v_o - v(t) = v_o - v_\infty \left\{1 - exp\left[-\left(\frac{t}{\tau}\right)^{\beta}\right]\right\} \tag{4-2}$$

where τ is a relaxation time constant and β is referred to as shape parameter.

Equation (4-2) was fitted to the experimental data to obtain τ and β. Figure 4-8 depicts the fitted curve to the experimental data.

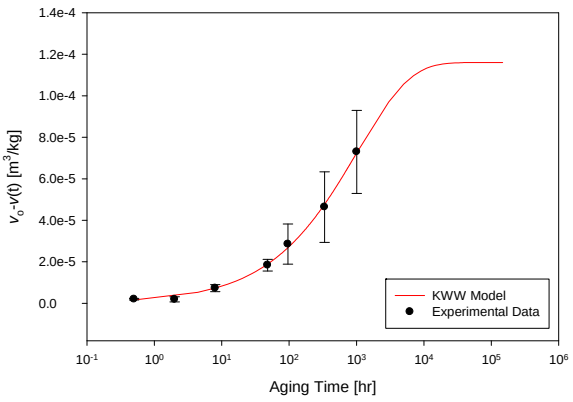

Figure 4-8 Fitted curve to the experimental data of volume relaxation at 80 °C.

According to the curve fitting results, τ is equal to 1043.4 *hr* and β is 0.56. The volume change at equilibrium is also equal to 1.16×10^{-4} m^3/kg. The time to reach at 98% of the equilibrium value is 11000 *hr*, which seems unrealistic when compared to the enthalpy relaxation results. These values can be obtained with more accuracy by conducting tests at longer aging times so that a better curve fitting is obtained. This will be further explained in the future work section in Chapter 6.

4.1.3 Specific Heat Capacity

The specific heat capacity of the PC/ABS blend was determined *before* and *after* hygrothermal aging of the blend under 9 different hygrothermal conditions. The obtained results for three replicates tested at the typical condition of 80 °C/50% RH for the glassy region (from room temperature to 80 °C) are illustrated in Figure 4-9.

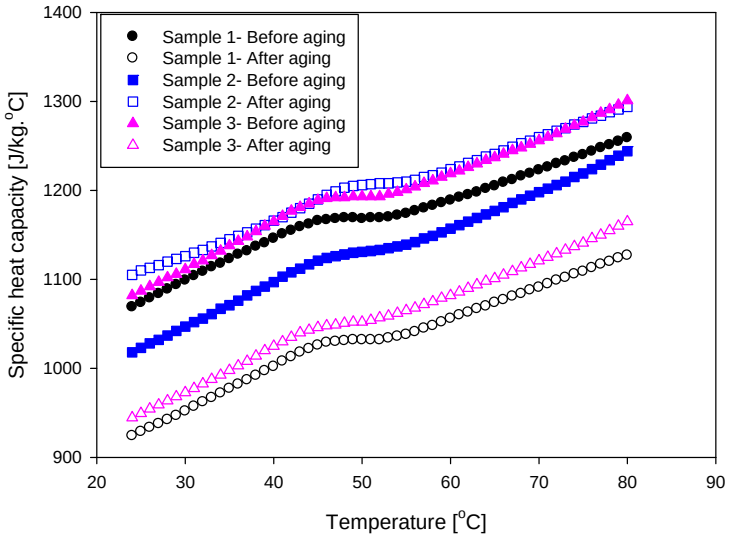

Figure 4-9 Comparison of specific heat capacity before and after hygrothermal conditioning at 80 °C/50% RH.

The comparison of the curves related to measurements performed *before* and *after* hygrothermal aging in Figure 4-9 reveals that the specific heat capacity for the first sample has decreased after aging whereas the specific heat capacity of the second and third samples has increased following aging. The average value of specific heat capacity of the three replicates is shown with the standard deviation in the form of bars in Figure 4-10.

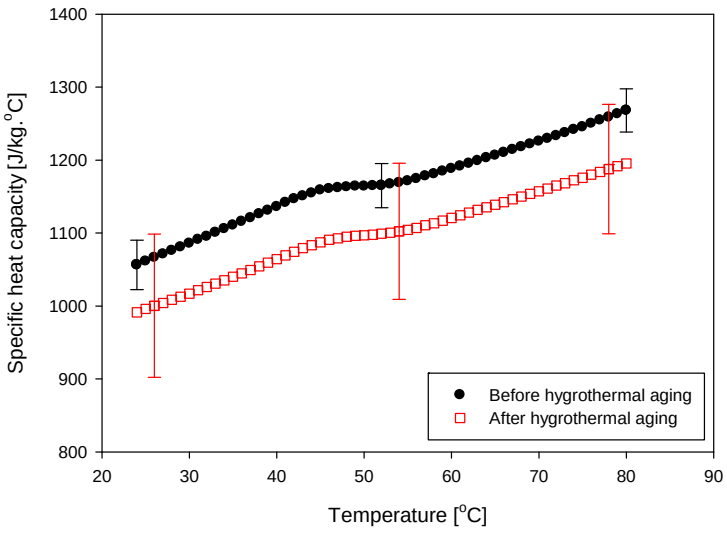

Figure 4-10 The average of specific heat capacity over the three replicates at 80 °C/50% RH.

As seen in Figure 4-10, the average specific heat capacity has decreased after hygrothermal aging at 80 °C/50% RH, but drawing such a conclusion will not be straightforward if the variation of the results is also considered (the bars in Figure 4-10). Therefore, a two-way repeated measures analysis of variance (ANOVA) was employed to study the effects of the two factors of *hygrothermal conditioning* and *scanning temperature* on the specific heat capacity, which is the response variable in this statistical analysis. The first factor, *hygrothermal conditioning*, has two levels of *before* and *after* conditioning and the levels of the *scanning temperature* factor are from 24 °C to 80 °C in an interval of 1 °C. The statistical analysis suggested that hygrothermal conditioning for 168 hours (the first factor) at the 9 hygrothermal conditions did not have a significant influence on the value of specific heat capacity. The specific heat capacity, however, was affected by the scanning temperature.

A regression analysis was, therefore, used to fit linear curves to the experimental values of specific heat capacity for the temperature range from room temperature up to 80 °C (glassy region of the material). As a result, a temperature-dependent expression has been proposed for the specific heat capacity of the blend at the glassy state:

$$c = 3.4T + 1028 \tag{4-3}$$

where c is the specific heat capacity in $J/kg.°C$ and T designate the scanning temperature in $°C$.

Equation (4-3) allows us to model the transient heat conduction in a coupled diffusion-heat transfer analysis for the blend in hygrothermal conditions. A discussion of the application of the relation in a numerical thermal analysis will be followed in the next chapter.

4.1.4 Moisture Uptake

4.1.4.1 Moisture Uptake Behaviour

The moisture uptake behaviour for the samples stored in environmental chambers at the four hygrothermal conditions of 50°C/50% RH, 50°C/93% RH, 65°C/50% RH, and 65°C/93% RH is illustrated in Figure 4-11. The equilibrium moisture content and the time to reach equilibrium for all conditions are presented in Table 4-6. The sharp differences in the uptake curves agree with similar observations by others, such as Narkis *et al.* [128] who showed distinct differences for glass-fibre reinforced PC in equilibrium liquid water sorption between 100°C and room temperature (0.6% and 0.3%, respectively).

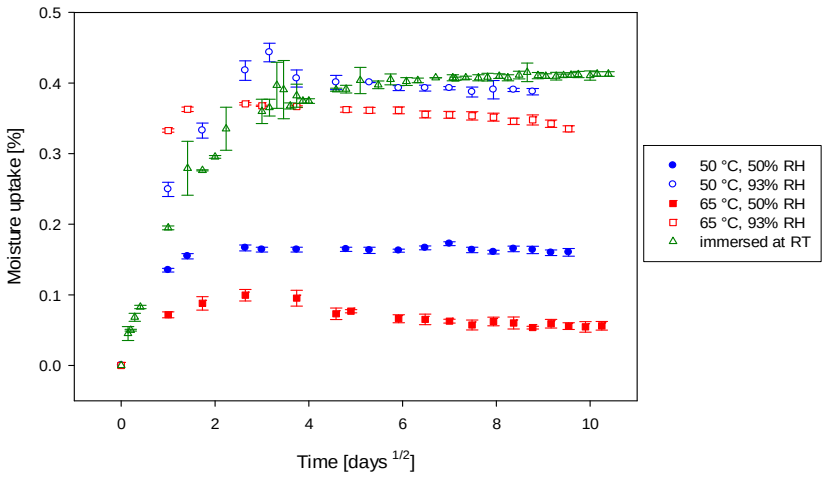

Figure 4-11 Moisture uptake behaviour of PC/ABS samples exposed to five different hygrothermal conditions.

Table 4-6 Corrected coefficient of diffusion, equilibrium moisture, and equilibrium time for the four hygrothermal conditions.

		Coefficient of Diffusion, $D_c \times 10^{-11}$ [m^2 / s]		**Equilibrium Moisture, M_∞ [%]**		**Equilibrium Time, t_∞ [days]**	
Relative Humidity [%]	**Sample No.**	**Aging Temperature [°C]**		**Aging Temperature [°C]**		**Aging Temperature [°C]**	
		50	**65**	***50***	***65***	***50***	***65***
50	1	1.28	7.92	0.17	0.06	9	49
	2	1.27	6.10	0.16	0.05	9	56
	3	1.81	5.54	0.16	0.06	9	56
	Average (± RSD)*	*1.45 (± 21.14%)*	*6.52 (± 19.08%)*	*0.16 (± 2.14%)*	*0.06 (± 13.55%)*	*9 (± 0%)*	*54 (± 7.53%)*
93	1	0.74	1.97	0.39	0.36	42	49
	2	0.69	1.93	0.40	0.36	42	42
	3	0.71	1.86	0.39	0.35	42	42
	Average (± RSD)	*0.71 (± 3.46%)*	*1.92 (± 2.78%)*	*0.39 (± 1.08%)*	*0.36 (± 1.36%)*	*42 (± 0%)*	*44 (± 9.12%)*

* Relative Standard Deviation

The governing equation of moisture diffusion in direction x of an infinite plate with thickness l, together with initial and boundary conditions is given as follows [129]:

$$\frac{\partial C}{\partial t} = D\frac{\partial^2 C}{\partial x^2} \tag{4-4}$$

$$C = C_i \qquad 0 < x < l, \;\; t \leq 0 \tag{4-5}$$

$$C = C_\infty \qquad x = 0; x = l, \;\; t > 0 \tag{4-6}$$

where C_i denotes the initial concentration of the plate and C_∞ represents the boundary concentration. The solution of Equation (4-4) with the initial and boundary conditions represented by relations (4-5) and (4-6) is [130]:

$$\frac{C(x,t)-C_i}{C_\infty-C_i}=1-\frac{4}{\pi}\sum_{i=0}^{\infty}\frac{1}{(2i+1)}sin\frac{(2i+1)\pi x}{l}exp\left[-\frac{(2i+1)^2\pi^2Dt}{l^2}\right] \tag{4-7}$$

An analytical solution to characterize the moisture weight gain of the plate, in which diffusion through the edges can be neglected, can be obtained by integrating the concentration over the thickness of the plate [131]:

$$\frac{M_t}{M_\infty}=1-\frac{8}{\pi^2}\sum_{n=0}^{\infty}\left\{\frac{1}{(2n+1)^2}\exp\left[-D(2n+1)^2\frac{\pi^2 t}{l^2}\right]\right\} \tag{4-8}$$

And the corresponding coefficient of diffusion is approximated as:

$$D=\frac{0.04919}{\left(\frac{t}{l^2}\right)_{\frac{1}{2}}} \tag{4-9}$$

where the coefficient of diffusion, D, is evaluated at the half-time of the absorption process. M_t and M_∞ are mass uptake of the sheet at time t and saturation, respectively, and l is the thickness of the sheet.

The normalized overall weight gain of the samples can also be experimentally determined as:

$$\frac{M_t}{M_\infty}=\frac{m_t-m_o}{m_\infty-m_o} \tag{4-10}$$

where m_t is the mass of the sample at time t, m_o is the mass of the dry sample, and m_∞ is the mass of the sample at saturation. The normalized overall weight gain of the samples has been drawn versus the square root of time in Figure 4-12. It is known that the coefficient of diffusion for a system is proportional to the initial slope of the moisture absorption behaviour. These coefficients are determined according to equation (4-9) based on the hourly measurements of moisture uptake and

they are corrected for the effect of diffusion through the edges of the samples using the following equation [129]:

$$D_c = D\left(1 + \frac{l}{h} + \frac{l}{w}\right)^{-2} \tag{4-11}$$

where l, h, and w are the thickness, length, and width of the samples, respectively. The correction factor for the samples used in this study is about 0.76, indicating that the "edge effects" (the effect of diffusion through the edges of the samples on the moisture uptake) cannot be neglected. The corrected coefficients of diffusion, D_c, are also tabulated in Table 4-6.

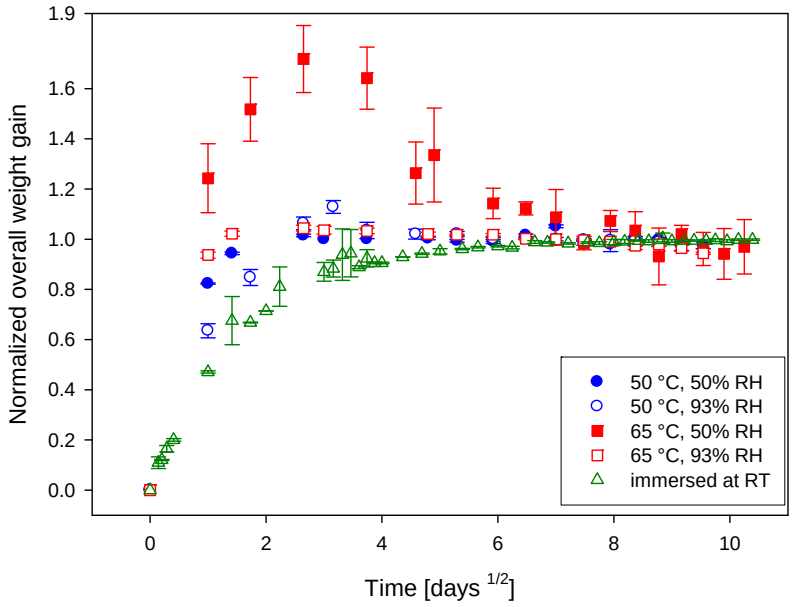

Figure 4-12 The effect of hygrothermal conditions on the coefficient of diffusion and anomalous behaviour in exposed samples.

One important characteristic of diffusion that can be seen in the moisture uptake curves of Figure 4-11 and more clearly on the normalized overall weight gain curves of Figure 4-12 is anomalous

diffusion behaviour, which appears as an overshoot on the curves. This anomalous (overshoot) behaviour has also occurred for the unfilled PC at 100 °C in the study of Narkis *et al.* [128].

The moisture uptake behaviour for the condition of fully immersed at room temperature is also illustrated in Figure 4-11. The moisture absorption curve indicates Fickian diffusion behaviour with an equilibrium moisture content of approximately 0.41%. This Fickian behaviour can be well compared with the overshoot behaviour of samples conditioned at the other four hygrothermal conditions illustrated in Figure 4-12.

4.1.4.2 Analysis on the Dependence of Moisture Uptake on Temperature and RH

There are several theories in literature that predict the equilibrium sorption uptake of a solvent-polymer system at both rubbery and glassy regions. The sorption behaviour in the rubbery state can be well described by the Flory-Huggins theory [132] of polymer solutions, but it fails to predict the nonlinear behaviour in a glassy polymer. Other theories, however, have been developed to describe the excess solvent uptake of glassy polymers. These theories are generally established based on the free volume theory of the amorphous state.

There are three models in the literature which can be used to predict the sorption isotherm of penetrant molecules into glassy polymeric systems: Vrentas-Vrentas [133]; Leibler-Sekimoto [111]; and Doumenc *et al.* [134]. They are extensions to the Flory-Huggins theory [132] and therefore, have the following general form:

$$a = (1 - \Phi_P)\exp(\Phi_P + \chi\Phi_P^2 + F) \tag{4-12}$$

where F for different models are expressed in Table 4-7.

Table 4-7 Different expressions of *F* in Equation (4-12).

Model	Expression	
Vrentas-Vrentas [133]	$\frac{M_s \omega_p^2 \Delta c_p \frac{dT_{gm}}{d\omega_s}\left(\frac{T}{T_{gm}}-1\right)}{RT}$	(4-13)
Leibler-Sekimoto [111]	$-\frac{v_s K_{gl}^o}{RT}\log\frac{\Phi_v}{\Phi_g(T)}$	(4-14)
Doumenc *et al.* [134]	$-\frac{v_s K_{gl}^o}{RT}\int_0^t \frac{\exp\left[-\tilde{t}(t',t)^{\beta'}\right]}{\Phi_p(t')}\cdot\frac{\partial\Phi_p(t')}{\partial t'}dt'$	(4-15)
	where	
	$\tilde{t}(t',t)=\int_{t'}^{t}\frac{dt''}{\tau_c[\Phi_p^*(t'')]}$	(4-16)
	and	
	$\tau_c\left(\Phi_p^*\right)=\tau_o\exp\left[\frac{B}{T-T_o-\Delta T_g\left(\Phi_p^*\right)}\right]$	(4-17)
	and	
	$\Phi_p^*(t)=\Phi_p(t)+\int_0^t\left\{1-\exp\left[-\tilde{t}(t',t)^{\beta'}\right]\right\}\cdot\frac{\partial\Phi_p(t')}{\partial t'}dt'$	(4-18)

The parameters used in Equations (4-12) to (4-18) are defined in Table 4-8. These three models were applied to obtain sorption isotherms of PC at two temperatures of 50 °C and 65 °C. The values of different parameters of the three models, expressed by Equations (4-13) to (4-18), are obtained from literature and are presented in Table 4-9.

Table 4-8 Definition of parameters in Equations (4-12) to (4-18).

Notation	Definition
a	solvent activity
B	Constant
c_p	specific heat capacity at const. pressure
Δc_p	difference in c_p between glassy & rubbery state
K_{gl}	bulk modulus at the glassy state
K^o_{gl}	bulk modulus at the dry state
M_s	solvent molecular weight
R	ideal gas constant
T	Temperature
T_{gm}	T_g of polymer-solvent system
T_o	Constant
ΔT_g	temperature shift
t, t', t''	Time
β'	exponent from stretched exponential
Φ_v	volume fraction
Φ_g	Φ_p at which glass transition takes place
Φ_p	polymer volume fraction
Φ_s	solvent volume fraction
τ_c	characteristic time
τ_o	Constant
χ	the Flory-Huggins interaction parameter
v_s	solvent molar volume
ω_p	polymer mass fraction

Table 4-9 Values of some of the parameters in Equations (4-13) to (4-18) obtained from literature.

Notation	Value	Ref.
Δc_p	0.2303 [J/gK]	[135]
K^o_{gl}	-0.008T [°C]+2.903 [GPa]	[136]
T_{gm}	-13 ω_s+422 [K]	[137]
τ	τ_o exp[-50000(1/T-1/415)]	[138]
τ_o	3850 [s]	[138]
χ	4.7-6.6 Φ_s	[139]

4.1.4.3 T_g Determination

The T_g's of the hygrothermally aged specimens were determined from the DMA tests and are tabulated together with the % moisture uptake after 7 days in Table 4-10. To determine reversibility of moisture absorption, the samples were then heated for 10 minutes at 135 °C which has been used for thermal history erasure. It was found that $T_{g,ABS}$ and $T_{g,PC}$ were in the range of 87-89 °C and 113-114 °C, respectively. Generally, most of the moisture was removed and the residual moisture content of the samples was below 35% of the 7-day moisture uptake of the corresponding samples.

Table 4-10 Dual T_g's of PC/ABS samples conditioned at the four hygrothermal conditions for 7 days.

Relative Humidity	Sample No.	Aging Temperature					
		50 [°C]			***65 [°C]***		
		Uptake [%]	*$T_{g,ABS}$ [°C]*	*$T_{g,PC}$ [°C]*	*Uptake [%]*	*$T_{g,ABS}$ [°C]*	*$T_{g,PC}$ [°C]*
50 [%]	1	0.15	88.0	113.1	0.11	86.6	112.7
	2	0.14	88.1	113.3	0.14	86.3	112.6
	Ave (± RSD)*	*0.15 (± 5%)*	*88.1 (± 0.1%)*	*113.2 (± 0.1%)*	*0.13 (± 17%)*	*86.5 (± 0.2%)*	*112.7 (± 0.1%)*
93 [%]	1	0.31	86.8	112.2	0.36	83.3	112.1
	2	0.27	86.6	112.5	0.37	82.6	111.7
	Ave (± RSD)	*0.29 (± 10%)*	*86.5 (± 0.5%)*	*112.4 (± 0.2%)*	*0.37 (± 2%)*	*83.0 (± 0.6%)*	*111.9 (± 0.3%)*

* Relative Standard Deviation

In the discussion to follow, it is reasonable to assume that the aging processes described closely represent low activation processes at the intermolecular scale associated with physical aging since the hygrothermal aging temperatures used in the study remained well below $T_{g,ABS}$ values. Moreover, no noticeable relaxation peak was detected in the aging temperature range used.

4.1.4.4 Discussion

4.1.4.4.1 Moisture Uptake Behaviour

As expected, Figure 4-11 shows that aging temperature and relative humidity strongly influence sample moisture uptake rate and saturation level. However, in order to fully evaluate the statistical significance of these two factors the method of analysis of variance (ANOVA) was applied, following a previous approach [140]. The aging temperature and relative humidity are the two factors, each with two levels, which were varied to study their effects on the saturation moisture. The analysis of a two-factor experiment with a and b levels of the factors (or treatments) is suitably analyzed by a two-factor ANOVA [141].

The two-factor ANOVA found that relative humidity had a significant effect (p-value < 0.001) on the equilibrium moisture; *i.e.*, the relative humidity increase of 43% (from 50% RH to 93% RH) increased the equilibrium moisture by average factors of 2.4 and 6.0 for aging temperatures of 50 °C and 65 °C, respectively (Table 4-6). The aging temperature also had an effect on the equilibrium moisture level although increasing aging temperature decreased the moisture levels, on average, by 62.5% and 7.7%, at relative humidity of 50% RH and 93% RH, respectively. The interaction between aging temperature and relative humidity was also significant.

In Figure 4-12, the different initial slopes of the curves represent the different coefficients of diffusion. A two-factor ANOVA was also applied to study the effects of aging temperature and relative humidity on the corrected coefficient of diffusion, D_c. The analysis revealed that aging temperature had a significant effect (p-value < 0.001) on the corrected coefficient of diffusion; *i.e.*, aging temperature increase of 15°C (from 50°C to 65°C) caused an increase in D_c with an average factor of 3.91. The relative humidity also had an effect; however, the increase of relative humidity led to a 67% decrease in D_c on average. The interaction between aging temperature and relative humidity was also significant.

Application of statistical analyses revealed that the two factors of relative humidity and aging temperature have opposite effects on both equilibrium level and D_c; *i.e.*, the equilibrium moisture

level increased with relative humidity but decreased with aging temperature. Conversely, the value of D_c decreased with relative humidity but increased with aging temperature. When combined, the two factors involve simultaneous mechanisms of moisture diffusion and physical aging. Thus, these two physical mechanisms need to be explored further to describe the observed effects.

4.1.4.4.1.1 Effects of the Two Factors on Equilibrium Moisture

The three models mentioned earlier were employed to predict the sorption isotherms of polycarbonate-water system at two different temperatures; *i.e.*, 50 °C and 65 °C. Since the experimental data for various parameters in these three models are not available for PC/ABS blend in open literature and as the 75/25 % PC/ABS blend is mostly composed of PC; its water sorption behaviour is expected to be close to that of PC. Therefore, the sorption isotherms of PC were taken as an estimate of those of PC/ABS blend.

The values of equilibrium moisture uptake are then calculated based on these models at two levels of relative humidity; *i.e.*, 50% and 93% RH, corresponding to activities of 0.50 and 0.93. These values can be used as an approximation for the equilibrium moisture uptake of the 75/25 % PC/ABS polymer blend. The theoretical results are compared with the experimental results obtained from hygrothermal aging of PC/ABS blends.

Figure 4-13 shows the sorption isotherms for PC-water system at two temperatures of 50 °C and 65 °C obtained by applying the three models. In this figure, the solubility of water in PC versus the water activity obtained from the Flory-Huggins theory is also plotted.

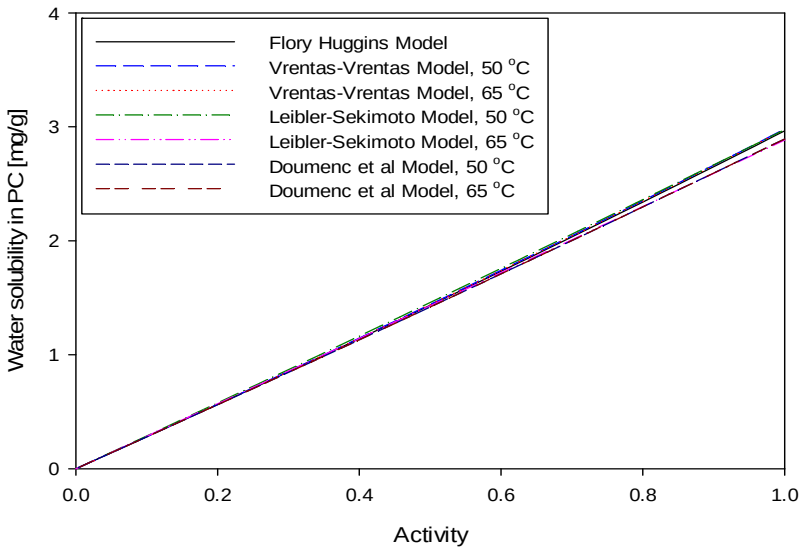

Figure 4-13 Comparison of sorption isotherms for PC-water system obtained by applying the three models.

As Figure 4-13 shows, there is negligible difference in the sorption behaviour of water in PC when analyzed by the three different models for glassy state, as well as the Flory-Huggins theory for the rubbery state. This can be attributed to the poor interaction between water and polycarbonate. This weak interaction is also reflected in the large value of Flory-Huggins interaction parameter, χ [142]. Although the values of different parameters in the three models are reported for PC materials with different molecular weights (Table 4-9), the effect of the interaction parameter on sorption isotherms is so large that the difference between those values is not influential.

In order to compare the results of the theoretical models with the hygrothermal experiments of 75/25 % PC/ABS, the values of equilibrium moisture uptake are calculated and tabulated in Table 4-11.

Table 4-11 Equilibrium moisture uptake in percentage obtained from the theoretical models.

		Vrentas-Vrentas model		Leibler-Sekimoto model		Doumenc *et al.* model	
		50% RH	93% RH	50% RH	93% RH	50% RH	93% RH
Aging Temperature [°C]	50	0.14	0.28	0.16	0.28	0.14	0.27
	65	0.14	0.28	0.14	0.27	0.14	0.27

The experimental values of equilibrium moisture uptake are comparable with models predictions. The slight difference between the values, however, is due to the difference in the sorption behaviours of PC and PC/ABS blend. The results of theoretical models also imply that the equilibrium moisture uptake is increased by relative humidity increase but is least affected by temperature changes, for the temperature range studied. This trend is also seen in the experimental results.

The increase of equilibrium moisture with relative humidity has also been reported by other investigators [4, 143, 144]. Akbar and Zhang [143], who studied moisture diffusion in carbon/epoxy composites in three different hygrothermal cases to determine moisture absorption as a function of relative humidity, observed that the maximum moisture content (or equilibrium moisture in the Fickian behaviour) increased with the relative humidity. In the study of moisture diffusion in composite sandwich structures, Katzman *et al.* [144] also reported that equilibrium moisture content increased with relative humidity. Golovoy and Zinbo [4] also reported increasing equilibrium moisture content of polycarbonate specimens with increasing relative humidity at 100 °C.

4.1.4.4.1.2 Effects of the Two Factors on the Coefficient of Diffusion

As explained in section 2.1.2, physical aging occurs during an isothermal hold following a rapid cooling from above T_g to the aging temperature, which is below T_g. Therefore, it is expected that physical aging does not have a strong influence on the moisture uptake when the beginning of the diffusion process coincides with the start of aging. Moisture flux to the polymer, however, is higher at higher temperatures, known as the Soret effect [145, 146]. It is therefore expected that higher temperatures lead to higher and faster initial moisture uptake; *i.e.*, the higher the temperature, the larger the coefficient of diffusion. Our experimental results are consistent with these well-known

theories and other studies which have compared hygrothermal effects [147, 148] in that the coefficient of diffusion is primarily dependent on temperature.

The dependence of the coefficient of diffusion on relative humidity deals with a comparison between the diffusion rate, on one hand, and the relaxation rate on the other. If the diffusion is Fickian, in which the diffusion rate is smaller than the rate of relaxation modes of the polymer chains [131], the coefficient of diffusion is independent of relative humidity. The humidity-independent coefficients of diffusion have been reported in the literature [144, 149]. However, when the coefficient of diffusion is a function of penetrant concentration, the diffusion process is non-Fickian, and this may occur when a polymer material is plasticized by the penetrant [13]. An increasing coefficient of diffusion with higher relative humidity has also been reported in the literature [143, 150]. At the beginning of the diffusion process, with all other conditions being the same, higher relative humidity produces larger moisture flux and therefore, in a non-Fickian diffusion is expected to lead to a larger coefficient of diffusion. Our experimental results, however, showed an opposite effect.

In general, it was found that aging temperature has the largest effect on the coefficient of diffusion: the higher the aging temperature, the higher the coefficient of diffusion. In comparison, the saturated moisture content appears to be mostly affected by relative humidity: the higher the relative humidity, the higher the saturated moisture content.

So far, the arguments presented have been based on concepts of the free volume theory. However, there are cases that this theory cannot be applied to explain the experimental results [151-153]. Pekarski *et al.* [153] in their study of diffusion of carbon dioxide and argon in aged and conditioned samples of BPA-PC reported that the diffusion in a conditioned matrix, which has more free volume, is slower than diffusion in a denser aged sample, and this is in direct contrast to the free volume theory. They defined three regimes of diffusion in materials based on a comparison between the penetrant size and the size of sorption sites or the holes in the polymer matrix, which are occupied by the penetrant molecules. When the penetrating gas molecules are smaller than the hole size, which is related to the first regime, the diffusion is not affected by aging or conditioning. There are reports in the literature that support this, such as the work of Akele *et al.* [154], in which aging did not have any effect on the diffusion of water into BPA-PC. The work of Pekarski *et al.* [153] belongs to the second regime, in which the penetrant and the hole sizes are comparable. In this regime, aging and conditioning has opposite effects to those expected from free volume theory. The third regime

includes the cases where the penetrant size is bigger than the hole size. In agreement with the free volume theory, the diffusion rate in this regime decreases with decreasing of free volume.

Based on the above definitions, it appears that the first regime would best characterize the moisture uptake for this blend since the second and third regimes are not applicable. Accordingly, the simultaneous heat-aging during hygrothermal exposure would have minimal influence on the diffusion process. Yet, it is seen for the hygrothermal conditions in Figure 4-12 that relaxation processes during heat-aging profoundly affected the shape of the uptake curves leading to distinct anomalous overshoots. Therefore, this strongly suggests that with prolonged exposure at elevated temperatures below T_g, the physical aging mechanism is a stronger driving force than the moisture diffusion process. After a threshold aging time, the free volume contraction during structural relaxation reaches a point where the diffusion mechanism can no longer move water molecules into the system. In the case of the polymer structure with distinct overshoot; *i.e.*, 65 °C/50% RH, the volumetric contraction process squeezes out the excess moisture to attain equilibrium. In other words, the effects of structural recovery have apparently dominated diffusion.

4.1.4.4.2 T_g Determination

As seen in Table 4-10, $T_{g,PC}$ has slightly changed with moisture content. However, $T_{g,ABS}$ has changed as the moisture uptake of the samples has increased. The effect of physical aging on the dual T_g's of the PC/ABS sample has previously been investigated [70]. It was found that the two T_g's of the blend were hardly influenced by aging up to the aging time of 1008 hours. Therefore, the changes seen in the T_g's after hygrothermal aging in this study can be related to the plasticization of the sample due to moisture absorption. The only discrepancy is seen in $T_{g,ABS}$ when temperature was changed from 50 °C to 65 °C at the relative humidity level of 50%. Although the moisture content has decreased, the T_g has decreased. This can be attributed to the oxidation of ABS, which is pronounced in the absorbance intensity of butadiene region [95].

4.2 Mechanical Properties

The results of the stress relaxation tests performed on PC/ABS bars are presented and discussed in this section.

4.2.1 Linear Viscoelastic Range

The changes in storage modulus as a function of time at increasing levels of strain, from 0.1 to 0.6 %, are plotted in Figure 4-14. There is no significant vertical shift in the curves of storage modulus, which indicates that within the force limit of the DMA instrument (maximum force limit of 18 *N*), the applied strain range is within the material's linear viscoelastic range.

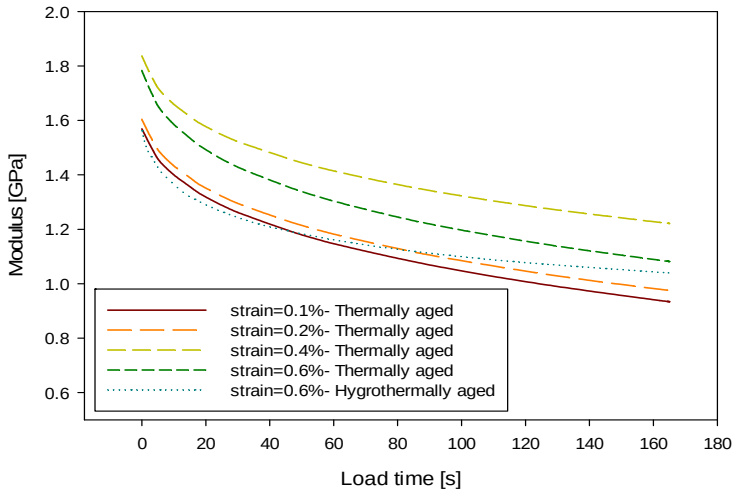

Figure 4-14 Linear viscoelastic range determination based on storage modulus curve at increasing strain level.

The storage modulus for samples that were aged in the 80 °C/fully immersed condition is also plotted in Figure 4-14. The stress relaxation test on these samples was conducted at a strain level of 0.6%. Since the corresponding curves are also within the range of the obtained curves from thermally aged samples, it can be concluded that the strain levels below 0.6% are within the linear viscoelastic range of the material. Therefore, all stress relaxation experiments were conducted at 0.5% strain.

4.2.2 Short Term Aging Tests

4.2.2.1 Thermal Aging Test

Stress relaxation tests were performed on thermally aged samples at three different aging temperatures of 50 °C, 65 °C and 80 °C; and momentary curves were obtained for the seven aging times, t_{a1} to t_{a7}. Figure 4-15 shows variation of modulus versus loading time at the seven aging times

for the three aging temperatures. The curves are the average of the modulus values over three replicates. Maximum relative standard deviation of the modulus over the three replicates was ± 7.4%, ± 2.1%, and ± 4.1% for aging temperatures of 50 °C, 65 °C, and 80 °C, respectively.

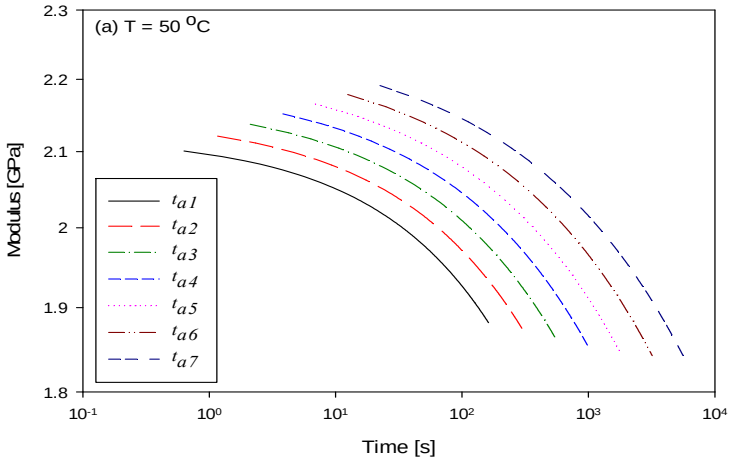

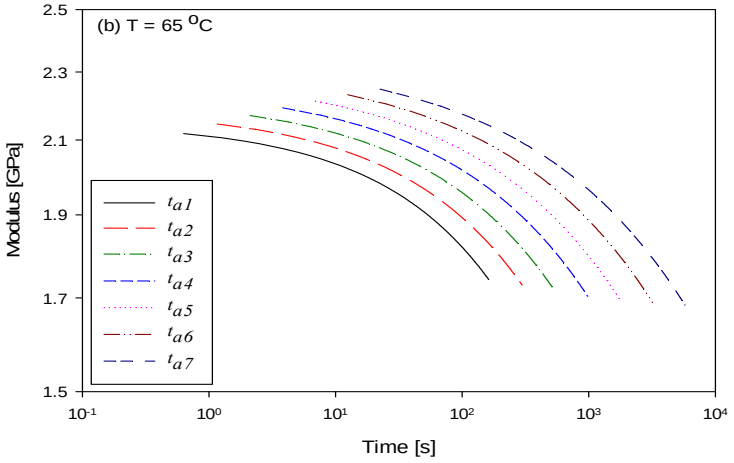

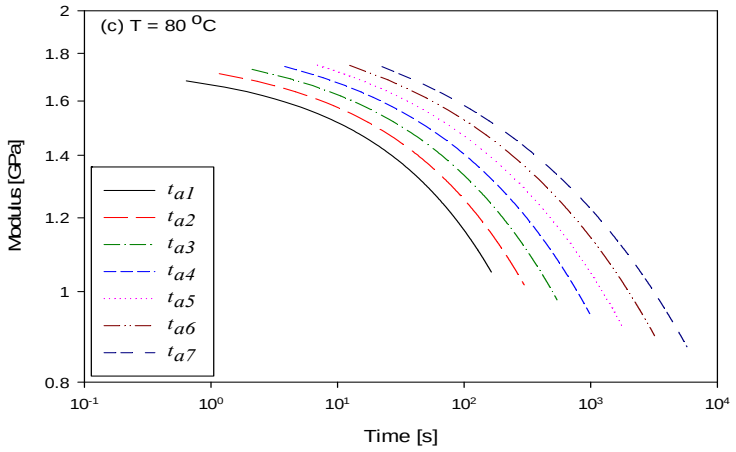

Figure 4-15 Momentary curves obtained from stress relaxation tests of thermally aged samples at (a) 50 °C, (b) 65 °C, and (c) 80 °C.

The time/aging-time superposition principle was employed to produce momentary master curves. The reference curve was the curve at t_{a7}; which means that the curves have been shifted horizontally to the right. Figure 4-16 shows the shifted curves for aging temperatures of 50 °C, 65 °C, and 80 °C.

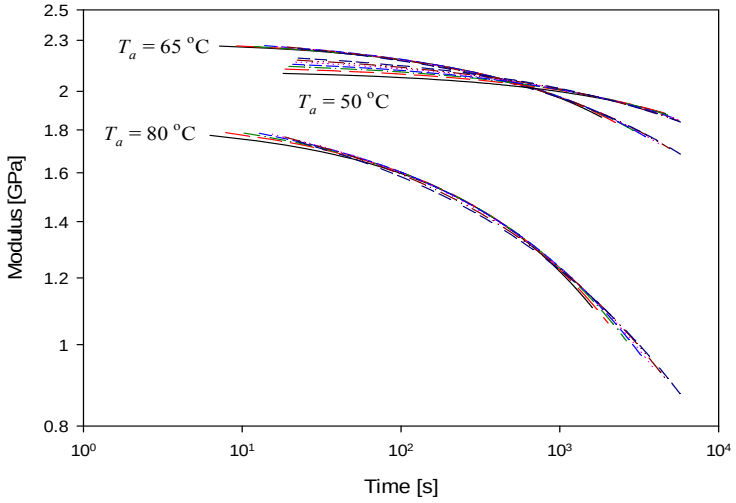

Figure 4-16 Momentary master curves obtained from stress relaxation tests of thermally aged samples at the three aging temperatures.

The obtained horizontal shift factors, a_{ta}, have also been plotted with respect to the aging time in Figure 4-17 for the three aging temperatures. Using the expression in Equation (4-19) [96], the values of the aging shift rate (μ_{ta}) were calculated and plotted in Figure 4-17:

$$\mu_{ta} = -\frac{\mathrm{d}\, log(a_{ta})}{\mathrm{d}\, log(t_a)} \tag{4-19}$$

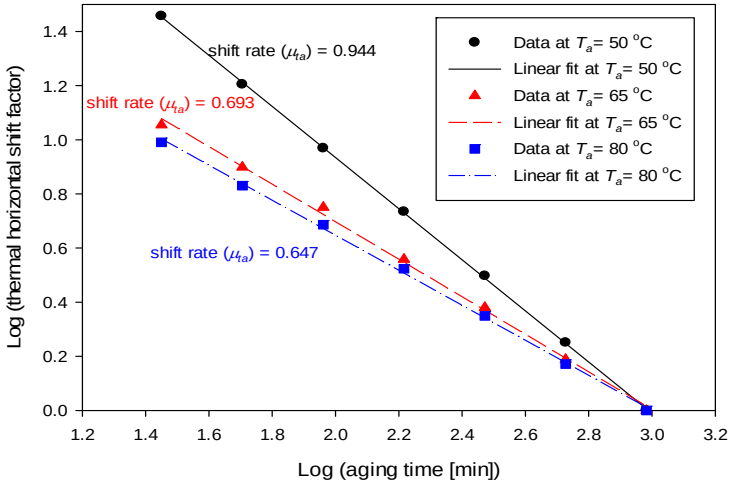

Figure 4-17 Horizontal shift factors and shift rates for thermal aging tests at the three aging temperatures.

It should also be noted that in order to superimpose all the curves into one single master curve, vertical shifting was also applied. The vertical shift factors, a_v, are small compared to the horizontal shift factors. The maximum values for $Log(a_v)$ were 0.0009, 0.0290, and 0.0228, for aging temperatures of 50 °C, 65 °C, and 80 °C, respectively. These maximum values correspond to the lowest aging time.

The experimental data were also curve fitted with the Kohlrausch-Williams-Watts (KWW) model [127, 155] as follows:

$$E(t) = E_o \mathrm{e}^{-(\mathrm{t}/\tau)^{\beta}} \tag{4-20}$$

where E_o, τ, and β are the initial modulus, relaxation time constant, and shape parameter, respectively. The three parameters for momentary master curve for the tests conducted at the reference aging time, t_{a7}, are shown in Table 4-12. The parameters listed in Table 4-12 are the average of the three replicates and the relative standard deviations are also included in parenthesis.

Table 4-12 Momentary master curve parameters for stress relaxation tests on thermally aged samples (reference t_{a7} = 960.2 min).

Aging Temp. *[°C]*	E_o *[GPa]*	τ $\times 10^3$*[s]*	β *[unitless]*
50	2.26 (±6.7%*)	659.6 (±2.7%)	0.331 (±0.2%)
65	2.36 (±2.1%)	130.4 (±1.7%)	0.348 (±0.1%)
80	2.09 (±2.5%)	9.2 (±3.4%)	0.282 (±1.2%)

* Relative Standard Deviation

The momentary curves can be related to the master curve at the reference aging time (t_{aref}) using the following relation [80]:

$$E(t)|_{t_a,T} = E_{ref}(a_{ta}t)|_{t_{aref},T} \tag{4-21}$$

The trend in Table 4-12 where the master curve parameters decrease with increasing aging temperature from 65 °C to 80 °C was expected. Higher temperatures cause a reduction in the material's initial modulus, E_o. However, this is less clear when the samples are aged at 50 °C, as seen in the master curves in Figure 4-16, where the 50 °C curve crosses over the 65 °C curve. This may be attributed to the high scatter in the data at lower temperatures [100], which will be described later. It is generally known that the relaxation time constant, τ, is sensitive to aging temperature; the higher the temperature, the shorter the relaxation time constant. This trend was also seen in the relaxation

time constant reported in Table 4-12 for the three different aging temperatures. Similar results have also been observed in heat aging studies of polycarbonate by O'Connell and McKenna [99] as well as Lee-Sullivan *et al.* [156].

Verification of modulus predictions from Equations (4-20) and (4-21) were done at the next sequential aging time (t_{a8}) following 16 hours (t_{a7}). Samples were thermally aged at 50 °C, 65 °C, and 80 °C, respectively, for t_{a8} = 1728.4 min ($t_{a8} = 1.8 \times t_{a7}$). Stress relaxation experiments were then performed on the aged specimens for 172.84 min, which is one tenth of the aging time. The modulus changes were recorded during stress relaxation test and are plotted in Figure 4-18 for the three aging temperatures. The predicted modulus for the aging time of t_{a8}, calculated using Equation (4-21), has also been plotted in Figure 4-18 for comparison. The shift factor, a_{ta}, was obtained using the linear relation of shift factor and aging time (depicted in Figure 4-17).

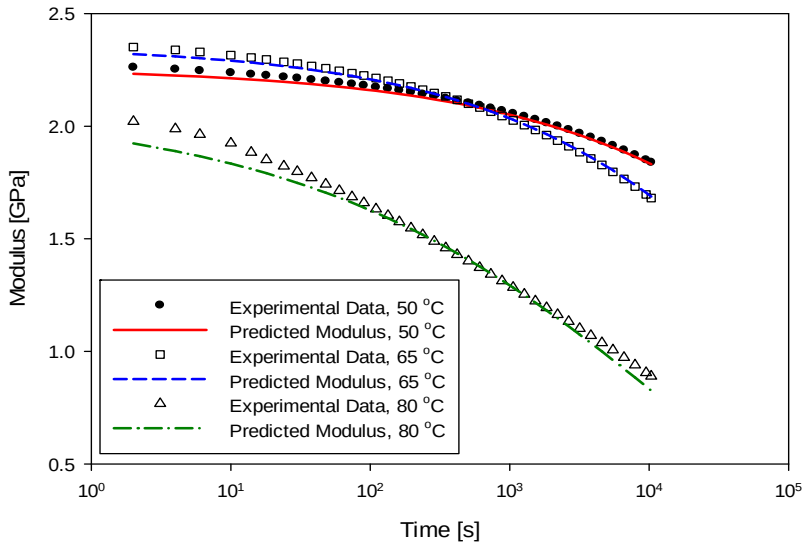

Figure 4-18 Comparison of the experimental and predicted values of modulus of the dry aged specimens for the aging time of t_{a8}.

It is evident from Figure 4-18 that the predictions agree quite well with experimental results with maximum error values of 1.3%, 2.0%, and 7.2% for the aging temperatures of 50 °C, 65 °C, and 80 °C, respectively.

4.2.2.2 Hygrothermal Aging Test

Stress relaxation tests were applied on specimens that were conditioned at the 9 hygrothermal conditions. Three replicates were employed for each condition. The average values of moisture uptake of the three samples after conditioning for 16 hours were calculated in percentage using the following formula and are presented in Table 4-13.

$$Moisture\ uptake = \frac{m_w - m_o}{m_o} \times 100\% \tag{4-22}$$

where m_o and m_w are mass of the *dry* and *wet* sample; *i.e.*, *before* and *after* hygrothermal conditioning.

Table 4-13 Moisture uptake in percentage for samples conditioned at the 9 hygrothermal conditions for 16 hours.

		Temperature [°C]		
		50	***65***	***80***
RH	***50%***	0.12	0.16	0.18
	93%*	0.25	0.36	0.30
	Fully Immersed	0.28	0.38	0.51

* 75% RH at 80 °C

Momentary curves were obtained for all tested samples. Figure 4-19 shows the variation of modulus in terms of loading time for the typical temperature of 65 °C. In this figure, the modulus curve obtained from the sample that was thermally aged at 65 °C at the reference aging time, t_{a7}, with moisture uptake of about zero (m ~ 0.0%) is also plotted.

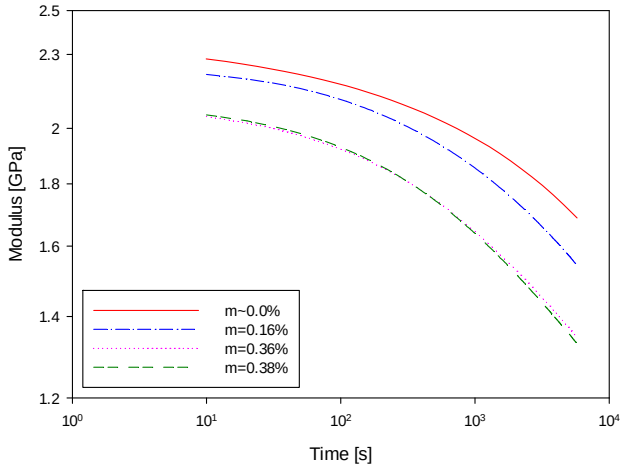

Figure 4-19 Typical momentary curves obtained from stress relaxation tests of hygrothermally aged samples at 65 °C.

The concept of time/moisture superposition was applied and the curves were all shifted to the reference curve to result in a master curve. The reference curve was selected to be the curve of the thermally aged sample (m ~ 0.0%). The master curves corresponding to the temperatures of 65 °C and 80 °C are shown in Figure 4-20. As the standard deviation of the momentary curves for the aging temperature of 50 °C was large, a master curve could not be generated.

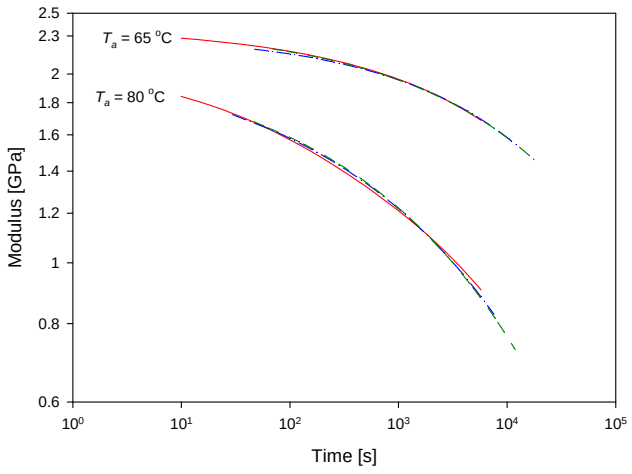

Figure 4-20 Momentary master curves obtained from stress relaxation tests of hygrothermally aged samples at the temperatures of 65 °C and 80 °C.

The so-called hygrothermal horizontal shift factors, a_H, were calculated and also plotted as a function of moisture uptake for the two temperatures of 65 °C and 80 °C in Figure 4-21. The values of the corresponding hygrothermal shift rate, μ_H, are also presented in Figure 4-21.

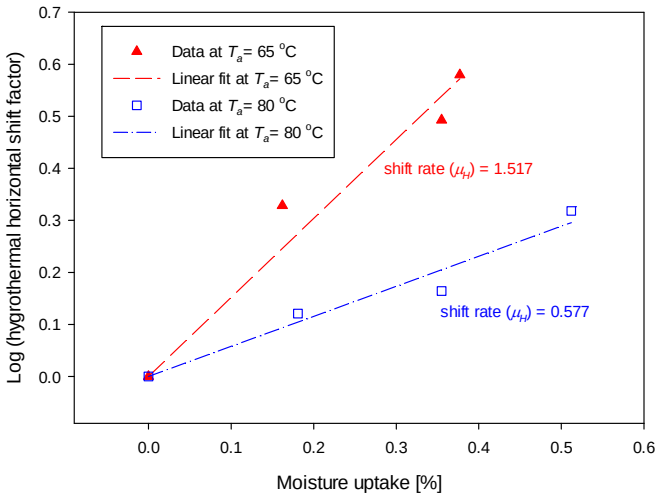

Figure 4-21 Horizontal shift factors and shift rates for hygrothermally aged samples at the two aging temperatures.

Similar to the thermal aging tests, the experimental data were curve fitted with the Kohlrausch-Williams-Watts (KWW) model [127, 155]. The corresponding parameters for the momentary curves at the two aging temperatures of 65 °C and 80 °C are presented in Table 4-14.

Table 4-14 Momentary curve parameters for stress relaxation tests on hygrothermally aged samples (reference moisture uptake ~ 0.0%).

Condition	E_o [GPa]	τ $\times 10^3$[s]	β [unitless]
65°C/50% RH	2.32 (±2.4%*)	73.5 (±1.5%)	0.347 (±2.4%)
65°C/93% RH	2.19 (±6.1%)	54.6 (±1.6%)	0.312 (±1.7%)
65°C/fully immersed	2.20 (±2.9%)	47.5 (±7.6%)	0.315 (±2.9%)
80°C/50% RH	1.88 (±2.9%)	6.2 (±15.5%)	0.248 (±1.9%)
80°C/75% RH	1.83 (±3.1%)	5.7 (±2.6%)	0.247 (±2.4%)
80°C/fully immersed	1.67 (±5.9%)	4.0 (±7.8%)	0.259 (±7.4%)

* Relative Standard Deviation

Similarly, the relation between momentary curves and master curves is established using the following relation:

$$E(t)|_{m,T} = E_{ref}(a_H t)|_{m_{ref},T} \tag{4-23}$$

Overall, both thermally and hygrothermally aged samples exhibited the same trends, Table 4-12 and Table 4-14; the three model parameters decrease with increasing temperature. However, a key difference is the relative drop in values. At both temperatures of 65 °C and 80 °C, the drop is much larger for the relaxation time, τ, than it is for initial modulus, E_o, and shape parameter, β.

Moisture content appears to have the same effect as temperature on momentary curve parameters; *i.e.*, increasing moisture content decreases the magnitude of the parameters. This is consistent with reports in the literature. Ishisaka and Kawagoe [10] in their study on the behaviour of moisture

absorption on polyamide 6 and epoxy samples reported equivalence between the effects of increasing water content and temperature on storage modulus. Comparison of the values in Table 4-14 shows that by considering the variation in the values of initial modulus, this parameter is relatively insensitive to relative humidity changes. However, there is a reduction of about 35% in the values of relaxation time constant when the relative humidity is doubled – this parameter is sensitive to the changes in the moisture content of the specimens. This can be attributed to increased plasticization with higher moisture content as observed by LaPlante and Lee-Sullivan [103] for FM300 structural film adhesive. They reported that when the moisture content of the adhesives did not exceed a threshold value, hygrothermal conditioning accelerated the relaxation mechanism.

4.2.3 Long Term Aging Tests

Similar to the short term aging tests, stress relaxation experiments were conducted on aged specimens. In long term aging tests, samples were aged at only one prolonged aging time; *i.e.*, 168 hours, and the stress relaxation period was set to be one tenth of the aging time; *i.e.*, 16.8 hours. Since the loading time is rather high, the ongoing aging process during loading cannot be neglected. Therefore, to consider the effect of physical aging during loading, an effective time, λ_t, can be used instead of the time, t, in Equation (4-20), following [96, 157]:

$$E(t) = E_o e^{-(\lambda_t/\tau(t_a^o))^\beta} \tag{4-24}$$

where λ_t is calculated based on:

$$\lambda_t = t_a^o ln\left(\frac{t}{t_a^o} + 1\right) \quad , \quad \mu_{ta} = 1 \tag{4-25}$$

$$\lambda_t = \frac{t_a^o}{1-\mu_{ta}}\left[\left(1 + \frac{t}{t_a^o}\right)^{1-\mu_{ta}} - 1\right] \quad , \quad \mu_{ta} \neq 1 \tag{4-26}$$

where t_a^o is the aging time before stress relaxation period (equal to 168 hours here), and t is the stress relaxation test time. The long term thermal aging test results are compared with the predictions obtained from Equations (4-24) to (4-26) in Figure 4-22.

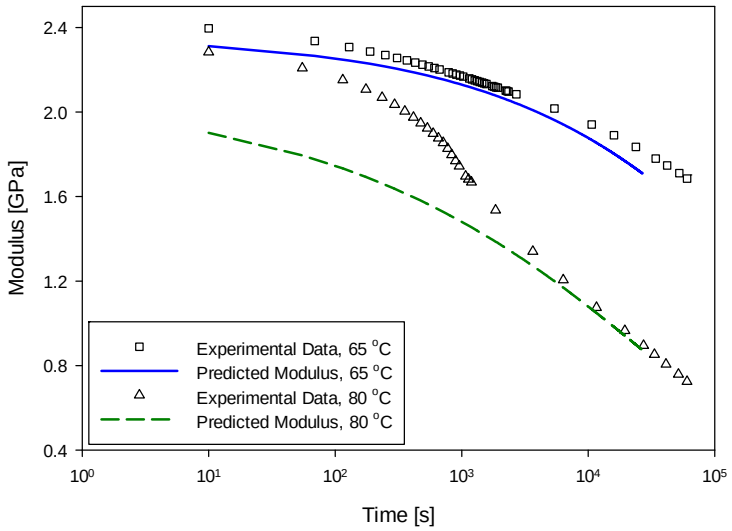

Figure 4-22 Comparison of experimental and predicted values of modulus for long term dry aged tests.

As seen in Figure 4-22, except for the first 16 minutes of stress relaxation of the samples at 80 °C, there is a reasonable agreement between the experimental and predicted values of modulus for both of the aging temperatures of 65 °C and 80 °C. Maximum error values of the predictions compared to the experimental values are 3.6% and 19.8% for the aging temperatures of 65 °C and 80 °C, respectively.

A common practice in long term predictions is to use only horizontal shift factors. It is also known that vertical shift factors, a_v, do not improve the results significantly. Tables 4-15 and 4-16 show the error values in prediction of modulus after t_{a8} aging time as well as long time modulus values with and without considering vertical shifting.

Table 4-15 Error values [%] in prediction of modulus after t_{a8} = 1728.4 min aging.

		without a_v	with a_v
Aging temperature [°C]	***50***	1.3	1.3
	65	2.0	1.9
	80	7.2	7.0

Table 4-16 Error values [%] in prediction of modulus following 168 hour aging.

		without a_v	with a_v
Aging temperature	***65***	3.6	3.6
[°C]	***80***	19.8	19.7

As seen in Tables 4-15 and 4-16, the calculated error values while vertical shift factors are considered (with a_v) are not significantly different from those obtained without applying vertical shift factors (without a_v).

Long term experiments were also conducted to study the effect of hygrothermal aging for 168 hours on stress relaxation behaviour of PC/ABS samples. Modulus curves were obtained from stress relaxation experiments on samples that were aged in the same nine hygrothermal conditions used in short term tests. Moreover, the long term modulus values were predicted by applying shift factors on the short term modulus values. The short term modulus values were first shifted using thermal shift factors (a_{ta}) to consider the effect of 168 hour aging and then the hygrothermal shift factors (a_H) were applied to account for the mass uptake increase during 168 hours of hygrothermal aging. Comparisons of the experimental and predicted modulus of the samples that were hygrothermally aged for 168 hours are presented in Figures 4-23 and 4-24 for the aging temperatures of 65 °C and 80 °C, respectively. The short term modulus values are also depicted in these figures.

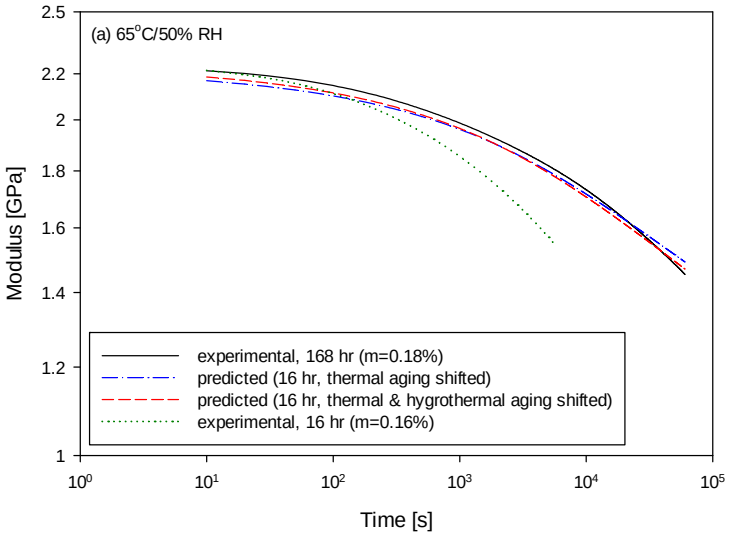
(a) 65°C/50% RH
Modulus [GPa]
Time [s]
experimental, 168 hr (m=0.18%)
predicted (16 hr, thermal aging shifted)
predicted (16 hr, thermal & hygrothermal aging shifted)
experimental, 16 hr (m=0.16%)

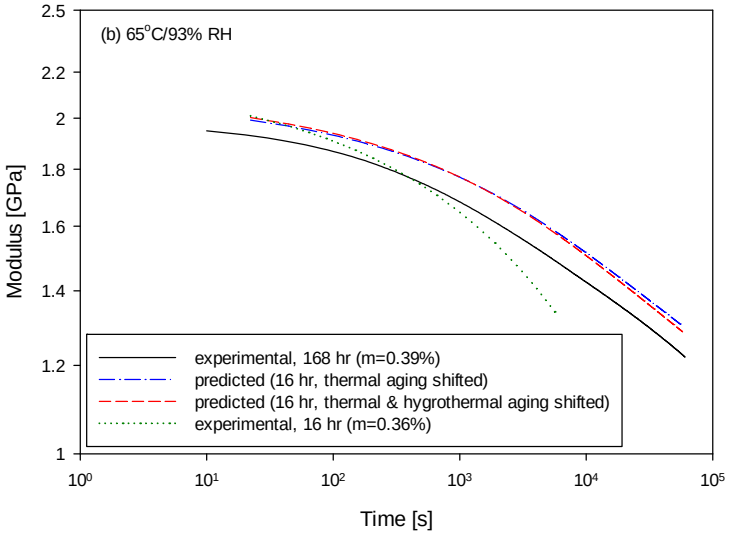
(b) 65°C/93% RH
Modulus [GPa]
Time [s]
experimental, 168 hr (m=0.39%)
predicted (16 hr, thermal aging shifted)
predicted (16 hr, thermal & hygrothermal aging shifted)
experimental, 16 hr (m=0.36%)

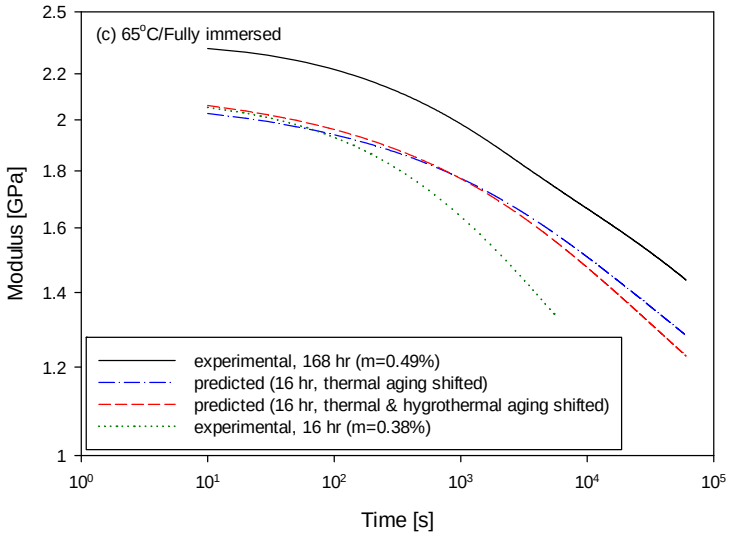

Figure 4-23 Comparison of modulus for samples hygrothermally aged at (a) 65 °C/50% RH, (b) 65 °C/93%RH, and (c) 65 °C/Fully immersed, for 168 hours.

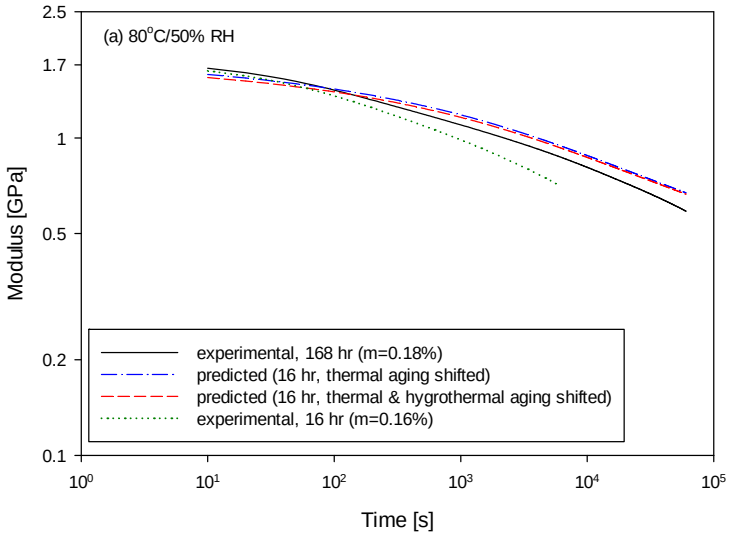

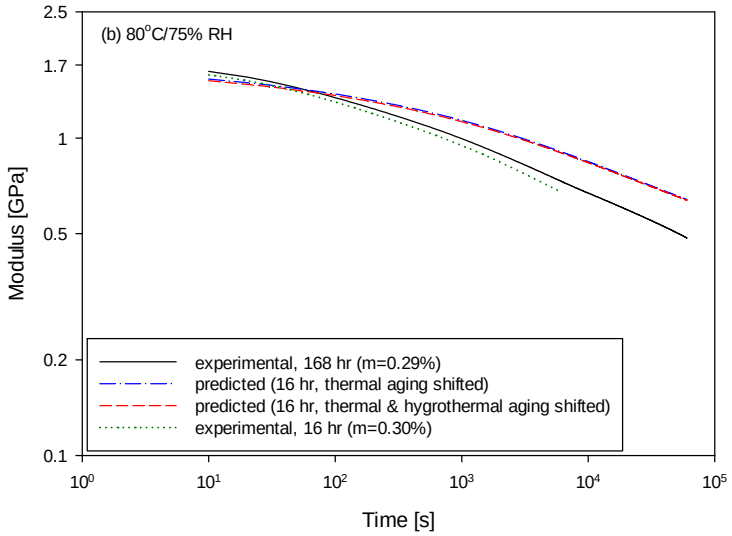

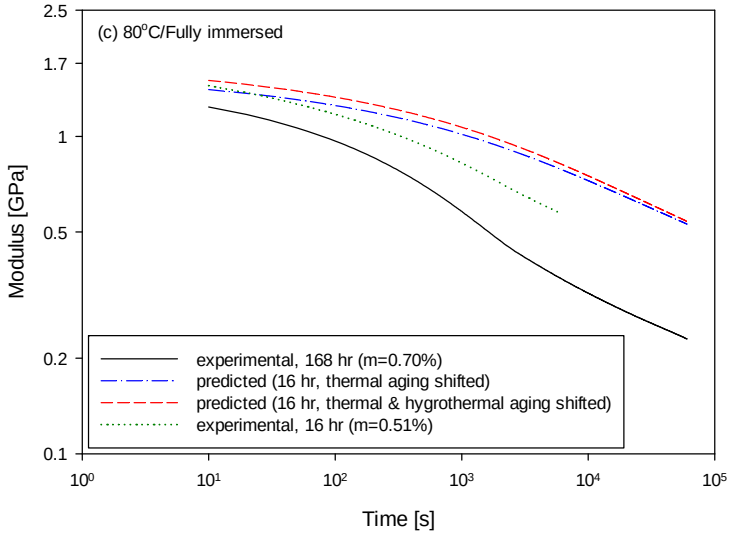

Figure 4-24 Comparison of modulus for samples hygrothermally aged at (a) 80 °C/50% RH, (b) 80 °C/75%RH, and (c) 80 °C/Fully immersed, for 168 hours.

It is seen that there is a reasonable agreement between the experimental and predicted values of modulus for both aging temperatures except for the full immersion condition. This suggests that short term aging test results cannot be simply extrapolated to predict long term behaviour for the full immersion condition. At the condition of 80 °C/fully immersed, the long term modulus is predicted

above short term modulus due to the effect of physical aging but the experimental value falls below the short term modulus. Although the material becomes stiffer as the aging process progresses, this stiffening effect is less pronounced at temperatures near T_g. The stiffening effect can also be further lessened as the moisture content increases, which is the case of 80 °C/fully immersed condition. This can be further investigated by testing samples that are saturated in fully immersed conditions.

It is also seen in Figures 4-23 and 4-24 that there is no significant difference between the thermal aging shifted curve and the one which has been obtained by applying both thermal and hygrothermal aging shift factors. This can be an indication of the prevalence of the effect of aging compared to moisture absorption in shifting the modulus of PC/ABS samples when the aging time is extended form 16 hours to 168 hours.

The experimental data of both thermal and hygrothermal long term aging tests were also curve fitted with the Kohlrausch-Williams-Watts (KWW) model. Tables 4-17 and 4-18 list initial modulus, relaxation time constant, and shape parameter obtained from curve fitting of thermal and hygrothermal long term aging tests, respectively. These parameters are the average of three replicates and the corresponding relative standard deviations are also shown in parenthesis.

Table 4-17 The KWW model parameters for stress relaxation tests on thermally long term aged samples.

Aging Temp. *[°C]*	E_o *[GPa]*	τ $\times 10^3$*[s]*	β *[unitless]*
50	2.30 (±8.5%*)	12348.1 (±1.6%)	0.282 (±0.7%)
65	2.46 (±1.8%)	2302.0 (±0.4%)	0.268 (±0.2%)
80	2.73 (±3.7%)	17.1 (±2.8%)	0.282 (±12.3%)

* Relative Standard Deviation

Table 4-18 The KWW model parameters for stress relaxation tests on hygrothermally long term aged samples.

Condition	E_o [GPa]	τ $\times 10^3$[s]	β [unitless]
65°C/50% RH	2.37 (±6.1%*)	1073.1 (±8.7%)	0.247 (±3.0%)
65°C/93% RH	2.31 (±7.2%)	924.1 (±10.8%)	0.162 (±2.6%)
65°C/fully immersed	2.84 (±9.6%)	79.6 (±20.9%)	0.146 (±1.6%)
80°C/50% RH	2.08 (±3.7%)	14.5 (±31.3%)	0.167 (±2.3%)
80°C/75% RH	2.23 (±2.2%)	3.4 (±18.8%)	0.151 (±0.7%)
80°C/fully immersed	1.88 (±8.8%)	0.2 (±11.3%)	0.139 (±0.9%)

* Relative Standard Deviation

Finally, in order to compare the effects of physical aging and moisture absorption on the stress relaxation behaviour of PC/ABS samples, the curves for thermal aging tests, hygrothermal aging tests, and un-aged tests for the three aging temperatures are compared for both short term and long term tests in Figures 4-25 and 4-26. In these figures, some of the data points and the corresponding error bars are also plotted to provide the values of standard deviation over the three replicates from which the average curves have been obtained.

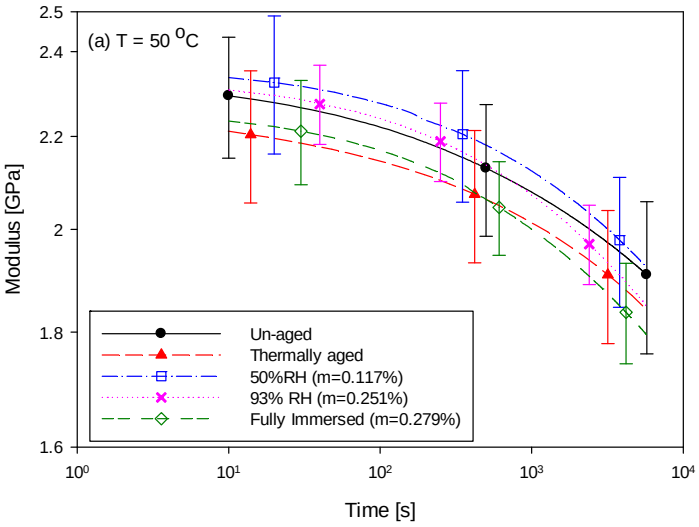
(a) T = 50 °C
Modulus [GPa]
Time [s]
Un-aged
Thermally aged
50%RH (m=0.117%)
93% RH (m=0.251%)
Fully Immersed (m=0.279%)

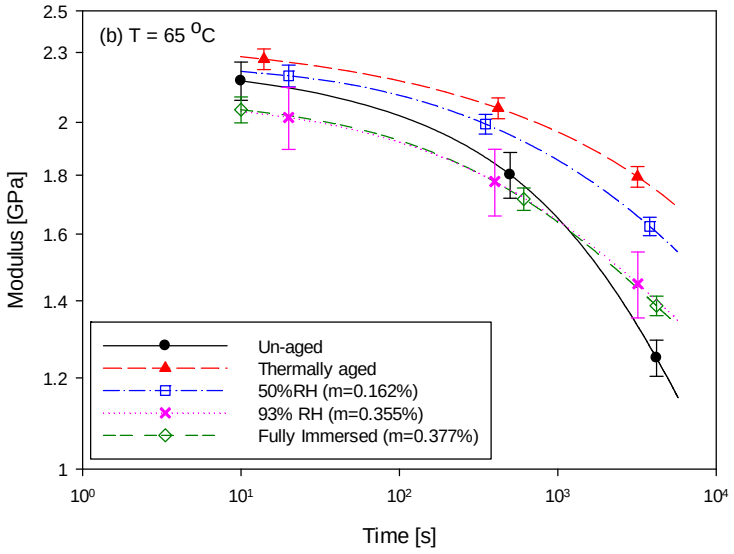
(b) T = 65 °C
Modulus [GPa]
Time [s]
Un-aged
Thermally aged
50%RH (m=0.162%)
93% RH (m=0.355%)
Fully Immersed (m=0.377%)

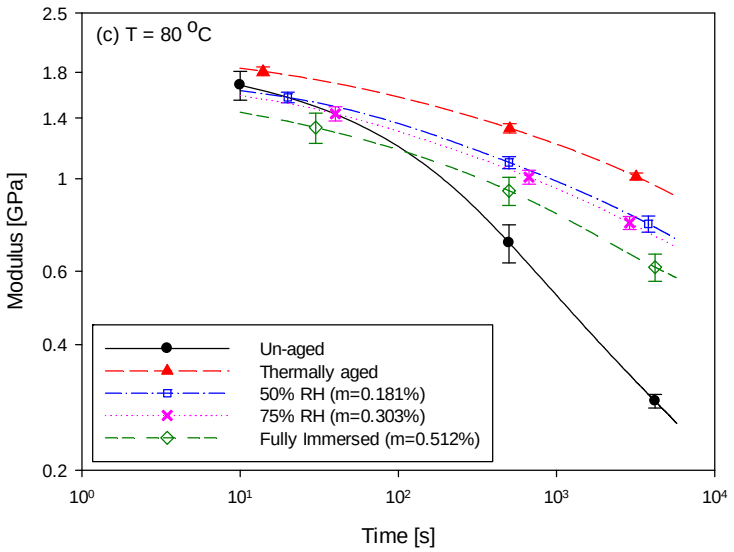

Figure 4-25 Comparison of the effects of thermal and hygrothermal aging for 16 hours on the modulus at temperatures of (a) 50 °C, (b) 65 °C, and (c) 80 °C.

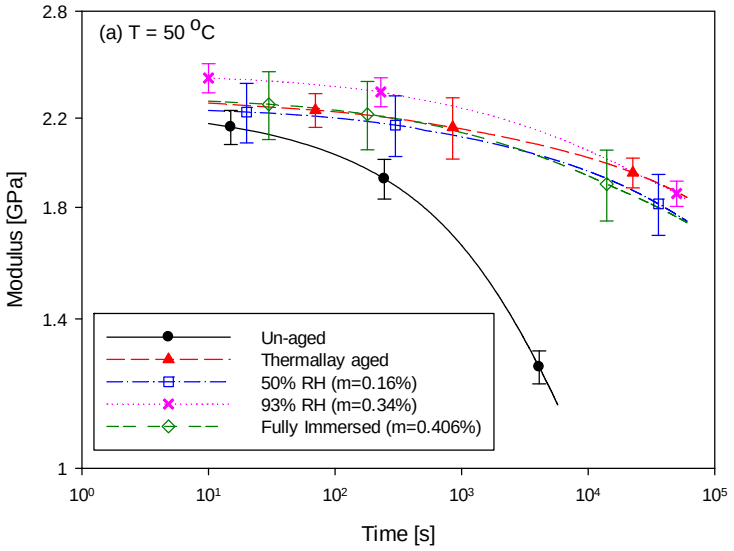

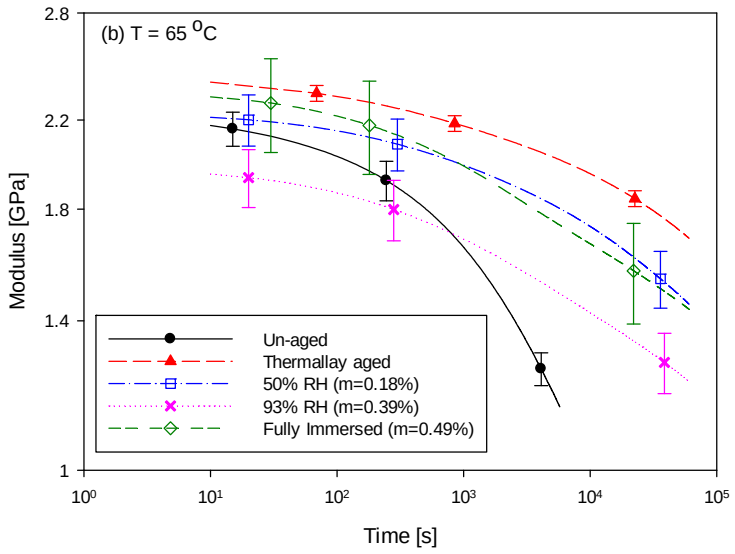

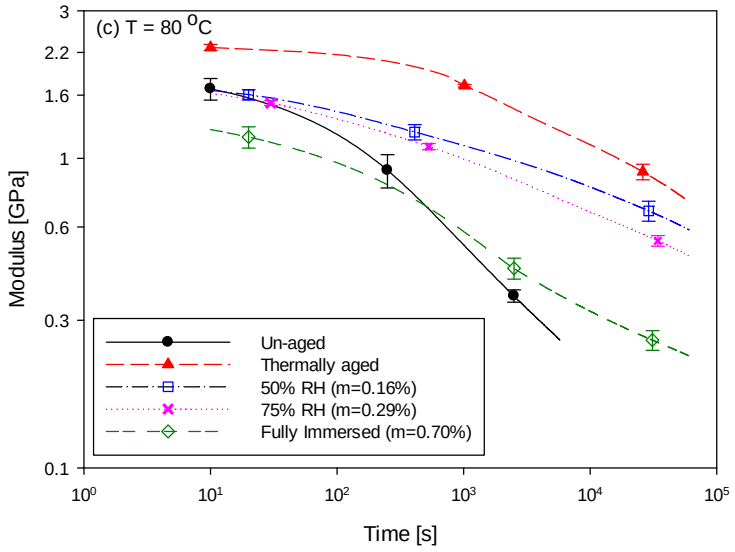

Figure 4-26 Comparison of the effects of thermal and hygrothermal aging for 168 hours on the modulus at temperatures of (a) 50 °C, (b) 65 °C, and (c) 80 °C.

As discussed earlier, the variation in the obtained values of modulus over the three replicates at aging temperature of 50 °C is so large that we do not have confidence in the significance of the detected changes when thermal and hygrothermal aging results are compared to un-aged results,

Figures 4-25 (a) and 4-26 (a). However, the variation in the modulus values at the two other aging temperatures; *i.e.*, 65 °C and 80 °C, is much lower. As expected and seen in Figures 4-25 and 4-26 (b) and (c), thermal aging causes an increase in the modulus of the material. This change is not statistically significant at the initial period of loading but it becomes more and more significant with prolonged loading times (as the material relaxes). This can be explained by the fact that thermal aging stiffens the material due to structural densification and reduced molecular relaxation, which is characteristic of physical aging. Moisture absorption, however, has an opposite effect. As the moisture content increases in the specimen, the material loses its stiffness and the modulus decreases as the material relaxes. Although moisture absorption decreases the material's modulus, its effect is not as strong as the effect of physical aging on modulus, especially at the end of loading time. If the values of relaxation time constant for un-aged samples at temperatures of 65 °C and 80 °C, which are 13.5×10^3 and 0.3×10^3 *s*, respectively, are compared with the values for thermally and hygrothermally aged specimens obtained from short term aging tests (Tables 4-12 and 4-14), the following trend is seen:

$$\tau_{\text{thermally aged}} > \tau_{\text{hygrothermally aged}} > \tau_{\text{un-aged}}$$

The increase in relaxation time constant due to thermal aging is considerably larger than at hygrothermal conditions, for the same temperature levels. A similar trend can also be seen in the relaxation time constants obtained for long term aging tests (Tables 4-17 and 4-18). Therefore, in hygrothermal aging of this blend for 16 and 168 hours, the relaxation properties are more affected by physical aging processes than absorbed moisture effects. This implies that physical aging is the dominant mechanism affecting relaxation behaviour of this blend even in the presence of relatively high levels of absorbed moisture.

4.3 Coupling Coefficients — First Set

The first set of coupling coefficients including the elastic coefficients of thermal and hygroscopic expansion has been determined using thermal analysis techniques and the obtained results are presented in the following sections.

4.3.1 Coefficient of Thermal Expansion

The coefficient of thermal expansion (CTE) was determined from the experimental results obtained from the T_g determination tests performed using the TMA. Table 4-19 shows the average values obtained for the CTE *before* and *after* T_g, which are denoted by α_g (CTE in *glassy* region) and α_r (CTE in *rubbery* region), respectively. These values were obtained for both of the blend components.

Table 4-19 Average values of CTE before and after T_g obtained from dilatometer and expansion modes.

Mode	ABS			PC		
	α_g *[1/°C]*	α_r *[1/°C]*	α_r / α_g	α_g *[1/°C]*	α_r *[1/°C]*	α_r / α_g
Expansion Probe	0.14	1.31	9.36	0.81	3.26	4.02
Dilatometer	1.00	23.43	23.43	1.36	20.07	14.76

As seen in Table 4-19, the ratio of α_r to α_g for ABS is almost twice that for PC (2.3 for expansion probe results and 1.6 for dilatometer ones). Apparently, the change of CTE at the glass transition is greater for ABS than PC.

4.3.2 Coefficient of Hygroscopic Expansion

The coefficient of hygroscopic expansion, α_d^e, is calculated using the method introduced by Zhou *et al.* [117]:

$$\alpha_d^e = \frac{(h_{sat} - h_o)/h_o}{(M_{sat} - M_o)/(h_{xo}h_{yo}h_{zo})} \qquad (4\text{-}27)$$

The coefficient of hygroscopic expansion can also be calculated from the slope of strain changes curve versus concentration. Figure 4-27 illustrates the change of strain versus concentration for the typical condition of 65 °C/fully immersed.

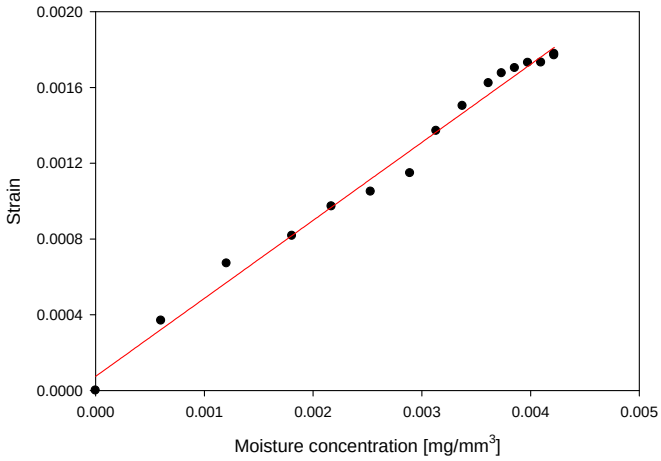

Figure 4-27 Calculation of the coefficient of hygroscopic expansion using the slope of the curve.

The coefficient of hygroscopic expansion was calculated using Equation (4-27) as well from the slope of the curve of strain versus concentration for each condition. Tables 4-20 and 4-21 list the obtained values of the hygroscopic expansion for each condition. The time for the samples to dry out at each condition is also obtained from the TGA test and is shown in Table 4-20.

Table 4-20 The coefficient of hygroscopic expansion calculated using Equation (4-27)

Condition	α_{il}^{e} [mm^3/mg]	Ave. (± RSD%) [mm^3/mg]	Time [min]
50 °C/50% RH	0.402	0.378 (±9.2%)	300
	0.353		
50 °C/93% RH	0.170	0.153 (±15.7%)	400
	0.136		
50 °C/fully immersed	0.478	0.336 (±59.8%)	590
	0.194		
65 °C/93% RH	0.319	0.339 (±8.3%)	240
	0.359		
65 °C/fully immersed	0.418	0.396 (±7.9%)	280
	0.374		
80 °C/50% RH	0.309	0.448 (±43.8%)	120
	0.586		
80 °C/75% RH	0.409	0.538 (±33.8%)	140
	0.666		
80 °C/fully immersed	0.721	0.782 (±10.9%)	200
	0.842		

Table 4-21 The coefficient of hygroscopic expansion obtained from the slope of strain vs. concentration curve.

Condition	α_d^e $[mm^3/mg]$	Ave. (±RSD%) $[mm^3/mg]$
50 °C/50% RH	0.293	0.187 (±80.2%)
	0.081	
50 °C/93% RH	0.067	0.080 (±23.0%)
	0.093	
50 °C/fully immersed	0.345	0.213 (±87.6%)
	0.081	
65 °C/93% RH	0.284	0.256 (±15.8%)
	0.227	
65 °C/fully immersed	0.326	0.323 (±1.5%)
	0.319	
80 °C/50% RH	0.176	0.315 (±62.3%)
	0.453	
80 °C/75% RH	0.411	0.484 (±21.2%)
	0.556	
80 °C/fully immersed	0.488	0.490 (±0.6%)
	0.492	

The obtained coefficients of hygroscopic expansion (tabulated in Tables 4-20 and 4-21) have significant variation at some conditions and therefore a specific trend cannot be found on the change of the coefficient of hygroscopic expansion with the hygrothermal condition. The high variation in the data can be decreased by testing more replicates. Nevertheless, the coefficient of hygroscopic expansion can be calculated as the average of all the values presented in Tables 4-20 and 4-21. The average coefficient of hygroscopic expansion is equal to 0.36 mm^3/mg.

4.4 Concluding Remarks

This chapter presented the results and the related discussion of experimental tests that were introduced in the previous chapter. The tests characterized the PC/ABS blend in terms of thermophysical and mechanical properties. The dual glass transition temperatures of constituent components of the PC/ABS blend were assigned using the dilatometry and expansion modes of the

TMA. Generally, the duality of T_g's for the blend could be reliably detected with scanning rates ranging between 0.5 and 5 °C/min. The T_g of the material was also determined using the three-point bending mode of the DMA. The obtained T_g, when compared to the T_g of hygrothermally aged samples, is useful to study the effect of moisture absorption on T_g. Physical aging experiments performed by TMA also revealed the volume relaxation behaviour of the material for up to 1008 hours of aging at 80 °C. A temperature-dependant linear relation was also obtained for the specific heat capacity of the material using MDSC tests on hygrothermally aged samples. There were two distinctly different moisture uptake curves observed for the PC/ABS blend aged at the hygrothermal conditions studied in the mass uptake tests. The approach to the equilibrium moisture content was a Fickian diffusion process when the blend was fully immersed at room temperature while clear overshoot behaviour was seen in the uptake curves when the blend was aged at elevated temperatures in relative humidity. It was proposed that anomalous overshoot curves represent the two opposing processes; first, diffusion of water molecules into the excess free volume of the polymer at the start of the aging process dominates, but is displaced by volumetric contraction triggered as aging-related structural relaxation progresses at elevated temperature. The effects of the latter process becomes increasingly more prominent with aging time and eventually squeezes excess water molecules out of the filled free volume of the polymer structure.

The competing effects of physical aging and moisture absorption on the viscoelastic behaviour of the blend were studied by curve fitting stress relaxation data of thermally and hygrothermally aged PC/ABS to the KWW model. Analysis of the two model parameters, initial modulus, E_o, and relaxation time constant, τ, were consistent with the literature in that moisture and aging temperature have similar effects on the material behaviour during aging; their increase caused decreases in the initial modulus and relaxation time constant. Overall, when the blend material was aged under hygrothermal conditions for up to 168 hours, the effects of physical aging were more prominent than relative humidity. This was evident when results were compared with both dry aged and un-aged results. Even in the presence of absorbed moisture, which plasticizes the material, the net effect was the increase in E_o and τ. The obtained experimental results for modulus can also be used for numerical modeling of viscoleastic behaviour of the blend in different hygrothermal conditions. This will be more explained in the following chapter. Eventually, the experimental results related to the elastic coefficients of thermal and hygroscopic expansion were presented. These coefficients will also be used for numerical modeling of the PC/ABS blend discussed in the next chapter.

Chapter 5
Numerical Modeling

As described in section 1.2, there are three main physical mechanisms or coupled physics involved in the study of coupled moisture diffusion and physical aging: structural mechanics, moisture diffusion, and heat conduction. From a thermodynamics point of view, the behaviour of each of these three physics can be represented by partial differential equations (PDE). These PDEs are coupled and can be solved to determine the state variables, which show the behaviour of the modeled material system. In this chapter, the coupled PDEs are numerically solved for PC/ABS blend material using finite element method. In the developed finite element model, some of the material properties are those obtained from the characteristic experiments presented in the preceding chapters and the other ones are determined using new experiments.

The framework for finite element analysis to model moisture diffusion coupled with physical aging in plastic thin plates is presented in this chapter. The numerical modeling approach consists of several parts. Figures 5-1, 5-2, and 5-3 show the various steps involved and the corresponding sections are presented in this chapter. First, in Figure 5-1, equation development is presented starting with the main equations followed by the governing equations on the coupled physics with two types of material behaviour: linear elastic and linear viscoelastic. Next, a series of numerical analyses are performed using the developed PDEs in the previous step. This is implemented using a commercial software package; *i.e.*, COMSOL Multiphysics®. This step is performed in two sections: uncoupled physics and coupled physics.

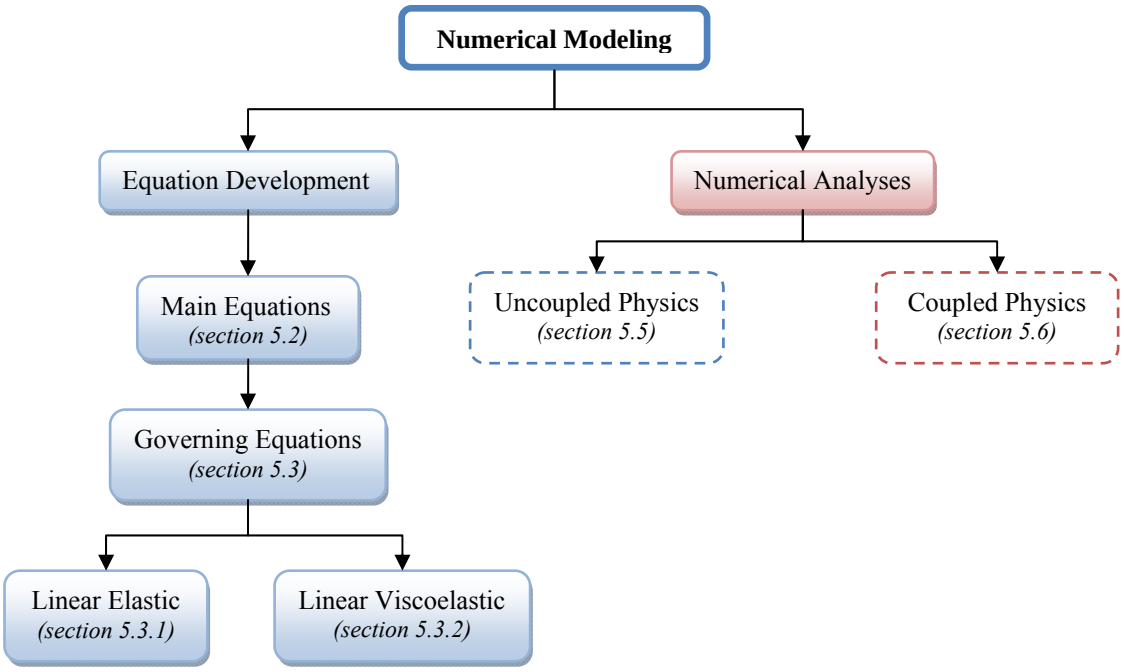

Figure 5-1 The steps of the numerical modeling work.

The uncoupled physics section (Figure 5-2) discusses the modeling of the three uncoupled physics including *structural mechanics*, *moisture diffusion*, and *heat conduction*. For the physics of *structural mechanics*, two kinds of material behaviour are considered; *i.e.*, *linear elastic* and *linear viscoelastic*, and each behaviour is analyzed under two modes of *plane strain* and *plane stress*.

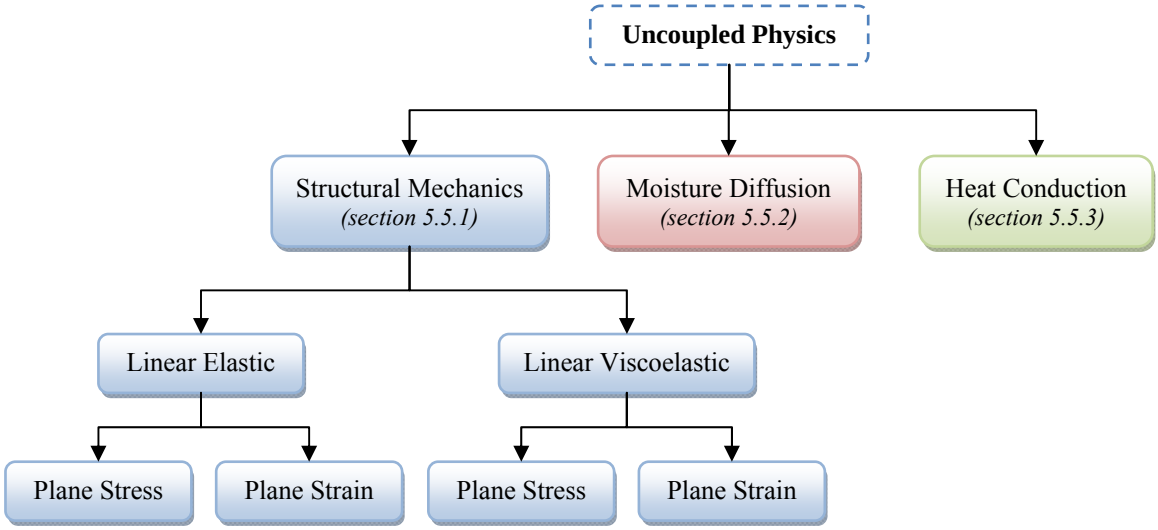

Figure 5-2 The steps of uncoupled physics modeling.

The coupled physics section, whose stages are depicted schematically in Figure 5-3, involves four main parts: linear elastic, linear viscoelastic, physical aging effects, and model verification. This part of the work is the main contribution of the thesis as there are no other reports in the literature on the finite element analysis on the quadruple coupled physical phenomena which requires the incorporation of the coupling coefficients. In the *linear elastic* part, a typical example is solved which enables us to compare the results of the current modeling with a parametric study available in literature. The coupling coefficients between the three physics of structural mechanics, moisture diffusion, and heat conduction are obtained in the part of *linear viscoelastic*. The part of *physical aging effects* deals with a discussion on the effects of physical aging on mechanical and diffusion behaviour. Eventually *model verification* is conducted to investigate the capability of the developed model to predict the material's behaviour in a representative case study.

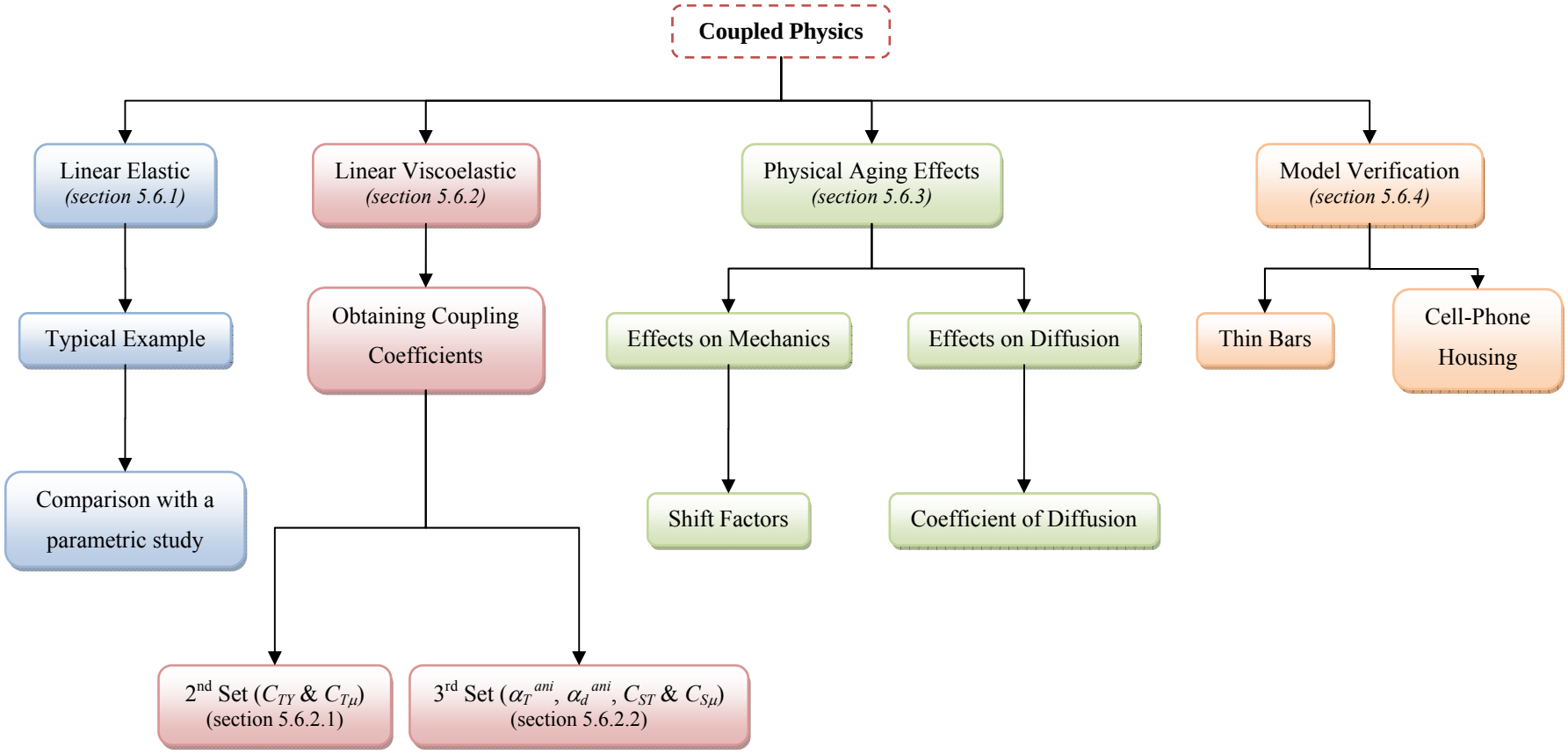

Figure 5-3 The steps involved in the coupled physics modeling.

5.1 Equation Development

The set of equations used to model the coupled physics of structural mechanics, moisture diffusion, and heat conduction have been developed by Rambert *et al.* [46-49]. These equations are derived within the framework of thermodynamics of irreversible processes and continuum mechanics. The details of the derivation can be found elsewhere (*e.g.* [48, 61, 158]). In the following sections, these equations are briefly introduced together with their derivation procedure.

5.2 Main Equations

First, the main equations from which the governing equations are derived are introduced [48]. In order to develop the equations, an elementary representative volume (ERV) needs to be defined based on the interaction of the polymer material and the diffusing substance. For a system obeying Fickian diffusion mode, the ERV is considered as a continuous medium which includes a homogenous mixture of polymer and the diffusing material. The ERV can then be represented by a set of state variables. The relationship between the thermodynamic forces to their dual variables can be established using two thermodynamic potentials; *i.e.*, specific free energy and dissipation potential. However, before using these potentials to derive the coupled constitutive equations, two main sets of equations need to be introduced.

5.2.1 Balance Equations

The balance laws include mass balance, mechanical balance, and thermodynamic balance laws, which are employed to develop the equations of state.

Mass Balance:

$$\rho \dot{Y}_d = -Div\, \vec{M}_d \tag{5-1}$$

$$Y_p + Y_d = 1 \tag{5-2}$$

$$\vec{M}_p = -\vec{M}_d \tag{5-3}$$

where ρ is the average density of ERV, Y and M denote the mass fraction and the relative flux; and the subscripts p and d refer to the polymer and the diffusing substance, respectively. The symbol "." above a variable denotes the time derivative of that variable.

Mechanical Balance:

$$Div\,\underline{\underline{\sigma}} + \rho\vec{f} = 0 \tag{5-4}$$

where σ is the Cauchy stress tensor (shown with double underbars), and f is the body force per unit of mass.

Thermodynamics Balance:

a) Energy Balance (first principle of thermodynamics)

$$\rho\dot{U} = \underline{\underline{\sigma}}:\underline{\underline{\dot{\varepsilon}}} - Div\,\vec{Q} + R \tag{5-5}$$

where U is the specific internal energy, ε is the infinitesimal strain tensor, Q denotes the heat flux, and R accounts for the external heat supply per volume. Divergence operator is also shown with *Div*.

b) Entropy Balance (second principle of thermodynamics)

- Gibbs Relation

$$T\dot{S} = \dot{U} - \frac{1}{\rho}\underline{\underline{\sigma}}:\underline{\underline{\dot{\varepsilon}}}^{e} - \Delta\mu\dot{Y}_d + A_j\dot{\xi}_j \tag{5-6}$$

where T represents temperature, S designates the specific entropy, $\Delta\mu$ is defined as the difference between the mass chemical potential of the diffusing substance (μ_d) and that of the polymer (μ_p), and ξ_j and A_j are the internal variable and its dual variable, respectively. Also, ε^{e} is the elastic strain with an assumption that ε can be partitioned into elastic strain, ε^{e}, and inelastic strain, ε^{in} ($\varepsilon = \varepsilon^{\mathrm{e}} + \varepsilon^{in}$).

- Entropy Variation

$$\rho\dot{S}^{e} = -Div\,\vec{J}_S + \frac{1}{T}R \tag{5-7}$$

$$\rho \dot{S}^i = \nabla\left[\frac{1}{T}\right].\vec{Q} - \nabla\left[\frac{\Delta\mu}{T}\right].\vec{M}_d + \frac{1}{T}\underline{\underline{\sigma}}:\underline{\underline{\dot{\varepsilon}}}^{in} + \frac{\rho}{T}A_j\dot{\xi}_j \tag{5-8}$$

where S^e and S^i are the variation of entropy due to *external* exchanges and *internal* evolutions, respectively. In Equations (5-8), ∇ represents the gradient operator. J_s denotes the entropy flux defined as follows:

$$\vec{J}_S = \frac{1}{T}\vec{Q} - \frac{\Delta\mu}{T}\vec{M}_d \tag{5-9}$$

- Volume Dissipation

$$\Phi = \Phi_1 + \Phi_2 + \Phi_3 \geq 0 \tag{5-10}$$

$$\Phi_1 = \underline{\underline{\sigma}}:\underline{\underline{\dot{\varepsilon}}}^{in} + \rho A_j\dot{\xi}_j \tag{5-11}$$

$$\Phi_2 = -\vec{J}_S.\nabla T \tag{5-12}$$

$$\Phi_3 = -\vec{M}_d.\nabla[\Delta\mu] \tag{5-13}$$

where Φ represents the volume dissipation, Φ_1 corresponds to the dissipation due to inelastic straining, Φ_2 relates to the thermal dissipation due to the heat transfer, and Φ_3 designates the diffusive dissipation caused by mass transport.

5.2.2 Constitutive Equations

The first set of constitutive equations are developed based on the first potential introduced previously; *i.e.*, the specific free energy. This potential is generally defined as a function of all the state variables (ε^e, T, Y_d, Y_p, ξ_j):

$$\Psi = U - TS = \Psi\left(\underline{\underline{\varepsilon}}^e, T, Y_d, Y_p, \xi_j\right) \tag{5-14}$$

The state equations can then be derived from (5-14). These equations relate the thermodynamic forces to their dual variables, as follows:

$$\underline{\underline{\sigma}} = \rho\left(\frac{\partial\Psi}{\partial\underline{\underline{\varepsilon}}^{e}}\right)_{T,Y_d,Y_p,\xi_j} \tag{5-15}$$

$$\mathrm{S} = -\left(\frac{\partial\Psi}{\partial T}\right)_{\underline{\underline{\varepsilon}}^{e},Y_d,Y_p,\xi_j} \tag{5-16}$$

$$\mu_i = \rho\left(\frac{\partial\Psi}{\partial Y_i}\right)_{T,\underline{\underline{\varepsilon}}^{e},Y_{k\neq i},\xi_j} \tag{5-17}$$

$$A_j = -\left(\frac{\partial\Psi}{\partial\xi_j}\right)_{T,\underline{\underline{\varepsilon}}^{e},Y_d,Y_p,\xi_{k\neq j}} \tag{5-18}$$

The second potential is the dissipative pseudo potential, δ^*, which is defined to develop another set of constitutive equations dealing with dissipative processes associated with diffusion, heat conduction, and viscoelasticity, as follows:

$$\delta^* = \delta^*\left(\underline{\underline{\sigma}}, \rho A_j, -\nabla T, -\nabla[\Delta\mu]\right) \tag{5-19}$$

$$\dot{\underline{\underline{\varepsilon}}}^{in} = \left(\frac{\partial\delta^*}{\partial\underline{\underline{\sigma}}}\right)_{\rho A_j,-\nabla T,-\nabla[\Delta\mu]} \tag{5-20}$$

$$\dot{\xi}_j = \left(\frac{\partial\delta^*}{\partial[\rho A_j]}\right)_{\underline{\underline{\sigma}},\rho A_{k\neq j},-\nabla T,-\nabla[\Delta\mu]} \tag{5-21}$$

$$\vec{J}_S = \left(\frac{\partial\delta^*}{\partial[-\nabla T]}\right)_{\underline{\underline{\sigma}},\rho A_j,-\nabla[\Delta\mu]} \tag{5-22}$$

$$\vec{M}_d = \left(\frac{\partial\delta^*}{\partial[-\nabla[\Delta\mu]]}\right)_{\underline{\underline{\sigma}},\rho A_j,-\nabla T} \tag{5-23}$$

For the coupled physics of structural mechanics, mass diffusion, and heat conduction the dissipative pseudo-potential can be reduced to a quadratic form resulting in linear constitutive equations:

$$\delta^* = \frac{1}{2}\underline{\underline{\sigma}}:\underline{\underline{K_S}}:\underline{\underline{\sigma}} + \frac{1}{2}K_{A_j}(\rho A_j)^2 + \frac{1}{2}\nabla T.\left(\underline{\underline{K_T}}\nabla T\right) + \frac{1}{2}\nabla[\Delta\mu].\left(\underline{\underline{K_\mu}}\nabla[\Delta\mu]\right) + \rho A_j\underline{\underline{C_{SA_j}}}:\underline{\underline{\sigma}}$$
$$-\frac{1}{2}\underline{\underline{\sigma}}:\left(\vec{C}_{ST}\otimes\nabla T + \nabla T\otimes\vec{C}_{ST}\right) - \frac{1}{2}\underline{\underline{\sigma}}:\left(\vec{C}_{S\mu}\otimes\nabla[\Delta\mu] + \nabla[\Delta\mu]\otimes\vec{C}_{S\mu}\right)$$
$$+\nabla T.\left(\underline{\underline{C_{T\mu}}}\nabla[\Delta\mu]\right) - \rho A_j\vec{C}_{TA_j}.\nabla T - \rho A_j\vec{C}_{\mu A_j}.\nabla[\Delta\mu] \tag{5-24}$$

$$\underline{\underline{\dot{\varepsilon}}}^{in} = \underline{\underline{K_S}}:\underline{\underline{\sigma}} + \rho A_j\underline{\underline{C_{SA_j}}} - \frac{1}{2}\left(\vec{C}_{ST}\otimes\nabla T + \nabla T\otimes\vec{C}_{ST}\right) - \frac{1}{2}\left(\vec{C}_{S\mu}\otimes\nabla[\Delta\mu] + \nabla[\Delta\mu]\otimes\vec{C}_{S\mu}\right) \tag{5-25}$$

$$\dot{\xi}_j = K_{A_j}\rho A_j + \underline{\underline{C_{SA_j}}}:\underline{\underline{\sigma}} - \vec{C}_{TA_j}.\nabla T - \vec{C}_{\mu A_j}.\nabla[\Delta\mu] \tag{5-26}$$

$$\vec{J}_S = -\underline{\underline{K_T}}\nabla T - \underline{\underline{C_{T\mu}}}\nabla[\Delta\mu] + \underline{\underline{\sigma}}\,\vec{C}_{ST} + \rho A_j\vec{C}_{TA_j} \tag{5-27}$$

$$\vec{M}_d = -\underline{\underline{K_\mu}}\nabla[\Delta\mu] - \underline{\underline{C_{T\mu}}}\nabla T + \underline{\underline{\sigma}}\,\vec{C}_{S\mu} + \rho A_j\vec{C}_{\mu A_j} \tag{5-28}$$

where K_S, K_T, K_μ, C_{SAj}, $C_{T\mu}$, C_{ST}, $C_{S\mu}$, C_{TAj}, $C_{\mu Aj}$, and K_{Aj} represent different coupling coefficients between the three physics. These coefficients, which are referred to as Onsager coefficients, are tensors (K_S, K_T, K_μ, C_{SAj}, and $C_{T\mu}$), vectors (C_{ST}, $C_{S\mu}$, C_{TAj}, and $C_{\mu Aj}$), and scalars (K_{Aj}).

Furthermore, the heat transfer equation can be developed based on the thermodynamic laws and the state equations (5-15) to (5-18):

$$\rho c_{\underline{\underline{\varepsilon}}^e,Y_d,Y_p,\xi_j}\dot{T} = \left\{ T\left(\frac{\partial \underline{\underline{\sigma}}}{\partial T}\right)_{\underline{\underline{\varepsilon}}^e,Y_d,Y_p,\xi_j} : \underline{\underline{\dot{\varepsilon}}}^{\boldsymbol{e}} + \underline{\underline{\sigma}} : \underline{\underline{\dot{\varepsilon}}}^{\boldsymbol{in}} - \underline{\underline{\sigma}} : \underline{\underline{\dot{\varepsilon}}}^{\boldsymbol{e}} - \rho \left[T\left(\frac{\partial A_j}{\partial T}\right)_{\underline{\underline{\varepsilon}}^e,Y_d,Y_p,\xi_j} - A_j \right] \dot{\xi}_j \right\}$$

$$+ \left\{ \rho \left[T\left(\frac{\partial \Delta\mu}{\partial T}\right)_{\underline{\underline{\varepsilon}}^e,Y_d,Y_p,\xi_j} - \Delta\mu \right] \dot{Y}_d \right\} + \left\{ -Div\vec{Q} + R \right\} \tag{5-29}$$

where c is the specific heat capacity and R represents the external heat supply.

5.3 Governing Equations

The governing equations can be developed from the main equations presented in the preceding section. The governing equations are derived assuming two different types of material behaviour: linear elasticity and linear viscoelasticity. The equations are presented based on the assumptions of isotropy and small perturbations [48].

5.3.1 Linear Elasticity

In elasticity, it is assumed that the internal variables do not exist and therefore, the specific free energy, Ψ, is a function of four variables; *i.e.*, ε^e, T, Y_d, and Y_p. A quadratic form is considered for Ψ so that it leads to linear state equations:

$$\rho\Psi\left(\underline{\underline{\varepsilon}}^e, T, Y_d, Y_p\right) = \underline{\underline{\sigma}}_o : \underline{\underline{\varepsilon}}^e + \frac{\lambda^e}{2}\left(tr\underline{\underline{\varepsilon}}^e\right)^2 + \mu^e tr\left(\underline{\underline{\varepsilon}}^e\right)^2$$

$$-(3\lambda^e + 2\mu^e)\alpha_T^e\, tr(\underline{\underline{\varepsilon}}^e)\Delta T - (3\lambda^e + 2\mu^e)\alpha_d^e\, tr(\underline{\underline{\varepsilon}}^e)\Delta Y_d - (3\lambda^e + 2\mu^e)\alpha_p^e\, tr(\underline{\underline{\varepsilon}}^e)\Delta Y_p$$

$$-\rho S_o \Delta T + \rho\mu_d^o \Delta Y_d + \rho\mu_p^o \Delta Y_p - \frac{1}{2}\frac{\rho}{T_o} c_{\underline{\underline{\varepsilon}}^e,Y_i}(\Delta T)^2 + \frac{1}{2} D_d \rho(\Delta Y_d)^2 + \frac{1}{2} D_p \rho\left(\Delta Y_p\right)^2$$

$$-d_d \Delta T \Delta Y_d - d_p \Delta T \Delta Y_p - d_{pd} \Delta Y_d \Delta Y_p \tag{5-30}$$

where λ and μ are Lamé's coefficients, α_T represents the coefficient of thermal expansion, α_d and α_p are respectively related to the coefficients of hygroscopic expansion of the diffusing material and polymer; and D_d and D_p designate the coefficient of diffusion of the diffusing material and polymer in

the mixture, respectively. The superscript "*e*" refers to elastic and the trace operator is depicted by "*tr*".

Therefore, the governing equations as developed by Rambert *et al.* [46] are as follows:

Structural Mechanics

$$\underline{\underline{\sigma}} = \underline{\underline{\sigma_{\boldsymbol{\rho}}}} + \lambda^e \left[tr\left(\underline{\underline{\varepsilon}}^e\right)\right]\underline{\underline{I}} + 2\mu^e\underline{\underline{\varepsilon}}^e - (3\lambda^e + 2\mu^e)[\alpha_T^e \Delta T + \alpha_d^e \Delta Y_d]\underline{\underline{I}} \tag{5-31}$$

Mass Diffusion

$$\rho\dot{Y}_d = \rho D\ Div(\nabla Y_d) + \left(C_{T\mu} - K_\mu C_{TY}\right)Div(\nabla T) - K_\mu \alpha_d^e \frac{(3\lambda^e + 2\mu^e)}{\rho} Div\left[\nabla\left[tr\left(\underline{\underline{\varepsilon}}^e\right)\right]\right] \tag{5-32}$$

Heat Transfer

$$\begin{aligned}
\rho c_{\underline{\underline{\varepsilon}}^e, Y_i, T}\dot{T} &= C_{TY}\left(K_\mu C_{TY} - 2K_{T\mu}\right)(\nabla T)^2 + \left(\frac{\lambda_T}{T} + C_{TY}\left(K_\mu C_{TY} - 2K_{T\mu}\right)\right)TDiv(\nabla T) \\
&+2\frac{\rho D}{K_\mu}\left(C_{T\mu} - C_{TY}K_\mu\right)\nabla T.\nabla Y_d\ + 2\alpha_d^e\frac{(3\lambda^e + 2\mu^e)}{\rho}\left(C_{TY}K_\mu - C_{T\mu}\right)\nabla T.\nabla\left[tr\left(\underline{\underline{\varepsilon}}^e\right)\right] \\
&+\frac{\rho D}{K_\mu}\left(C_{T\mu} - C_{TY}K_\mu\right)TDiv(\nabla Y_d) + \frac{\rho^2 D^2}{K_\mu}(\nabla Y_d)^2 - 2D\alpha_d^e(3\lambda^e + 2\mu^e)\nabla Y_d.\nabla\left[tr\left(\underline{\underline{\varepsilon}}^e\right)\right] \\
&+\alpha_d^e\frac{(3\lambda^e + 2\mu^e)}{\rho}\left(C_{TY}K_\mu - C_{T\mu}\right)TDiv\left[\nabla\left[tr\left(\underline{\underline{\varepsilon}}^e\right)\right]\right] + K_\mu\left[\alpha_d^e\frac{(3\lambda^e + 2\mu^e)}{\rho}\right]^2\left[\nabla\left[tr\left(\underline{\underline{\varepsilon}}^e\right)\right]\right]^2 \\
&-\alpha_T^e(3\lambda^e + 2\mu^e)T\left[tr\left(\dot{\underline{\underline{\varepsilon}}}^e\right)\right] + R
\end{aligned} \tag{5-33}$$

where K_μ is the coefficient related to the effect of chemical potential gradient on the diffusant mass flux. Other than the two coefficients of $\alpha_T{}^e$ and $\alpha_d{}^e$, which represent the interaction between structural mechanics with temperature and moisture, respectively, there are two other coupling coefficients in Equations (5-31) to (5-33): C_{TY} which corresponds to the effect of temperature (concentration) variation on the chemical potential (entropy); and $C_{T\mu}$ which relates to the temperature (chemical potential) gradient effect on the mass (entropy) flux.

5.3.2 Linear Viscoelasticity

Viscoelastic materials are usually represented by a combination of elastic springs and viscous dashpots. One of these models is the generalized Kelvin-Voigt model (also referred to as the Poynting-Thomson model [159]), which consists of a linear spring connected in series with a Kelvin-Voigt element. Rambert *et al.* [48] used this model (shown in Figure 5-4) to develop equations for a linear viscoelastic material.

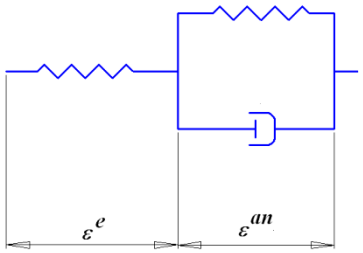

Figure 5-4 Generalized Kelvin-Voigt model

Based on the representation shown in Figure 5-4, the total strain, ε, can be partitioned into two parts: elastic strain, ε^e, and anelastic strain, ε^{an}. Anelastic strain is an internal variable and is related to its dual variable, A, which is equal to $(-\sigma^{an}/\rho)$. The specific free energy can then be written as the sum of two components, an elastic component, Ψ^e, and anelastic one, Ψ^{an}, (shown in bold):

$$\Psi = \Psi\left(\underline{\underline{\varepsilon}}^e, T, Y_d, Y_p, \underline{\underline{\varepsilon}}^{an}\right) = \Psi^e\left(\underline{\underline{\varepsilon}}^e, T, Y_d, Y_p\right) + \boldsymbol{\Psi^{an}}\left(\boldsymbol{T, Y_d, Y_p, \underline{\underline{\varepsilon}}^{an}}\right) \tag{5-34}$$

where Ψ^e is defined in Equation (5-33) and Ψ^{an} is:

$$\rho\Psi^{an}\left(T, Y_d, Y_p, \underline{\underline{\varepsilon}}^{an}\right) = \underline{\underline{\sigma}}^{an} : \underline{\underline{\varepsilon}}^{an} + \frac{\lambda^{an}}{2}\left(tr\underline{\underline{\varepsilon}}^{an}\right)^2 + \mu^{an} tr\left(\underline{\underline{\varepsilon}}^{an}\right)^2$$
$$-(3\lambda^{an} + 2\mu^{an})\alpha_T^{an}\, tr(\underline{\underline{\varepsilon}}^{an})\Delta T - (3\lambda^{an} + 2\mu^{an})\alpha_d^{an}\, tr(\underline{\underline{\varepsilon}}^{an})\Delta Y_d$$
$$-(3\lambda^{an} + 2\mu^{an})\alpha_p^{an}\, tr(\underline{\underline{\varepsilon}}^{an})\Delta Y_p \tag{5-35}$$

In this work, a similar procedure to that by Rambert *et al.* [48] has been adopted with one difference: two Kelvin-Voight elements are considered to be connected in series with a linear spring because it can better represent the viscoelastic behaviour of PC/ABS blend used in this study. Therefore, the governing equations for the three physics of structural mechanics, mass diffusion, and heat transfer are developed as follows (The anelastic terms are shown in bold):

Structural Mechanics

$$\underline{\underline{\sigma}} = \underline{\underline{\sigma_o}} + \lambda^e\left[tr\left(\underline{\underline{\varepsilon}}^e\right)\right]\underline{\underline{I}} + 2\mu^e\underline{\underline{\varepsilon}}^e - (3\lambda^e + 2\mu^e)[\alpha_T^e\Delta T + \alpha_d^e\Delta Y_d]\underline{\underline{I}}$$

$$\underline{\underline{\boldsymbol{\sigma}}}^{\boldsymbol{an_i}} = \underline{\underline{\boldsymbol{\sigma_o}}}^{\boldsymbol{an_i}} + \boldsymbol{\lambda^{an_i}}\left[\boldsymbol{tr}\left(\underline{\underline{\boldsymbol{\varepsilon}}}^{\boldsymbol{an_i}}\right)\right]\underline{\underline{\boldsymbol{I}}} + \boldsymbol{2\mu^{an_i}}\underline{\underline{\boldsymbol{\varepsilon}}}^{\boldsymbol{an_i}} - (\boldsymbol{3\lambda^{an_i} + 2\mu^{an_i}})\left[\boldsymbol{\alpha_T^{an_i}\Delta T + \alpha_d^{an_i}\Delta Y_d}\right]\underline{\underline{\boldsymbol{I}}},$$

$$i = 1{,}2\ (no\ summation\ convention)$$

$$\underline{\underline{\dot{\boldsymbol{\varepsilon}}}}^{\boldsymbol{an_i}} = \frac{\boldsymbol{1+\nu}}{\boldsymbol{\eta^{v_i}}}\underline{\underline{\boldsymbol{\sigma}}}^{\boldsymbol{v_i}} - \frac{\boldsymbol{\nu}}{\boldsymbol{\eta^{v_i}}}\left[\boldsymbol{tr}\left(\underline{\underline{\boldsymbol{\sigma}}}^{\boldsymbol{v_i}}\right)\right]\underline{\underline{\boldsymbol{I}}} - \frac{\boldsymbol{1}}{\boldsymbol{2}}\boldsymbol{C_{ST_i}}\left(\vec{\boldsymbol{1}}\otimes\boldsymbol{\nabla T} + \boldsymbol{\nabla T}\otimes\vec{\boldsymbol{1}}\right)$$
$$-\frac{\boldsymbol{1}}{\boldsymbol{2}}\boldsymbol{C_{S\mu_i}}\left(\vec{\boldsymbol{1}}\otimes\boldsymbol{\nabla}[\Delta\boldsymbol{\mu}] + \boldsymbol{\nabla}[\Delta\boldsymbol{\mu}]\otimes\vec{\boldsymbol{1}}\right) \tag{5-36}$$

$$i = 1{,}2\ (no\ summation\ convention)$$

Mass Diffusion

$$\rho\dot{Y}_d = \rho D\ Div(\nabla Y_d) + \left(C_{T\mu} - K_\mu C_{TY}\right)Div(\nabla T) - K_\mu\alpha_d^e\frac{(3\lambda^e + 2\mu^e)}{\rho}Div\left[\nabla\left[tr\left(\underline{\underline{\varepsilon}}^e\right)\right]\right]$$
$$-\boldsymbol{K_\mu\alpha_d^{an_i}}\frac{\boldsymbol{(3\lambda^{an_i} + 2\mu^{an_i})}}{\boldsymbol{\rho}}\boldsymbol{Div}\left[\boldsymbol{\nabla}\left[\boldsymbol{tr}\left(\underline{\underline{\boldsymbol{\varepsilon}}}^{\boldsymbol{an_i}}\right)\right]\right] - \boldsymbol{C_{s\mu_i}Div}\left[\underline{\underline{\boldsymbol{\sigma}}}^{\boldsymbol{v_i}}\vec{\boldsymbol{1}}\right] \tag{5-37}$$

$$i = 1{,}2\ (summation\ convention)$$

Heat Transfer

$$\rho c_{\underline{\underline{\varepsilon}}^e, Y_i, T, \underline{\underline{\varepsilon}}^{an}} \dot{T} = C_{TY}\left(K_\mu C_{TY} - 2K_{T\mu}\right)(\nabla T)^2 + \left(\frac{\lambda_T}{T} + C_{TY}\left(K_\mu C_{TY} - 2K_{T\mu}\right)\right) T Div(\nabla T)$$

$$+2\frac{\rho D}{K_\mu}\left(C_{T\mu} - C_{TY}K_\mu\right)\nabla T.\nabla Y_d \; + 2\alpha_d^e \frac{(3\lambda^e + 2\mu^e)}{\rho}\left(C_{TY}K_\mu - C_{T\mu}\right)\nabla T.\nabla\left[tr\left(\underline{\underline{\varepsilon}}^e\right)\right]$$

$$+\frac{\rho D}{K_\mu}\left(C_{T\mu} - C_{TY}K_\mu\right) T Div(\nabla Y_d) + \frac{\rho^2 D^2}{K_\mu}(\nabla Y_d)^2 - 2D\alpha_d^e(3\lambda^e + 2\mu^e)\nabla Y_d.\nabla\left[tr\left(\underline{\underline{\varepsilon}}^e\right)\right]$$

$$+\alpha_d^e \frac{(3\lambda^e + 2\mu^e)}{\rho}\left(C_{TY}K_\mu - C_{T\mu}\right) T Div\left[\nabla\left[tr\left(\underline{\underline{\varepsilon}}^e\right)\right]\right] + K_\mu\left[\alpha_d^e \frac{(3\lambda^e + 2\mu^e)}{\rho}\right]^2 \nabla\left[tr\left(\underline{\underline{\varepsilon}}^e\right)\right]^2$$

$$-\alpha_T^e(3\lambda^e + 2\mu^e) T\left[tr\left(\underline{\underline{\dot{\varepsilon}}}^e\right)\right] + R$$

$$+\boldsymbol{2\alpha_d^{an_i}\frac{(3\lambda^{an_i} + 2\mu^{an_i})}{\rho}\left(C_{TY}K_\mu - C_{T\mu}\right)\nabla T.\nabla\left[tr\left(\underline{\underline{\varepsilon}}^{an_i}\right)\right]}$$

$$+\boldsymbol{\alpha_d^{an_i}\frac{(3\lambda^{an_i} + 2\mu^{an_i})}{\rho}\left(C_{TY}K_\mu - C_{T\mu}\right) T Div\left[\nabla\left[tr\left(\underline{\underline{\varepsilon}}^{an_i}\right)\right]\right]}$$

$$+\boldsymbol{K_\mu\left[\alpha_d^{an_i}\frac{(3\lambda^{an_i} + 2\mu^{an_i})}{\rho}\right]^2\left[\nabla\left[tr\left(\underline{\underline{\varepsilon}}^{an_i}\right)\right]\right]^2}$$

$$-\boldsymbol{2D\alpha_d^{an_i}(3\lambda^{an_i} + 2\mu^{an_i})\nabla Y_d.\nabla\left[tr\left(\underline{\underline{\varepsilon}}^{an_i}\right)\right]}$$

$$+\boldsymbol{2K_\mu\alpha_d^e\alpha_d^{an_i}\frac{(3\lambda^e + 2\mu^e)(3\lambda^{an_i} + 2\mu^{an_i})}{\rho^2}\nabla\left[tr\left(\underline{\underline{\varepsilon}}^e\right)\right].\nabla\left[tr\left(\underline{\underline{\varepsilon}}^{an_i}\right)\right]}$$

$$-\boldsymbol{\left(C_{ST_i} - C_{S\mu_i}C_{TY}\right)\nabla T\underline{\underline{\sigma}}^{v_i}\vec{1} - \left(C_{ST_i} - C_{S\mu_i}C_{TY}\right) T Div\left(\underline{\underline{\sigma}}^{v_i}\vec{1}\right) - C_{S\mu_i}C_{TY}\nabla Y_d\underline{\underline{\sigma}}^{v_i}\vec{1}}$$

$$+\boldsymbol{C_{S\mu_i}\alpha_d^e\frac{(3\lambda^e + 2\mu^e)}{\rho}\nabla\left[tr\left(\underline{\underline{\varepsilon}}^e\right)\right]\underline{\underline{\sigma}}^{v_i}\vec{1} + C_{S\mu_i}\alpha_d^{an_i}\frac{(3\lambda^{an_i} + 2\mu^{an_i})}{\rho}\nabla\left[tr\left(\underline{\underline{\varepsilon}}^{an_i}\right)\right]\underline{\underline{\sigma}}^{v_i}\vec{1}}$$

$$+\boldsymbol{\underline{\underline{\dot{\varepsilon}}}^{an_i}:\underline{\underline{\sigma}}^{v_i} - \alpha_T^{an_i}(3\lambda^{an_i} + 2\mu^{an_i}) T\left[tr\left(\underline{\underline{\dot{\varepsilon}}}^{an_i}\right)\right]}$$

$$i = 1{,}2\ (summation\ convention) \tag{5-38}$$

where σ^{an} and σ^{v} are the stress components related to the spring and dashpot in the Kelvin-Voigt element. C_{ST} and $C_{S\mu}$ are the coupling coefficients related to the interaction of viscoelastic component of structural mechanics with heat conduction and moisture diffusion, respectively.

5.4 Finite Element Analysis (FEA)

There are different software packages available to model finite element analysis (FEA) problems. Of the various commercial packages available, COMSOL Multiphysics® is particularly strong for modeling coupled PDEs. This software (COMSOL Multiphysics® 4.0a) was therefore selected for numerical modeling in this work. Some of the specific capabilities of this software are described in the following sections.

5.4.1 COMSOL Multiphysics

COMSOL Multiphysics® is a powerful modeling software package which is based on the MATLAB® programming language. COMSOL was first known as FEMLAB, which was developed in 1998 and was introduced in its current format in 2005. It acts as a computational tool for PDEs with the possibility of equation customization. Its multiphysics modeling capability is extendable to include complicated problems and it also provides MATLAB® m-file source code, which makes programming easier. COMSOL Multiphysics® uses finite element method (FEM) as a tool to calculate PDEs. It actually translates PDEs into the assembly of FEM stiffness matrix and load vector, then solves for equations on smaller subdomains; *i.e.*, finite elements. Mathematically, COMSOL Multiphysics® converts a PDE to its weak form through using finite element concepts, in which Lagrange basis functions (or shape functions) are used to represent field variables discontinuously over the domain. This discontinuous representation of functions is then integrated to result in the solution [160].

5.4.2 Partial Differential Equations

The software package of COMSOL Multiphysics® has different modules for modeling physics such as structural mechanics, heat transfer, diffusion, etc. One of these modules is the PDE module, which is used for equation based modeling [161]. Using the PDE module of COMSOL Multiphysics® makes the modeling of a set of complicated PDEs very straight forward because of several advantages it has such as being open source, easy to modify; and there is no need to write a user-defined element code (UEL). The PDE module provides the users with three forms of PDEs: coefficient form, general form,

and weak form. Since the two coefficient form PDE and general form PDE are applied for modeling in this study, these two forms are introduced for a time dependant problem below.

Coefficient Form PDE

The coefficient form PDE has the following form:

$$e_a \frac{\partial^2 u}{\partial t^2} + d_a \frac{\partial u}{\partial t} + \nabla.(-c\nabla u - \alpha u + \gamma) + \beta.\nabla u + au = f \tag{5-39}$$

where u is a dependant variable over the computational domain, denoted by Ω in COMSOL Multiphysics®.

The boundary conditions in the coefficient form PDE is shown as:

$$n.(c\nabla u + \alpha u - \gamma) + qu = g - h^T \mu \tag{5-40}$$

$$hu = r \tag{5-41}$$

These two boundary conditions are defined over the boundary, $\partial\Omega$, and are referred to as generalized Neumann and Dirichlet boundary conditions, respectively.

General Form PDE

The general form PDE, as its name shows, is a more general form of the coefficient form PDE in the following form:

$$e_a \frac{\partial^2 u}{\partial t^2} + d_a \frac{\partial u}{\partial t} + \nabla.\Gamma = F \tag{5-42}$$

where Γ and F are functions of the dependant variable, u, and its space derivatives over the computational domain, Ω.

The boundary conditions in the general form PDE is:

$$-n.\Gamma = G + \left(\frac{\partial R}{\partial u}\right)^T \mu \tag{5-43}$$

$$0 = R \tag{5-44}$$

where the first equation represents the generalized Neumann boundary condition and the second one relates to the Dirichlet boundary condition defined over the boundary, $\partial\Omega$. Different coefficients and terms in Equations (5-39) to (5-44) are defined in COMSOL Multiphysics® so that the corresponding PDEs form the governing PDE in the desired problem.

5.5 Uncoupled Physics Modeling

The final model of this study includes the coupled physics of structural mechanics, moisture diffusion, and heat conduction. These models will be built using the governing equations of each mechanism, which are in the form of PDEs. However, the uncoupled physics should be first modeled using the corresponding PDE and verified against the built-in modules of the software to ensure that the PDEs are modeled correctly for each mechanism. The coupled physics modeling will then be developed based upon the verified uncoupled models.

5.5.1 Structural Mechanics

The first physics which is modeled is the structural mechanics, which is developed considering two kinds of material behaviour: linear elastic and linear viscoelastic.

5.5.1.1 Linear Elastic

For the case of linear elastic behaviour, a typical 2-dimensional problem similar to the model of Rambert *et al.* [46] is considered. A time-dependant transient analysis is carried out on a pipe made up of a material having linear elastic behaviour. The pipe has an internal radius of 5 *mm* with wall thickness of 1 *mm*. The reason a pressurized pipe is considered for modeling is that it provides a good example of a geometry with curved edges that can be modeled in different modes. Moreover, this is the same geometry used for the coupled physics modeling discussed later in section 5.6.1. Because of

the part symmetry, only a quarter of the pipe geometry is modeled. The meshed pipe as well as the applied boundary conditions is illustrated in Figure 5-5.

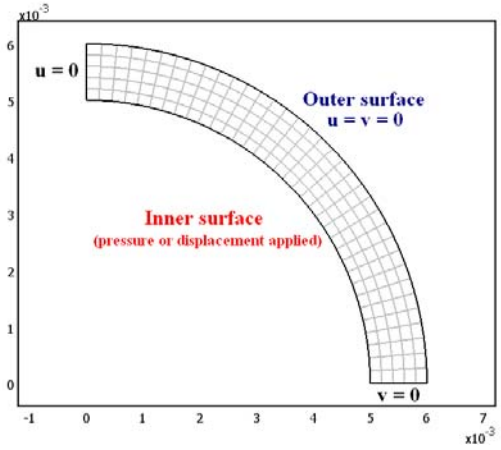

Figure 5-5 The geometry and boundary conditions of a quarter of a typical pipe.

The governing equations for this material system for plane strain and plane stress cases are:

$$Div\ \underline{\sigma} = 0 \tag{5-45}$$

Plane Strain:

$$\begin{Bmatrix}\sigma_{xx}\\ \sigma_{yy}\\ \sigma_{xy}\end{Bmatrix} = \frac{E}{(1+\nu)(1-2\nu)}\begin{bmatrix}1-\nu & \nu & 0\\ \nu & 1-\nu & 0\\ 0 & 0 & \frac{1-2\nu}{2}\end{bmatrix}\begin{Bmatrix}\varepsilon_{xx}\\ \varepsilon_{yy}\\ \varepsilon_{xy}\end{Bmatrix} \tag{5-46}$$

Plane Stress:

$$\begin{Bmatrix}\sigma_{xx}\\ \sigma_{yy}\\ \sigma_{xy}\end{Bmatrix} = \frac{E}{(1-\nu^2)}\begin{bmatrix}1 & \nu & 0\\ \nu & 1 & 0\\ 0 & 0 & \frac{1-\nu}{2}\end{bmatrix}\begin{Bmatrix}\varepsilon_{xx}\\ \varepsilon_{yy}\\ \varepsilon_{xy}\end{Bmatrix} \tag{5-47}$$

where E and ν are the modulus of elasticity and Poisson's ratio, respectively. In Equation (5-45), it is assumed that the second time derivative of the displacement (acceleration) and body force can be

neglected. It should be noted that in the case of plane stress, the geometry can be considered as a thin disc with a central circular hole instead of a pipe.

Equations (5-45) to (5-47) can be modeled using the general form of PDEs, Equation (5-42), in COMSOL Multiphysics®. The modulus of elasticity and Poisson's ratio were set equal to 2.16 *GPa* and 0.37, respectively. The inner surface of the pipe was also exposed to a pressure of 1 *MPa* simulating the creep loading behaviour. Figures 5-6 (a) and 5-6 (b) depict the radial strain contour of the modeled pipe for the cases of plane strain and plane stress, respectively.

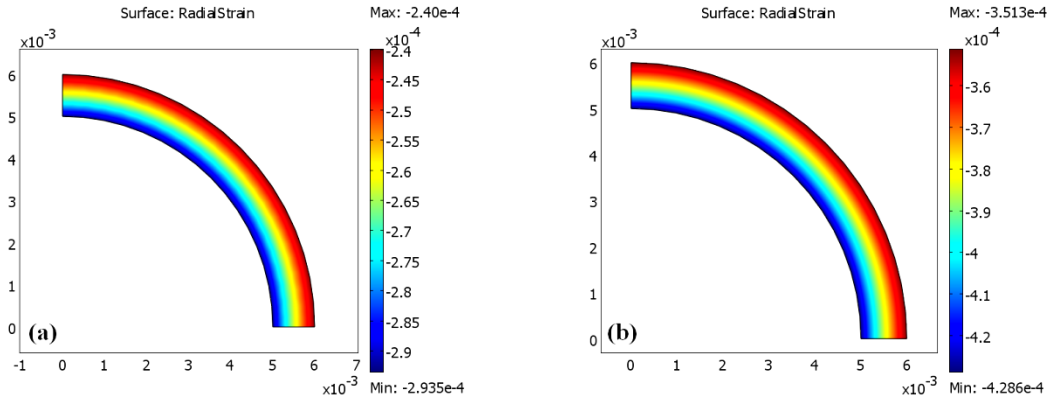

Figure 5-6 Radial strain contour obtained from a 2D analysis of an elastic pipe for (a) plane strain and (b) plane stress conditions.

The radial strain contours presented in Figures 5-6 (a) and 5-6 (b) exactly match with those obtained from the analyses using the built-in structural module of COMSOL Multiphysics®. This validates the modeling using PDEs for the uncoupled structural mechanics with elastic behaviour in a 2D analysis.

5.5.1.2 Linear Viscoelastic

Similar to the linear elastic behaviour described in the previous section, a 2D analysis of the same pipe is conducted assuming that the pipe is made of a material having linear viscoelastic behaviour. The viscoelastic behaviour can be modeled using two famous rheological models; *i.e.*, generalized Kelvin-Voigt (Figure 5-7) and generalized Maxwell models (Figure 5-8).

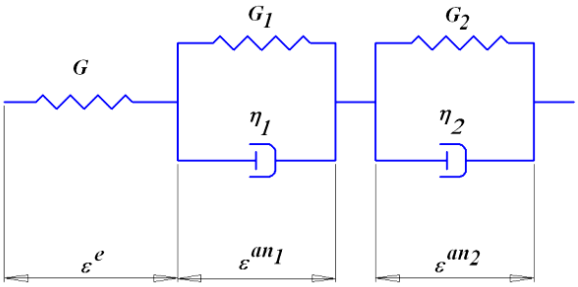

Figure 5-7 Schematic representation of the generalized Kelvin-Voigt model.

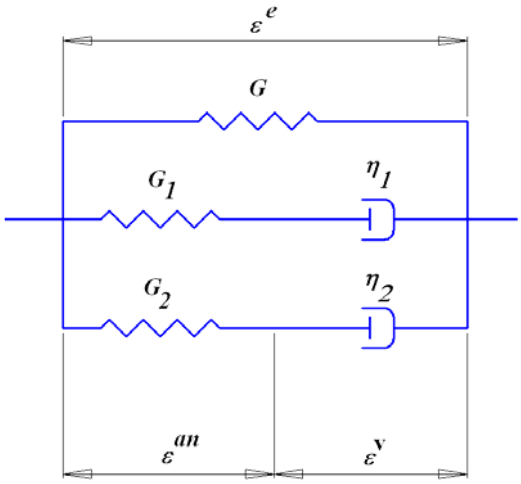

Figure 5-8 Schematic representation of the generalized Maxwell model

In the generalized Kelvin-Voigt model, two elements of Kelvin-Voigt model are linked in series with an elastic spring; and in the generalized Maxwell model, two Maxwell elements are connected in parallel to an elastic spring. Using of two elements of the Kelvin-Voigt and Maxwell model in the generalized models would better represent the viscoelastic behaviour of the PC/ABS blend used in this study. Strain components and the properties related to the springs and dashpots are also illustrated in Figures 5-7 and 5-8. The elastic and viscoelastic components of stress and strain for the models of Figures 5-7 and 5-8 have the following relation:

Generalized Kelvin-Voigt Model:

$$\underline{\underline{\varepsilon}} = \underline{\underline{\varepsilon}}^{e} + \underline{\underline{\varepsilon}}^{an_1} + \underline{\underline{\varepsilon}}^{an_2}, \qquad \underline{\underline{\varepsilon}}^{an_1} = \underline{\underline{\varepsilon}}^{v_1},\ \underline{\underline{\varepsilon}}^{an_2} = \underline{\underline{\varepsilon}}^{v_2} \tag{5-48}$$

$$\underline{\underline{\sigma}} = \underline{\underline{\sigma}}^{e} = \underline{\underline{\sigma}}^{an_1} + \underline{\underline{\sigma}}^{v_1} = \underline{\underline{\sigma}}^{an_2} + \underline{\underline{\sigma}}^{v_2} \tag{5-49}$$

Generalized Maxwell Model:

$$\underline{\underline{\varepsilon}} = \underline{\underline{\varepsilon}}^{e} = \underline{\underline{\varepsilon}}^{an_1} + \underline{\underline{\varepsilon}}^{v_1} = \underline{\underline{\varepsilon}}^{an_2} + \underline{\underline{\varepsilon}}^{v_2} \tag{5-50}$$

$$\underline{\underline{\sigma}} = \underline{\underline{\sigma}}^{e} + \underline{\underline{\sigma}}^{an_1} + \underline{\underline{\sigma}}^{an_2}, \qquad \underline{\underline{\sigma}}^{an_1} = \underline{\underline{\sigma}}^{v_1}, \underline{\underline{\sigma}}^{an_2} = \underline{\underline{\sigma}}^{v_2} \tag{5-51}$$

The governing equations for a viscoelastic material following two models of generalized Kelvin-Voigt and generalized Maxwell and for both cases of plane strain and plane stress are presented in Appendix A.

A transient analysis was performed on the pipe (Figure 5-5) assuming that the pipe's material follows the two rheological models of generalized Kelvin-Voigt and generalized Maxwell. The parameters of these models and their derivation will follow this section. The 2D analysis was performed in two cases of plane strain and plane stress. The outer surface of the pipe was fixed and the inner surface was exposed to two different loading conditions: a radial constant displacement of 0.1 *mm* inducing stress relaxation condition and a constant internal pressure equal to 1 *MPa* producing creep loading condition. The results were then compared to results obtained from similar analyses conducted using the software package of ABAQUS®. Figures 5-9 and 5-10 depict hoop stress contours obtained from the stress relaxation analyses of the pipe in, respectively, plane stress and plane strain modes performed in COMSOL Multiphysics®. Similarly, the results of creep analyses are illustrated in the form of radial strain contours in Figures 5-11 and 5-12 for plane stress and plane strain modes, respectively. The results of corresponding analyses performed in ABAQUS® are also shown in Figures 5-13 and 5-14 for the purpose of comparison.

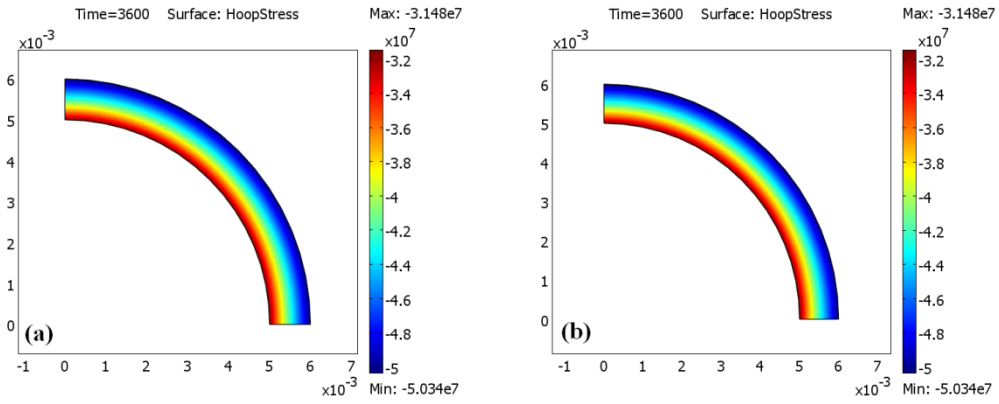

Figure 5-9 Hoop stress contour [*Pa*] obtained from a plane stress analysis using (a) generalized Kelvin-Voigt model, and (b) generalized Maxwell model conducted in COMSOL Multiphysics®.

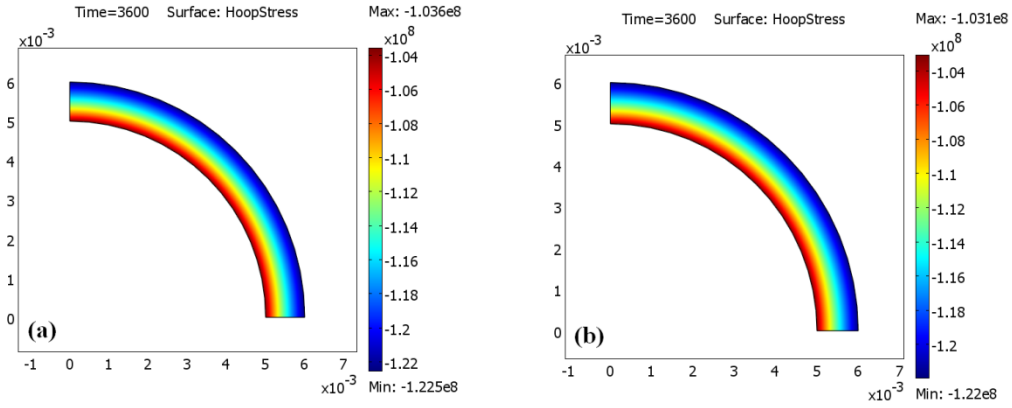

Figure 5-10 Hoop stress contour [*Pa*] obtained from a plane strain analysis in using (a) generalized Kelvin-Voigt model, and (b) generalized Maxwell model conducted in COMSOL Multiphysics®.

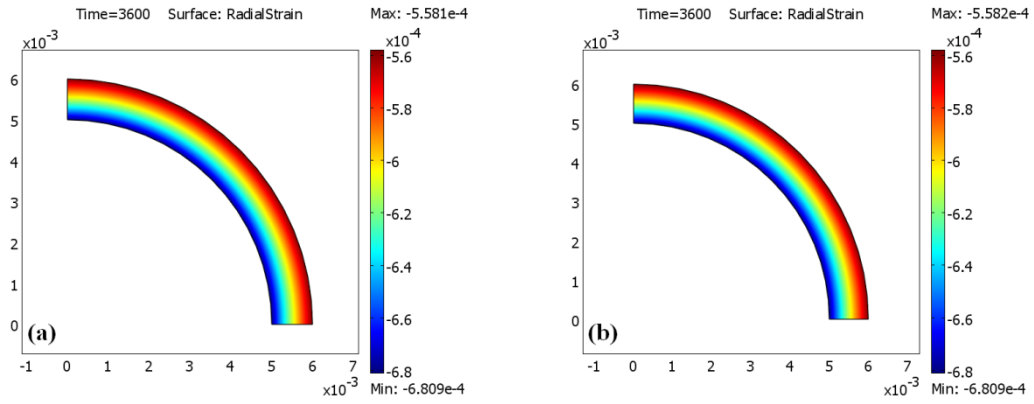

Figure 5-11 Radial strain contour obtained from a plane stress analysis in using (a) generalized Kelvin-Voigt model, and (b) generalized Maxwell model conducted in COMSOL Multiphysics®.

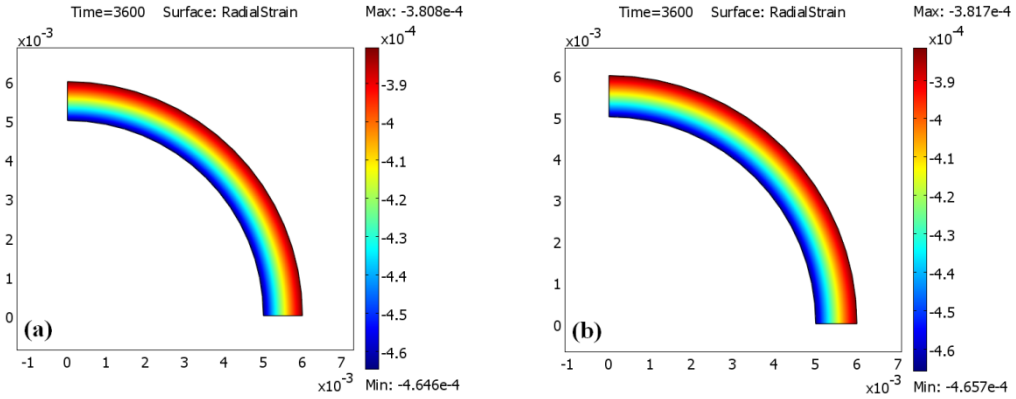

Figure 5-12 Radial strain contour obtained from a plane strain analysis in using (a) generalized Kelvin-Voigt model, and (b) generalized Maxwell model conducted in COMSOL Multiphysics®.

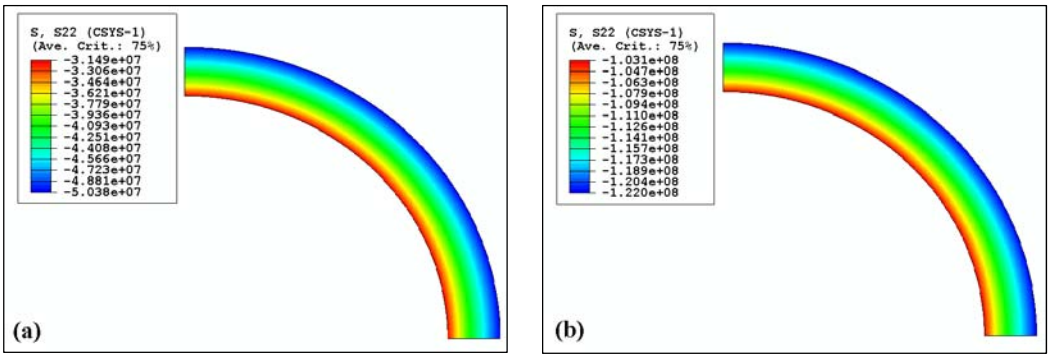

Figure 5-13 Hoop stress contour [*Pa*] obtained in (a) plane stress and (b) plane strain analyses in ABAQUS®.

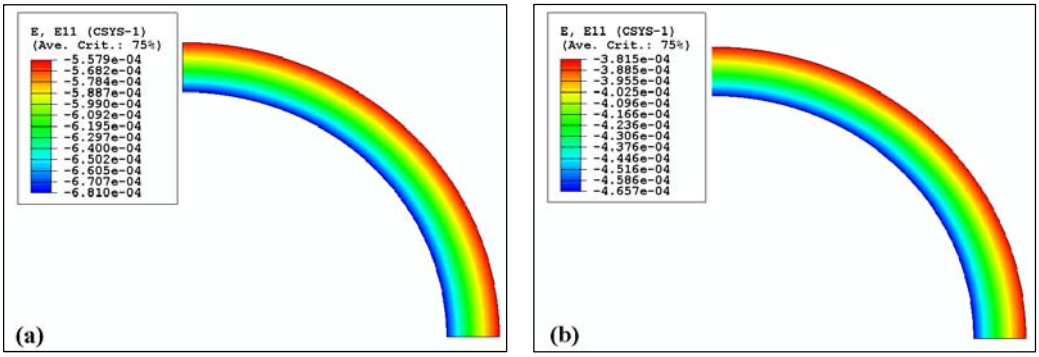

Figure 5-14 Radial strain contour obtained in (a) plane stress and (b) plane strain analyses in ABAQUS®.

There is a very good agreement between the results of COMSOL Multiphysics® analyses and the corresponding results from ABAQUS®, which confirms the validity of the PDE modeling in COMSOL Multiphysics® for linear viscoelastic materials.

5.5.1.2.1 Rheological Model Parameters

Two rheological models were used to model the linear viscoelastic behaviour: the generalized Kelvin-Voigt model and the generalized Maxwell model, with two branches of Kelvin-Voigt and Maxwell elements, respectively (Figures 5-7 and 5-8). The compliance and modulus of these two models are represented in the form of Prony series:

$$D = D_e + D_1\left(1 - \exp\left(-\frac{t}{\tau_1}\right)\right) + D_2\left(1 - \exp\left(-\frac{t}{\tau_2}\right)\right) \quad (5\text{-}52)$$

$$E = E_e + E_1 \exp\left(-\frac{t}{\tau_1}\right) + E_2 \exp\left(-\frac{t}{\tau_2}\right) \quad (5\text{-}53)$$

where D represents compliance and E refers to modulus. Compared to the KWW models presented in section 4.2.2.1, the Prony series form of the two models can be better used in finite element modeling [162].

There are five parameters in the modulus of the generalized Maxwell model; *i.e.*, E_e, E_1, E_2, τ_1, and τ_2, which can be obtained by fitting a curve to the experimental data obtained from stress relaxation experiments discussed in section 4.2.2.1. For example, the modulus of the un-aged samples at 65 °C, which is used for the linear viscoelastic modeling using the generalized Maxwell model presented in previous section, has the following form:

$$E\ [GPa] = 1.033 + 0.851\ exp(-t / 3023) + 0.273\ exp(-t / 260)$$

In order to find the values of the five parameters of the generalized Kelvin-Voigt model (D_e, D_1, D_2, τ_1, and τ_2), which is equivalent to the model above; a 2D analysis is performed using the parameters of the generalized Maxwell model on a rectangular plate. A constant uniaxial stress is applied on the plate which simulates the creep loading. If the value of the uniaxial stress is set to unit, the obtained strain will become equivalent to the compliance of the material. The strain data points are then curve fitted to the compliance equation (5-52) to get the following form:

$$D\ [1/GPa] = 0.464 + 0.444\ (1 - exp(-t / 5547)) + 0.061\ (1- exp(-t / 296))$$

The above formula can then be used for modeling compliance of an un-aged sample at 65 °C using the generalized Kelvin-Voigt model. The obtained compliance is also verified using the relation it has with modulus [80] as follows:

$$\int_0^t E(t)D(t-\tau)d\tau = t \quad (5\text{-}54)$$

It was seen that the obtain parameters for compliance also satisfies Equation (5-54).

Similar procedure was taken to obtain the equivalent compliance for thermally aged samples at 65 °C at different aging times, t_{a1} to t_{a7}. The curves, which are depicted in Figure 5-15, were then shifted to the reference curve at t_{a7} to obtain the shift factors, a_{ta}, and the corresponding aging shift rate, μ_{ta}:

$$\log(a_{ta}) = \mu_{ta} \log(t_a) + 2.712 \tag{5-55}$$

where t_a is the aging time in minutes and μ_{ta} is equal to -0.905.

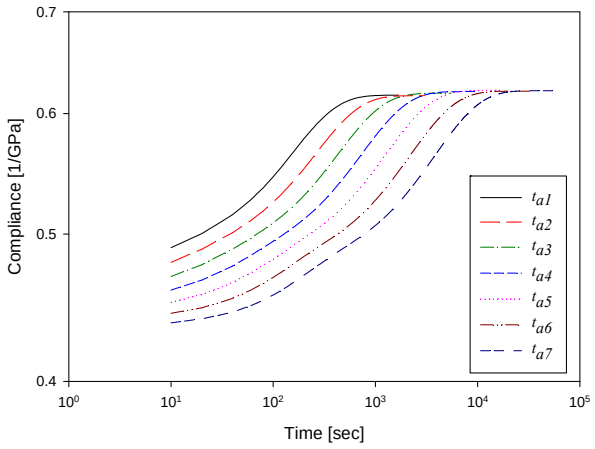

Figure 5-15 Compliance of thermally aged samples at 65 °C.

The application of the obtained curves in Figure 5-15 in modeling of aged PC/ABS material is later discussed in section 5.6.3.1.

5.5.2 Moisture Diffusion

The next phenomenon which is modeled is the physics of moisture diffusion inside a thin plate. The transient analysis of moisture diffusion inside a thin plate using finite element analysis software packages such as COMSOL Multiphysics® can sometimes lead to erroneous results. A case in point is obtaining negative values of concentration inside a modeled plate after the outset of mass uptake by the plate. Such results, which are physically unrealistic, occur when the coefficient of diffusion is very small. The coefficient of moisture diffusion to the polymer material used in this study, PC/ABS,

is in the order of 10^{-11} m^2/s and therefore, the transient analysis of moisture diffusion could lead to physically incorrect results.

This problem can be overcome (at least to some extent, if not completely) by applying certain numerical techniques. Although Madduri *et al.* [163] in their study on 3D thermal-diffusion analysis on a moisture loaded epoxy sample have applied a number of techniques to remove the effect of the unrealistic results for long-time analysis, the techniques turned out to be not effective. The techniques they have applied were mesh refinement, time stepping options, using different solver, and using different element types. In this study, however, the mesh refinement technique has been employed in 1D and 2D analyses to diminish the error produced in the results.

A 1D moisture diffusion model was built in COMSOL Multiphysics® using the PDE coefficient form. The initial concentration of the line (1D model) was considered to be zero and the concentration at the two ends of the line was set at a constant value of 0.0016 after the start of the analysis ($t > 0$). The coefficient of diffusion was also set equal to 6.5×10^{-11} m^2/s. Since the negative values of concentration are produced in the vicinity of the edges of the plate, the mesh size was decreased towards the end points of the 1D model (Figure 5-16).

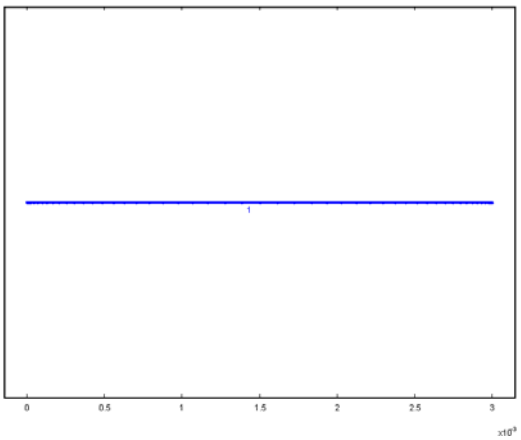

Figure 5-16 Mesh size decreases towards the end points of the line.

By considering 50 elements with element ratio of 0.04 for the line of 3 *mm* long, the negative value of concentration along the line decreases to 0.15% of the concentration at the boundary condition. The negative value of concentration, however, disappears after about 8 *sec* of the analysis.

To investigate the effect of these negative values on the long time response, the results of the model were compared against the analytical results (Equation (4-7)). Figure 5-17 shows the values of concentration at the midpoint of the 1D model obtained from both numerical and analytical solutions.

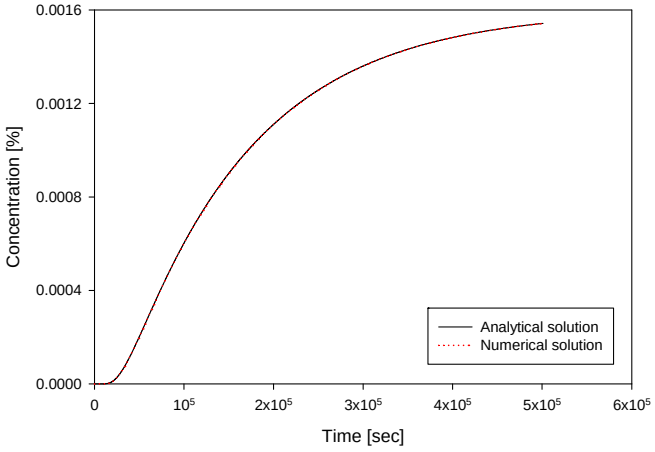

Figure 5-17 Comparison between concentration values at midpoint obtained from numerical and analytical analyses.

As the figure shows, the two curves of analytical and numerical solutions overlay. Before the concentration at the midpoint reaches at 25% of the saturated value (corresponding to about 4 hours after the start of moisture uptake) there are some discrepancies between the numerical and analytical results. After that, however, the difference reduces to less than 1% and quickly approaches zero thereafter.

Figure 5-18 also shows the values of concentration at a point near the edge of the line; *i.e.*, at a distance of $l/12$ (l is the length of the line and is equal to 3 *mm*) from the end point. The error after 16 minutes from the start of the diffusion is less than 1%, which reduces very rapidly to zero as the diffusion process progresses.

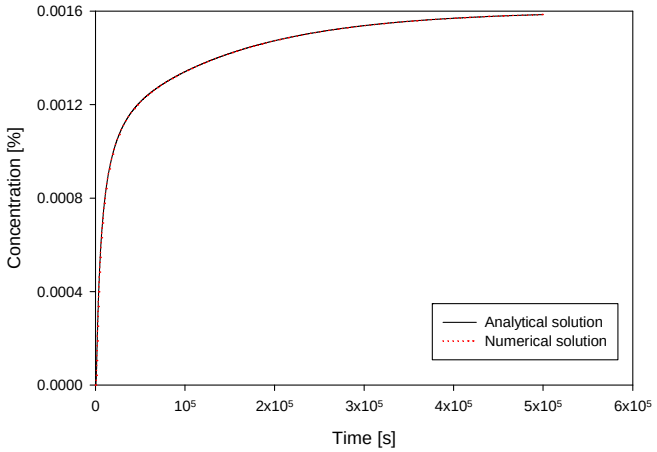

Figure 5-18 Comparison of numerical and analytical results at a point near the edge.

In experiments dealing with diffusion, the mass uptake of the samples is usually calculated. Therefore, the mass uptake of the line obtained from numerical and analytical analyses is also compared. The analytical mass of the absorbed moisture is presented by Equation (4-8). A comparison of the mass uptake from both numerical and analytical analyses is depicted in Figure 5-19. The maximum error in the estimation of mass uptake is 0.13%.

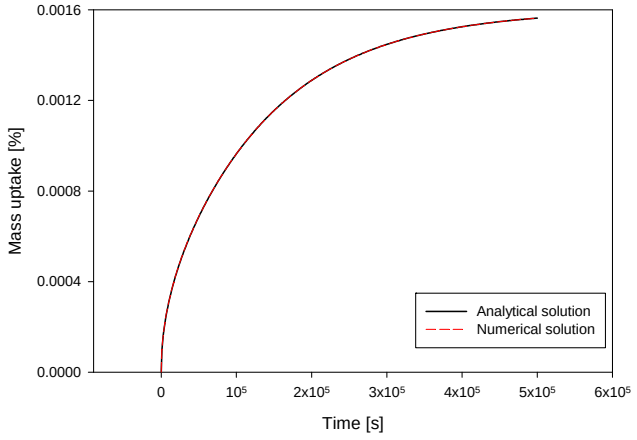

Figure 5-19 Mass uptake obtained from numerical and analytical analyses.

In a similar way, a 1D analysis over the length of 25 *mm* was conducted. The results were improved by considering 100 elements with element ratio of 0.04. Results similar to those of the 1D analysis of the 3 *mm* line were extracted: the concentration at the midpoint and at a distance of $1/100^{th}$ of the length from the end point (Figures 5-20 and 5-21, respectively) as well as the mass uptake of the line (Figure 5-22). Maximum error of the mass uptake results obtained from numerical analysis was about 0.3%.

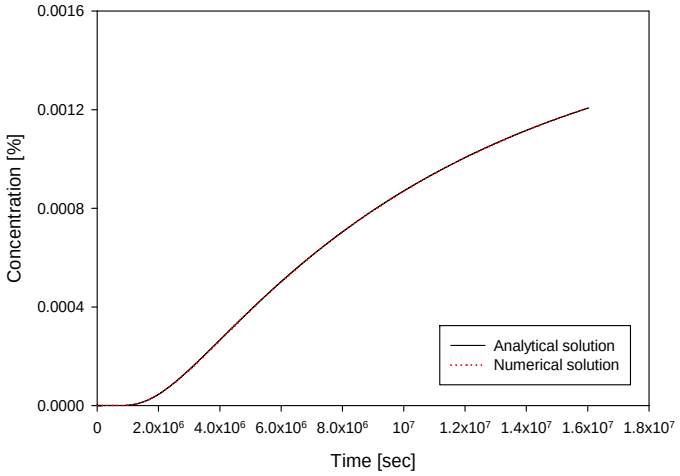

Figure 5-20 Comparison of the moisture concentration at the midpoint of the 25 *mm* line obtained from the two analyses.

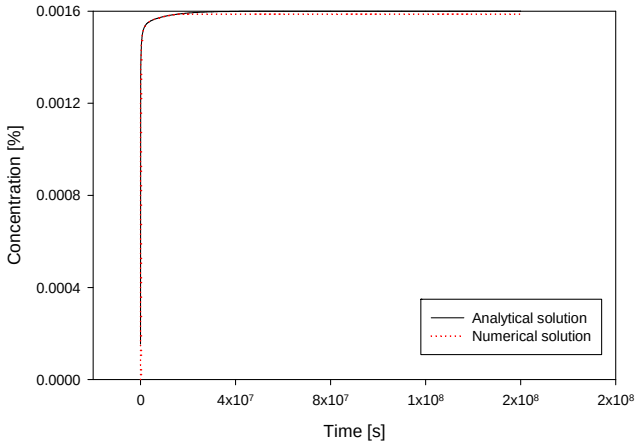

Figure 5-21 Moisture concentration at a point near the edge of the 25 *mm* line obtained from the two analyses.

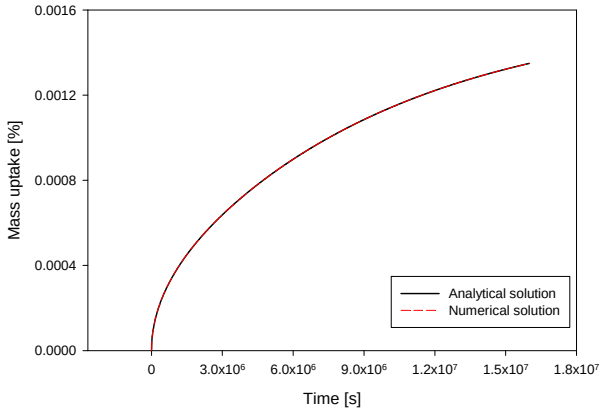

Figure 5-22 Mass uptake of the 25 *mm* line.

Next, a 2D analysis of a rectangular plate with dimensions 25×3 *mm* was conducted. Due to the part symmetry, only 1/4th of the plate was modeled. The 2D analysis was performed in three cases of boundary conditions: lateral gradient, longitudinal gradient, and both gradient. In lateral gradient case, the two longitudinal sides of the plate were at non-zero (here, at 0.0016) concentration and the two other sides had zero fluxes and therefore a lateral concentration gradient was produced in the plate. Similarly, in longitudinal gradient case, the non-zero concentration was considered for the lateral sides and a longitudinal gradient was created. For both lateral and longitudinal gradient cases the mass uptake obtained from the numerical analysis was within maximum error of 0.13% and 0.3%, respectively, compared to the analytical solution.

In the case of both gradients, the mass uptake was obtained and the comparison between the two analytical and numerical analyses was made by calculating the coefficient of diffusion. The coefficient of diffusion is obtained from the initial slope of normalized weight gain curve versus square root of time ($t^{0.5}$) according to the following equation [129]:

$$D = \frac{\pi}{16}\left(\frac{M_2 - M_1}{M_\infty}\right)^2 \left(\frac{h}{\sqrt{t_2} - \sqrt{t_1}}\right)^2 \tag{5-56}$$

And if t_1 and M_1 are taken to be zero and M_2 is considered as half the equilibrium moisture (M_∞), then D can be calculated from Equation 4-4.

The calculated coefficient of diffusion from the numerical analysis results using Equation (5-56) and considering t_1 and t_2 equal to the two initial times of moisture uptake had an error of 2.1% compared to the analytical results. Therefore, the 2D model can also reasonably analyze the diffusion mechanism using PDE module of COMSOL Multiphysics®.

5.5.3 Heat Conduction

The last phenomenon considered for uncoupled physics modeling is the physics of heat conduction. In order to verify the capability of PDE module of COMSOL Multiphysics® in modeling the heat conduction in a typical PC/ABS bar, two numerical analyses are performed and the results are compared. The first analysis is the reference one developed using the built-in module of heat transfer in COMSOL Multiphysics® and the second one includes the PDE equation of uncoupled physics developed using the PDE module. For this purpose, a 2D analysis of a PC/ABS bar with dimensions 25×3 *mm* is modeled. There are two parameters involved in modeling heat conduction in the PC/ABS bar: specific heat capacity, c, and heat conductivity, λ_T. The value of c was experimentally determined in section 4.1.3 for the range of 24 °C to 80 °C. For the 2D analysis, the average value of c in the range of 24 °C to 80 °C; *i.e.*, 1200 $J/kg.K$, is considered. For the value of λ_T, the corresponding value for PC material, 0.19 $W/m.K$, available in literature is used. The PC/ABS bar was supposed to be initially at 135 °C then moved to an environment at 65 °C. Therefore, the initial temperature of the bar was set at 135 °C; and for the boundary conditions, the edges of the bar were exposed to a convectional heat flux with convective heat transfer coefficient, h_c, of 9.2 $W/m^2.K$ and surrounding temperature of 65 °C. The calculation of the convective heat transfer coefficient can be found in Appendix B. Because of the part symmetry, only a quarter of the bar was modeled. The temperature at the midpoint of the bar is compared between the numerical analyses performed by the heat transfer module and the PDE module in Figure 5-23.

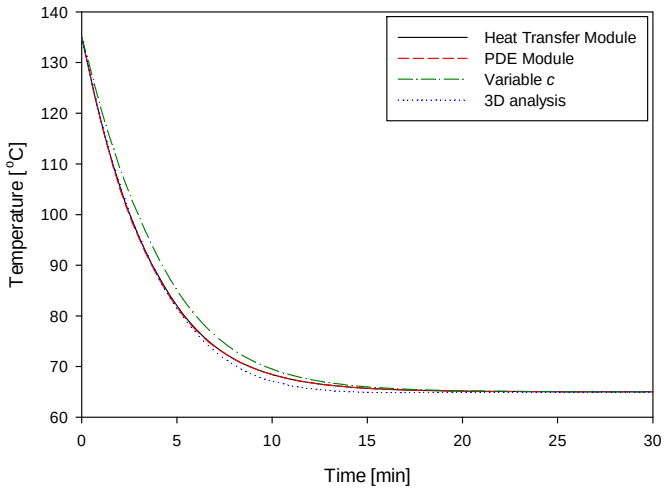

Figure 5-23 Midpoint temperature of the PC/ABS bar in heat conduction analyses.

As seen in Figure 5-23, the two curves corresponding to the analyses conducted by heat transfer and PDE modules overlay. This shows that the heat conduction physics can be correctly modeled using the PDE module.

Next, an analysis was performed using the temperature-dependant specific heat capacity obtained in section 4.1.3 to investigate the difference between using constant and variable c in the heat conduction analysis. Figure 5-23 also illustrates the midpoint temperature of the PC/ABS bar determined using temperature dependant c. It is seen that the maximum difference between the constant and variable c curves is about 4.4 °C suggesting that using the temperature-dependant c does not make a significant difference in the midpoint temperature. Therefore, in the analyses of coupled physics that follow this section, the constant c equal to 1200 $J/kg.K$ is applied. Also depicted in Figure 5-23 is the midpoint temperature of the PC/ABS bar performed using a 3D analysis. For the 3D analysis, a PC/ABS bar with dimensions 64×25×3 *mm* was modeled. The comparison between the obtained curve from the 3D analysis and the corresponding curve obtained from the 2D analysis shows no noticeable difference (maximum difference of 1.4 °C) between the midpoint temperatures obtained from the two analyses. This verifies using a 2D analysis instead of a 3D analysis for heat conduction analyses in the coupled physics modeling.

5.6 Coupled Physics Modeling

5.6.1 Coupled Linear Elasticity-Diffusion-Heat Conduction

This section presents an example of 2D modeling of triple coupled physics of structural mechanics, mass diffusion, and heat conduction. For the structural mechanics it is assumed that the material has a linear elastic behaviour. The governing equations used for modeling are the set of coupled equations (5-31) to (5-33) developed by Rambert *et al.* [46]. These equations are modeled using the PDE module of COMSOL Multiphysics® and the results are compared with the corresponding results from the work of Rambert *et al.* [46], which have already been experimentally verified by other researchers in the field [50]. The comparison, therefore, enables us to validate the current modeling for the coupled linear elasticity-diffusion-heat conduction using the PDE module of COMSOL Multiphysics®.

In order to model the three coupled physics in COMSOL Multiphysics®, a known example problem has been investigated. A 2D model was developed for a gas pipe, Figure 5-24, to facilitate a parametric analysis of the coupling conditions. This is the example Rambert *et al.* [46] have considered for their parametric study on the triple coupled physics. Rambert *et al.* [46] employed finite element analysis of ABAQUS® for numerical implementation of the direct coupling in the governing equations and developed a user-defined element (UEL) for this purpose. The technique they have applied considers the coupling between the three physics involved in the problem; however, the software package they employed requires developing a new type of element for analysis using programming packages such as Intel® FORTRAN.

The pipe geometry, which is identical to that used for uncoupled physics presented in 5.5.1, has an internal diameter of 5 *mm* and a thickness of 1 *mm*. Because of the symmetry of the pipe only a quarter of it has been modeled. In this analysis, the pipe is made of polyvinylidene fluoride (PVDF) with material characteristics presented in Table 5-1.

Table 5-1 Material characteristics of a PVDF sample and CO_2 at 21 °C [47]**.**

ρ	λ	μ	c	λ_t	α_T^e	s_g	D	α_d^e
[kg/m^3]	*[MPa]*	*[MPa]*	*[J/kg.K]*	*[W/m.K]*	*[1/K]*	*[1/MPa]*	*[m^2/s]*	*[-]*
1745	2000	631	1045	0.26	10^{-5}	5.539×10^{-3}	9.8×10^{-12}	2.2×10^{-13}

In Table 5-1, s_g indicates the solubility coefficient of CO_2 in PVDF-CO_2 mixture and is used to normalize the gas concentration expressed in *MPa*. The pipe is used for transporting carbon dioxide (CO_2) and therefore, is under internal pressure, temperature, and gas concentration variations. The boundary conditions and initial conditions as well as loading diagrams are shown in Figures 5-24 and 5-25, respectively.

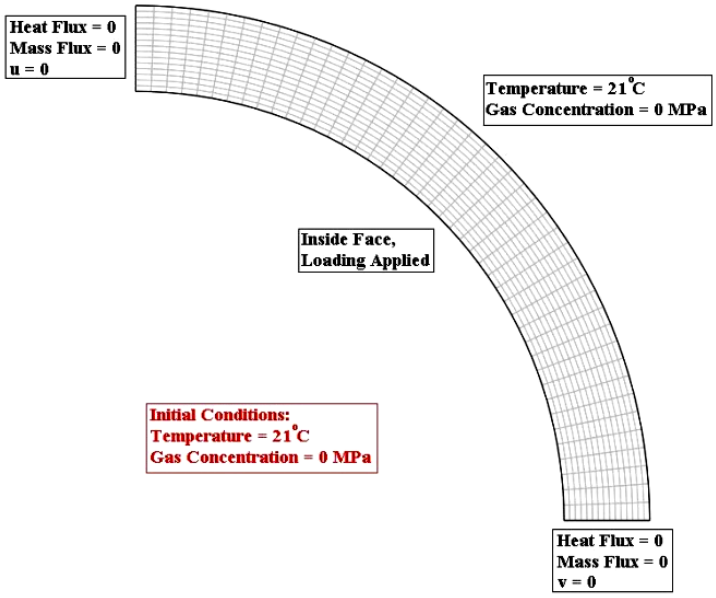

Figure 5-24 Meshed pipe model with boundary conditions and initial conditions (adopted from reference [47]**).**

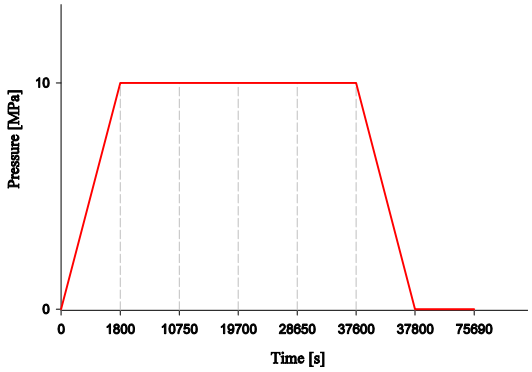

(a)

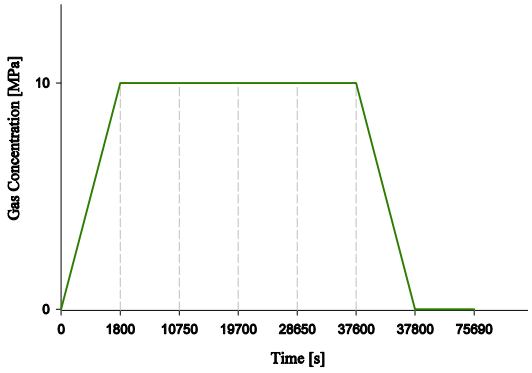

(b)

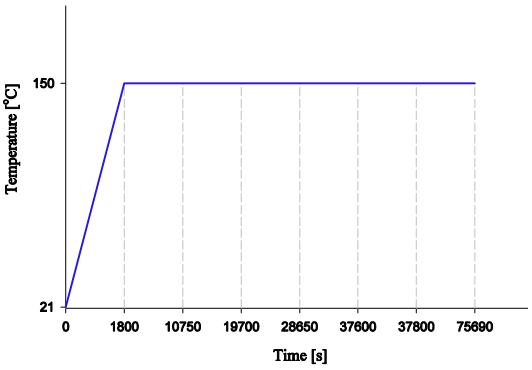

(c)

Figure 5-25 Applied loading diagrams on the inside face of the pipe, (a) pressure, (b) gas Concentration, (c) temperature (adopted from reference [46]**).**

There are five coupling coefficients in the governing equations (5-31) to (5-33): α_T^e, α_d^e, K_μ, $C_{T\mu}$, and C_{TY}. The coupled equations were solved by introducing the five coefficients to the model successively. The effects of different values of the coupling coefficients on displacement, gas concentration, and temperature were investigated and the results were compared with the results reported by Rambert *et al.* [46].

The first coefficient being studied was K_μ. When all coupling coefficients are zero except K_μ, the only physical behaviour which is affected by this coefficient is heat transfer. Figure 5-26 shows the effect of K_μ on radial nodal values of temperature (T) compared with the uncoupled case (T_1) at different times.

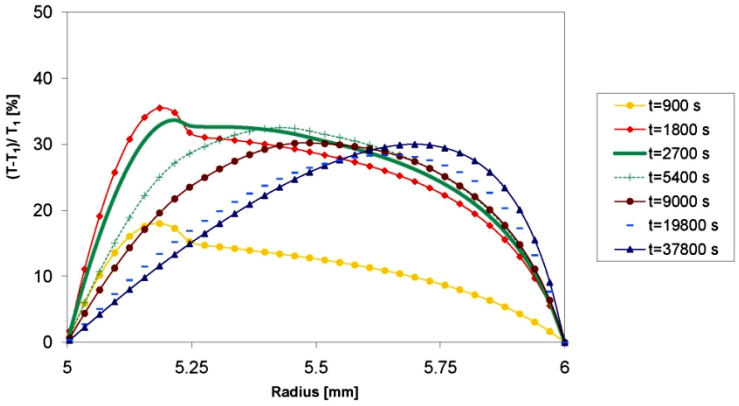

Figure 5-26 The effect of K_μ on radial nodal temperature (T) compared with the uncoupled case (T_1) for $K_\mu = 2\times10^4$ kg.s/m^3.

The next coupling coefficients studied were the elastic coefficients of thermal and hygroscopic expansion (α_T^e and α_d^e). These coefficients affect the stress analysis by introducing expansions due to temperature and concentration changes in the material. The effects of thermal and hygroscopic expansions on radial displacement of the pipe's nodes for different values of K_μ are depicted in Figure 5-27. These values were obtained for a point at a distance of 0.25 *mm* from the internal face of the pipe's wall. A comparison of these curves show a competition between the effect of internal gas pressure and the effects of thermal and diffusion expansion on radial displacement.

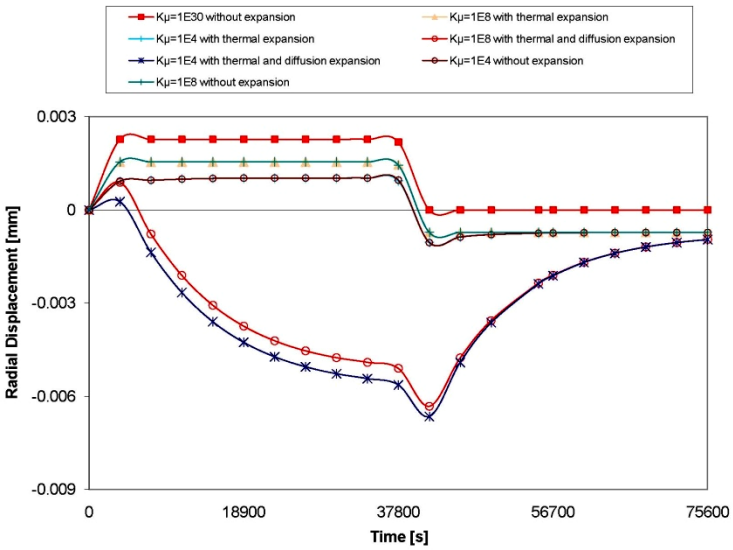

Figure 5-27 The effect of expansion coefficients on radial displacement for different values of K_μ obtained at r = 5.25 mm.

As seen in Figure 5-27, hygroscopic and thermal expansions affect the radial displacement, but the effect of hygroscopic expansion is greater than that of thermal expansion for this type of material and loading conditions. K_μ has also an effect on radial displacement but the effect is not that significant.

$C_{T\mu}$ was the next coupling coefficient that was studied. Figures 5-28 and 5-29 show how this coefficient influences the radial nodal values of temperature and concentration at different times. However, this effect is not obviously great (less than 1% for temperature and 0.005 MPa for concentration) since the value of $C_{T\mu}$ is small. For larger values of $C_{T\mu}$, the effect is more pronounced.

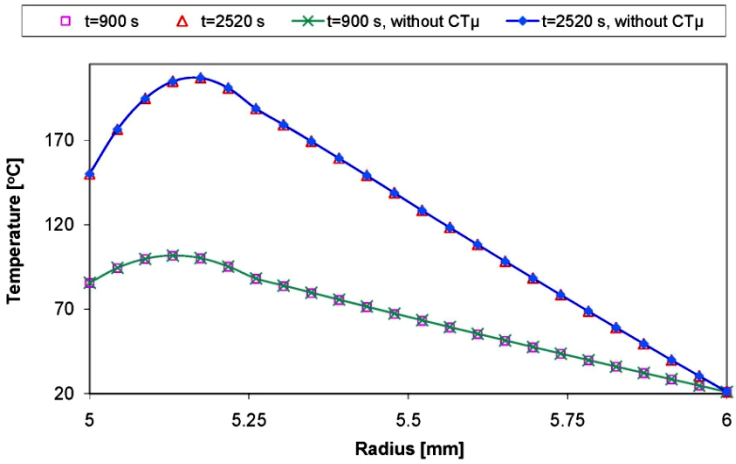

Figure 5-28 The effect of $C_{T\mu}$ value (10^{-2} $kg/(m.s.K)$) on radial values of temperature.

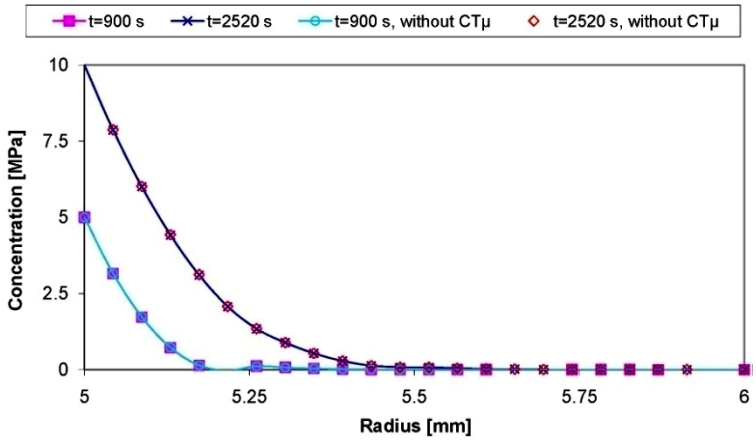

Figure 5-29 The effect of $C_{T\mu}$ value (10^{-2} $kg/(m.s.K)$) on radial values of gas concentration.

Finally, the effect of the coupling coefficient C_{TY} was modeled. Figures 5-30 to 5-32 show the effect of this coefficient on temperature, concentration, and radial displacement, respectively. These are the results of the total coupled case, in which all the five coupling coefficients are nonzero.

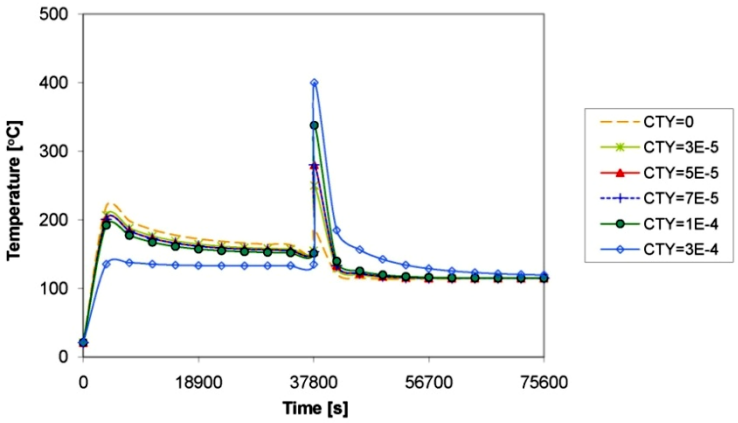

Figure 5-30 The effect of different values of C_{TY} on temperature at the radius of 5.25 *mm*.

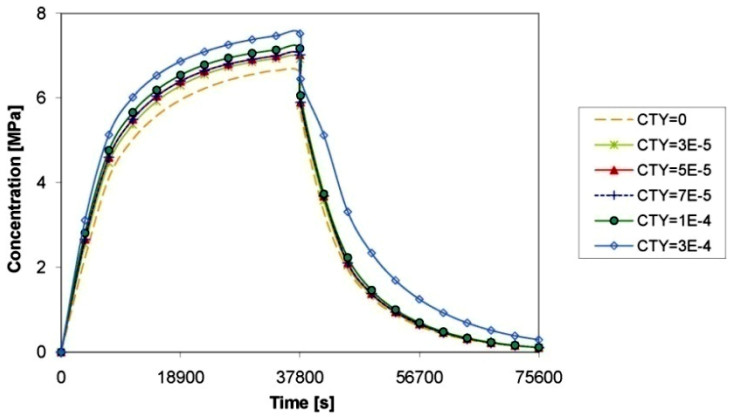

Figure 5-31 The effect of different values of C_{TY} on concentration at the radius of 5.25 *mm*.

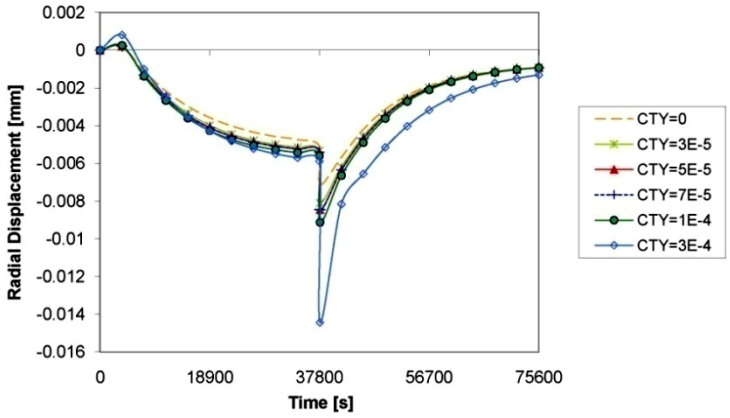

Figure 5-32 The effect of different values of C_{TY} on radial displacement at the radius of 5.25 *mm*.

As seen in figures above, C_{TY} has a direct effect on the values of temperature and concentration; and changes the values of radial displacement through changing the values of temperature and concentration.

There is a good agreement between the results of all the coupling coefficients modeled with COMSOL Multiphysics® and the results presented in the work of Rambert *et al.* [46]. The corresponding figures from work of Rambert *et al.* [46] as they relate to Figures 5-26 to 5-32 are provided in Appendix C for the purpose of comparison.

5.6.2 Coupling Coefficients — Second and Third Sets

There are several coupling coefficients which link the three physics of structural mechanics, moisture diffusion, and heat conduction to one another. These coefficients, which are presented in the governing equations (5-31)-(5-33) and (5-36)-(5-38), can be categorized into three sets, as follows:

i. α_T^e and α_d^e

These coefficients deal with the interaction of temperature and moisture changes with the elastic part of the structural mechanics (indicated by the superscript *e*). These coefficients have been obtained experimentally and the results were presented in sections 4.3.1 and 4.3.2, respectively.

ii. $C_{T\mu}$ and C_{TY}

These two coupling coefficients link the transfer of mass with heat. The coefficient $C_{T\mu}$ represents the effect of temperature (chemical potential) gradient effect on the mass (entropy) flux, and C_{TY} corresponds to the effect of temperature (concentration) variation on the chemical potential (entropy). These coefficients are obtained based on a comparison between experimental results and numerical analyses.

iii. α_T^{ani}, α_d^{ani}, C_{ST}, and $C_{S\mu}$

These coefficients deal with the interaction of temperature and moisture changes with the viscoelastic part of the structural mechanics. α_T^{ani} and α_d^{ani} are approximated using the corresponding elastic coefficients; *i.e.*, α_T^e and α_d^e. The coefficients C_{ST} and $C_{S\mu}$ are obtained using a similar method to that employed for obtaining the coefficients $C_{T\mu}$ and C_{TY}.

5.6.2.1 Coupled Moisture Diffusion and Heat Conduction — 2nd Set

The induction of mass flux by temperature gradient in a material system is referred to in thermophysics as the Soret effect (or Ludwig-Soret effect). This effect is represented in this work by the coupling coefficient, $C_{T\mu}$. The Soret effect has been first formulated in detail by Charles Soret in 1978 [145] and many experimental methods were developed since then to obtain the Soret coefficient for different material systems. Platten [146] has reviewed some of these techniques in two categories of Convectionless Systems and Convective Coupling. These methods, which are used for measuring the Soret coefficient in solutions and liquid systems, include the standard Soret cell, the beam deflection technique, the thermal diffusion forced Rayleigh scattering technique, the Rayleigh-Benard configuration, and the thermogravitational process.

There are also studies in literature related to the thermodiffusion and the Soret effect in solid systems. For instance, Janek *et al.* [164] studied the transport of ionic charges induced by temperature gradient in ionic solids and conductors. The Soret effect has also been studied in porous systems by some authors. A recent example is the work of Davarzani *et al.* [165], in which a new technique is developed to measure the Soret effect in a porous medium using a two bulb apparatus. To the best of the author's knowledge, there is no work in literature on the experimental method of finding the Soret effect in water-polycarbonate systems.

Therefore, due to the practical difficulties in obtaining the coupling coefficients; namely, $C_{T\mu}$ and C_{TY}, to describe the process of moisture diffusion into the PC/ABS material, the coefficients were estimated by comparing between experimental results and the numerical analyses. As these two coefficients deal with the interaction of temperature and mass flux, the numerical analysis also involves modeling moisture diffusion coupled with heat conduction in a PC/ABS bar.

The premise of this estimation technique is that the moisture uptake of the bar obtained from a 2D analysis can be compared with the moisture uptake of samples used in moisture uptake experiments (section 4.1.4). Since the sample moisture uptake is physically affected by the values of the coupling coefficients, $C_{T\mu}$ and C_{TY}, the values of these coefficients can be set in such a way that the numerical moisture uptake gets as close as possible to the experimental moisture uptake. This can be accomplished using an optimization algorithm.

This method of using an optimization method has been applied by other researchers. For instance, Benjelloun-Dabaghi and Benali [166] used an optimization method together with a parameter

sensitivity study to find the coefficient of diffusion and the maximum gas concentration in the permeation tests of CO_2-polyethylene (PE) system. A similar approach has been followed in another study by Scheichl *et al.* [167]. They used a nonlinear least-squares optimization method to find the characteristic gas transport parameters in different polymer-gas systems.

The optimization method used in this study employs a nonlinear least-squares curve fitting solver (*lsqcurvefit*) in MATLAB® (MATLAB® R2010b). The objective is to find the best values of the coupling coefficients, $C_{T\mu}$ and C_{TY}, for curve fitting the moisture uptake versus time curve determined experimentally. In mathematical language, if we assume that the vector x contains the variables that provide the best curve fitting, the optimization function *lsqcurvefit* finds the vector x that solves the following problem [168]:

$$\min_x \sum_i (F(x, xdata_i) - ydata_i)^2 \tag{5-57}$$

where *xdata* and *ydata* are the input variables and observed output variables, respectively, and F is a function which returns the objective function (moisture uptake in this study) evaluated at x. *xdata* and *ydata* are experimental time points and the corresponding sample moisture uptake results obtained from mass uptake experiments. The algorithm used for the *lsqcurvefit* solver was the *trust region reflective* algorithm, which is suitable for problem containing constraints on the vector x.

The objective function in the optimization method used in this work is provided by a 2D analysis conducted in COMSOL Multiphysics®, from which moisture uptake can be obtained. Therefore, COMSOL Multiphysics® and MATLAB® were linked to perform the optimization method.

Since the 2D analysis only involves the coupled models of moisture diffusion and heat conduction, the PDE equations (5-32) and (5-33) are used without the terms related to structural mechanics effect, as follows:

Mass Diffusion

$$\rho \dot{Y}_d = \rho D \; Div(\nabla Y_d) + \left(C_{T\mu} - K_\mu C_{TY}\right) Div(\nabla T) \tag{5-58}$$

Heat Transfer

$$\rho C_{\boldsymbol{\varepsilon}^e,Y_i,T}\dot{T} = C_{TY}\left(K_\mu C_{TY} - 2K_{T\mu}\right)(\nabla T)^2 + \left(\frac{\lambda_T}{T} + C_{TY}\left(K_\mu C_{TY} - 2K_{T\mu}\right)\right)TDiv(\nabla T)$$

$$+2\frac{\rho D}{K_\mu}\left(C_{T\mu} - C_{TY}K_\mu\right)\nabla T.\nabla Y_d + \frac{\rho D}{K_\mu}\left(C_{T\mu} - C_{TY}K_\mu\right)TDiv(\nabla Y_d) + \frac{\rho^2 D^2}{K_\mu}(\nabla Y_d)^2 + R \tag{5-59}$$

According to Equations (5-58) and (5-59), the coupling coefficients $C_{T\mu}$ and C_{TY} together with the coefficient K_μ form multiplicative factors for different terms of the PDEs. Therefore, these factors, which are functions of $C_{T\mu}$, C_{TY}, and K_μ, are defined as three new coefficients, *coeff1*, *coeff2* and *coeff3*, from which the coupling coefficients $C_{T\mu}$ and C_{TY} as well as the coefficient K_μ can be derived. The new coefficients, *coeff1 to coeff3*, are defined as follows:

$$coeff1 = C_{T\mu} - K_\mu C_{TY} \tag{5-60}$$

$$coeff2 = C_{TY}\left(K_\mu C_{TY} - 2K_{T\mu}\right) \tag{5-61}$$

$$coeff3 = \frac{\rho^2 D^2}{K_\mu} \tag{5-62}$$

The PDE expressions (5-58) and (5-59) will then get the following form:

Mass Diffusion

$$\rho\dot{Y}_d = \rho D\ Div(\nabla Y_d) + (coeff1)Div(\nabla T) \tag{5-63}$$

Heat Transfer

$$\rho C_{\boldsymbol{\varepsilon}^e,Y_i,T}\dot{T} = (coeff2)(\nabla T)^2 + \left(\frac{\lambda_T}{T} + coeff2\right)TDiv(\nabla T)$$

$$+2\frac{(coeff1)(coeff3)}{\rho D}\nabla T.\nabla Y_d + \frac{(coeff1)(coeff3)}{\rho D}TDiv(\nabla Y_d) + (coeff3)(\nabla Y_d)^2 \tag{5-64}$$

Therefore, the 2D analysis conducted in COMSOL Multiphysics® returns the mass uptake (objective function) as a function of the three coefficients, *coeff1* to *coeff3*, from which the coefficients $C_{T\mu}$, C_{TY}, and K_{μ} can be calculated. The PC/ABS bar used for the 2D analysis has dimensions of 25×3 *mm* and due to the part symmetry, only 1/4th of the bar was modeled. The numerical model was run using experimental conditions in order to compare moisture uptake of the bar with experimental results. As described in section 3.3.1.4, the mass uptake experiments were performed by storing the samples at four hygrothermal conditions after thermal history erasure at 135 °C. Therefore, the initial values of moisture concentration and temperature were set at 0 and 135 °C, respectively, and the boundary conditions are the equilibrium moisture uptake and the aging temperature, which are applied at the two exterior surfaces of the bar (shown in Figure 5-33). In order to consider the symmetry, the moisture and heat flux at the other two surfaces are set equal to zero. The numerical analysis was performed for 3 hours, which is longer than the time it takes for the temperature to equilibrate. Before the temperature equilibrates, the effects of the terms in PDE equation containing the coupling coefficients are more pronounced and once the temperature equilibrates, these terms become negligible.

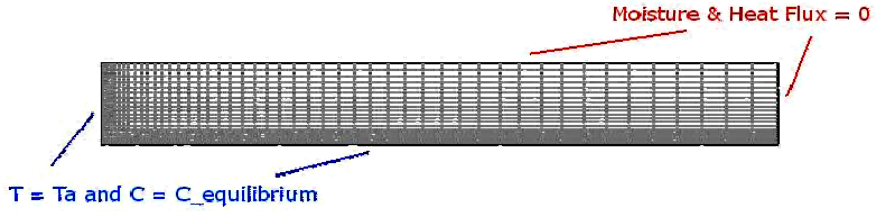

Figure 5-33 A quarter of the bar modeled for the coupled analysis of moisture diffusion and heat conduction.

The optimization method has been applied for the four hygrothermal conditions and the results of the coefficients, $C_{T\mu}$, C_{TY}, and K_{μ} are tabulated in Table 5-2. In this table, the coefficient of determination, R^2, is also presented for each condition.

Table 5-2 The values of the coefficients obtained from MATLAB® optimization method.

Condition	$C_{T\mu}$ [kg/(m.s.K)]	C_{TY} [J/(kg.K)]	K_{μ} [kg.s/m^3]	R^2
50°C/50%RH	2.88×10^{-12}	3.95	7.23×10^{-13}	0.70
65°C/50%RH	2.79×10^{-9}	710.0	3.83×10^{-12}	0.92
50°C/93%RH	2.08×10^{-9}	79.7	2.61×10^{-11}	0.85
65°C/93%RH	1.83×10^{-9}	14.0	1.31×10^{-10}	0.79

The obtained coefficients at each condition are then employed to obtain the moisture uptake at the other three conditions to determine how the moisture uptake behaviour is affected by the coefficients and which sets of coefficients can provide the best result for all the 4 conditions. It was found out that the coefficients obtained for condition of 50°C/93%RH can best represent the experimental data for all the conditions.

Moreover, another experiment was performed in which a higher temperature gradient was imposed at the beginning of the moisture uptake so that the coupling coefficients become more influential in affecting the moisture uptake. The PC/ABS bars were conditioned inside an environmental chamber after thermal history erasure at 135 °C. The condition of the sample at the beginning of the moisture uptake stage was 50°C/50% RH but the temperature was ramped to 65 °C in 30 minutes and then was held constant. Therefore, the gradient of temperature was expected to be more than the case where the hygrothermal conditioning involved constant temperature levels. A numerical analysis modeling the coupled moisture diffusion and heat conduction was performed for the new hygrothermal condition with the coupling coefficients obtained for the condition of 50°C/93% RH. It was found that the numerical moisture uptake curve fits to the experimental results with a coefficient of determination of 0.94. This is while the coefficient of determination of the curve fit for a case with zero coupling coefficients is 0.93. The maximum difference between the numerical and experimental results also decreased from 7.3% to 6.7% when the coupling coefficients were changed from zero to those obtained for the condition of 50°C/93% RH.

5.6.2.2 Coupling with Structural Mechanics — 3rd Set

5.6.2.2.1 α_T^{ani} and α_d^{ani}

The anelastic coefficients of thermal expansion, α_T^{ani}, and the anelastic coefficients of hygroscopic expansion, α_d^{ani}, are related to the interaction of temperature and moisture changes with the viscoelastic part of the structural mechanics. These coefficients are approximated using the corresponding elastic coefficients; *i.e.*, α_T^e and α_d^e.

To obtain an approximate value for the anelastic coefficients, a typical example is considered. A bar is assumed to be constrained at the two ends and a temperature change is applied to the material resulting in a thermal stress state. If the bar is assumed to be made of PC/ABS following the rheological model of generalized Kelvin-Voigt, the thermal stress will be:

$$\sigma = \sigma^e = \sigma^{an_i} + \sigma^{\mathrm{v}} \tag{5-65}$$

$$-3K^e\alpha_T^e\Delta T = -3K^{an_i}\alpha_T^{an_i}\Delta T + \sigma^{\mathrm{v}} \tag{5-66}$$

σ^{v} can be neglected and therefore:

$$\alpha_T^{an_i} = \frac{K^{an_i}}{K^e}\alpha_T^e \tag{5-67}$$

If we consider the properties of an un-aged sample of PC/ABS at 65 °C, we will have:

$$\alpha_T^{an_1} = 0.96\,\alpha_T^e \quad , \qquad \alpha_T^{an_2} = 0.13\,\alpha_T^e \tag{5-68}$$

Similarly, we can obtain the following relation between elastic and anelastic coefficients of hygroscopic expansion:

$$\alpha_d^{an_1} = 0.96\ \alpha_d^e \quad , \qquad \alpha_d^{an_2} = 0.13\ \alpha_d^e \tag{5-69}$$

where α_T^e and α_d^e are equal to the experimental values obtained in sections 4.3.1 and 4.3.2.

5.6.2.2.2 C_{ST} and $C_{S\mu}$

The third set of coupling coefficients also include the coefficients C_{ST} and $C_{S\mu}$, which are related to the interaction of structural mechanics with heat conduction and moisture diffusion, respectively. These coefficients are obtained using an optimization method similar to the one applied to obtain the second set of coupling coefficients. The experiments whose results are compared against numerical analyses include applying mechanical load on a PC/ABS sample while it is being exposed to humid environments. The mechanical loading system is applied in creep mode by exerting a constant force on a PC/ABS bar in a 3-point bending mode. As the test is conducted in a humid environment, moisture diffusion occurs simultaneously with mechanical loading, and therefore a 3D analysis can appropriately model the experimental setup. However, due to the high number of elements required to do a correct 3D analysis and because of significantly large degrees of freedom, an unreasonably long run-time is required to obtain the coupling coefficients using an optimization method. This problem can be overcome by doing a 2D analysis provided that the 2D model can substitute the 3D analysis without producing noticeable errors.

5.6.2.2.2.1 2D vs. 3D analysis

In order to validate the 2D analysis, a comparison is first made between the mass uptake of a PC/ABS bar obtained from 2D and 3D analyses of moisture diffusion. Figure 5-34 shows the mass uptake of a PC/ABS bar under the condition of 65C/50% RH within the first 10 hours of diffusion obtained from both 2D and 3D analyses.

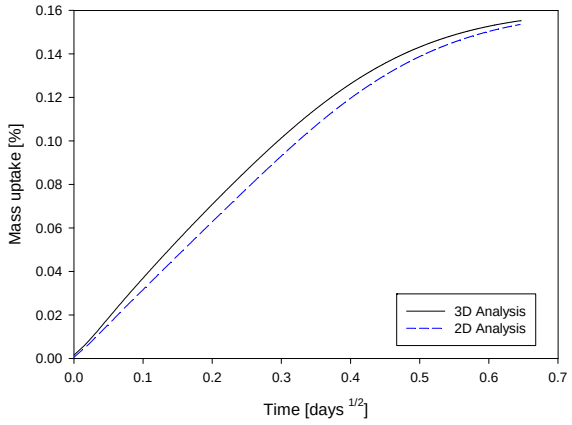

Figure 5-34 Moisture uptake of a PC/ABS bar obtained from 2D and 3D diffusion analyses.

The comparison of the moisture uptake curves in Figure 5-34 reveal a maximum error of about 9% when a 3D moisture diffusion analysis is replaced by the corresponding 2D analysis.

Next, the three-point bending mode of a rectangular bar is analyzed using plane strain mode of the structural mechanics module in COMSOL Multiphysics® to verify the applicability of a 2D analysis for modeling structural mechanics of a bending beam. In a three-point bending mode, the loads, boundary conditions, and geometry are symmetric and therefore, only half of the beam is modeled. A rectangular beam with dimensions 32×3 *mm* and Young's modulus and Poisson's ratio of 2.2 *GPa* and 0.37, respectively, is modeled in the plane strain mode with the thickness of 13 *mm* (equal to the width of a PC/ABS bar used in creep experiments). The beam is under a three-point bending mode and therefore, the lower surface was fixed vertically at a point located at a distance of 25 *mm* from the midpoint of the beam (which is the left edge of the half beam). This boundary condition represents one of the rollers of the three-point bending clamp. The concentrated force in the middle of the beam was simulated with a force (equal to 5 *N*) per area on the left edge of the half beam (shown in Figure 5-35) because this is the way the boundary condition can be applied in PDE mode of COMSOL Multiphysics®. The meshed beam and the schematic of loading and boundary conditions are illustrated in Figure 5-35.

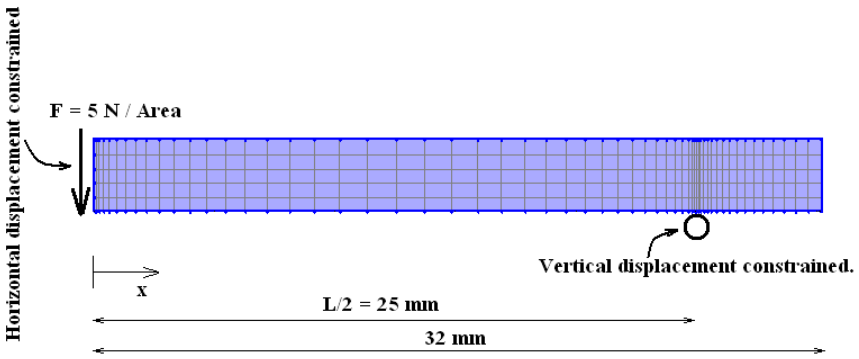

Figure 5-35 The meshed beam and the applied loading and boundary conditions.

The deflection and the *x*-component of stress obtained along the beam length from the static analysis are shown in Figures 5-36 and 5-37, respectively.

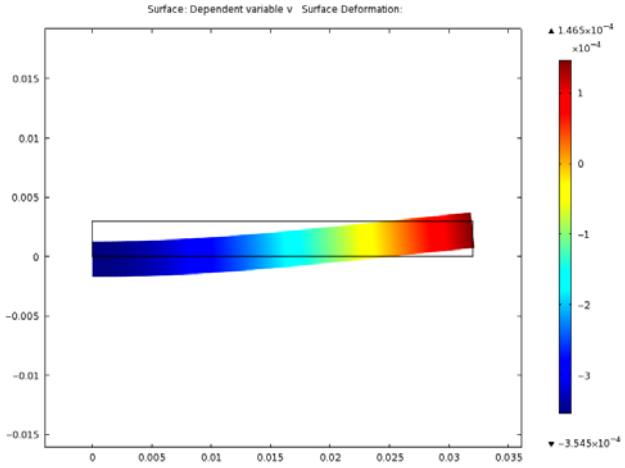

Figure 5-36 The contour of vertical deflection [*m*] of the beam.

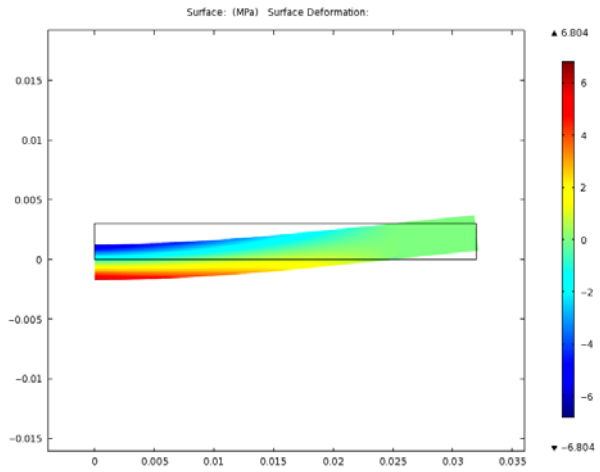

Figure 5-37 The contour of the *x*-component of stress [*MPa*] along the beam.

The numerical results are compared with the theoretical values of deflection, δ_v, and the *x*-component of stress, σ_x, obtained using the following equations, in Figures 5-38 and 5-39, respectively:

$$\delta_v = \frac{F\left(\frac{L}{2} - x\right)(4x^2 - 4Lx - 2L^2)}{48EI} \quad , \quad 0 \le x \le \frac{L}{2} = 25\ mm \tag{5-70}$$

$$\delta_v = \frac{F\left(\frac{L}{2}\right)^2\left(x - \frac{L}{2}\right)}{4EI} \quad , \quad \frac{L}{2} \le x \le 32\ mm \tag{5-71}$$

$$\sigma_x = \frac{F\left(\frac{L}{2} - x\right)t}{4I} \quad , \quad 0 \le x \le \frac{L}{2} = 25\ mm \tag{5-72}$$

$$\sigma_x = 0 \quad , \quad \frac{L}{2} \le x \le 32\ mm \tag{5-73}$$

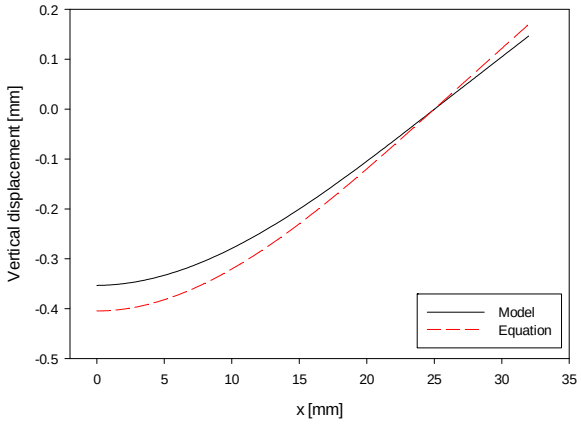

Figure 5-38 The vertical deflection of the beam along its length obtained from the model and equation.

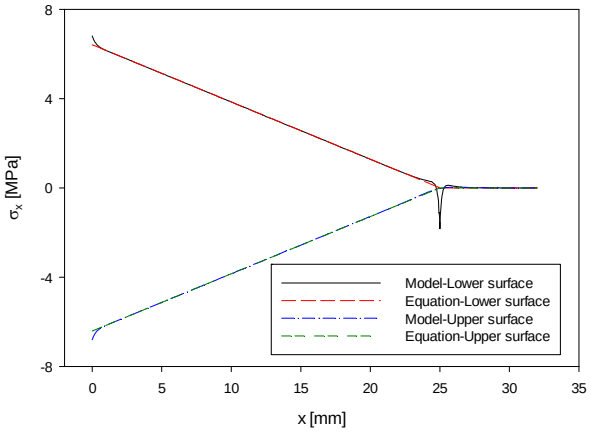

Figure 5-39 The *x* component of stress along the beam obtained from the model and equation.

As seen in Figure 5-39, the stress obtained from the 2D analysis exactly matches with the theoretical stress except in the vicinity of the points where the load ($x = 0$) and the boundary condition ($x = 25$ *mm*) were applied. The high stresses in these regions indicate the stress concentration caused by constrained loading nodes. Figure 5-38 also shows a similar trend between the deflection obtained from the 2D analysis and the theoretical value and the difference between the two values reaches at a maximum value of 13%. This difference can be attributed to the fact that the thickness of 13 *mm* used for plane strain mode is not large enough as compared to the beam dimensions.

Considering the two analyses mentioned above, a 2D analysis was used to find the coupling coefficients between the structural mechanics with the physics of heat conduction and moisture diffusion; *i.e.*, C_{ST} and $C_{S\mu}$.

5.6.2.2.2.2 Experiments

To determine the coupling coefficients, C_{ST} and $C_{S\mu}$, the numerical analysis results are compared with the corresponding results from experimental tests. The tests are performed on a PC/ABS bar with nominal dimensions 64×13×3 *mm*. The sample is first stored in a desiccator for 48 hours, and then placed inside an oven at 135 °C for 10 minutes to remove the thermal history of the material. Next, the PC/ABS bar is loaded in a three-point bending mode inside an environmental chamber at 65 °C/50% RH. A load of 8.48 N is applied at the mid-point of the sample by two brass pieces suspended at the two ends of a thin rod. The constant load simulates the creep loading condition. The three-point loading of the sample is illustrated in Figure 5-40.

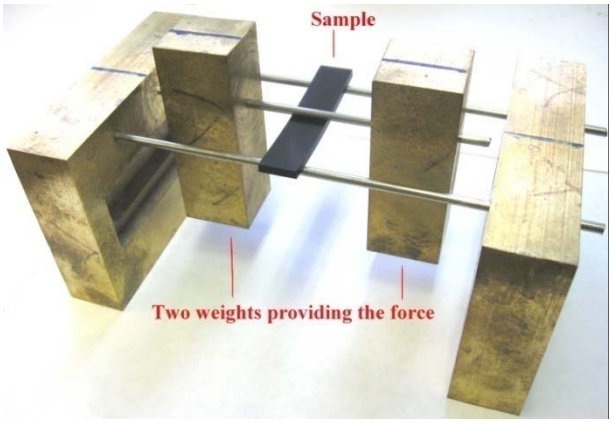

Figure 5-40 The three-point bending clamp.

The sample is loaded for the duration of creep loading (t_1, t_2, and t_3) and then the maximum deflection of the sample is measured after it is removed from the creep clamp. The measurement is performed using a stereo microscope which is supplied with an attachment that measures the microscope stage travel in both *x* and *y* directions with an accuracy of 0.001 *mm*. This measurement technique will be referred from here on as the *microscopic measurement technique*. Figure 5-41 shows a deformed PC/ABS bar following a creep test of 10 hours. In this figure, two kinds of

deflection are depicted: δ_{v1} related to the deflection of the midpoint of the bar with respect to the undeformed state, and δ_{v2} corresponding to the deflection of the end point of the bar.

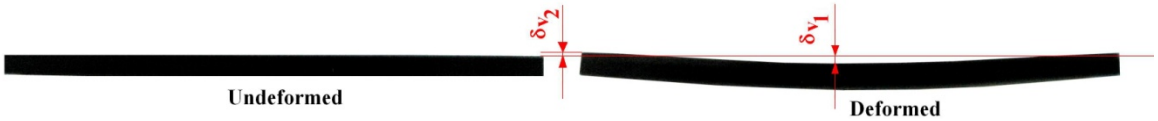

Figure 5-41 Deflections of a PC/ABS bar due to three-point bending creep.

The deflection of the bar is measured by attaching the deformed sample to a reference straight plate and therefore the measured deflection reflects the summation of δ_{v1} and δ_{v2}. Since the measurement is performed after the sample is removed from the clamp, the measured deflection does not include the elastic part.

In order to verify the accuracy of the microscopic measurement technique, similar tests are conducted inside an oven at 65 °C and the measured deflection values are corrected with the results of similar tests performed using a DMA. The deflection measured by DMA is the deflection in the middle of the plate, δ_{v1}. A numerical analysis is also performed to obtain δ_{v2}. The tests in the oven were performed for three creep loading durations of 2, 5, and 10 hours. A new sample was used for each creep loading duration and 2 replicates were tested for each time measurement. The DMA tests were done for two replicates tested for 10 hours of aging. Figure 5-42 compares the deflection values measured using the microscopic measurement technique with those obtained from tests conducted in the DMA.

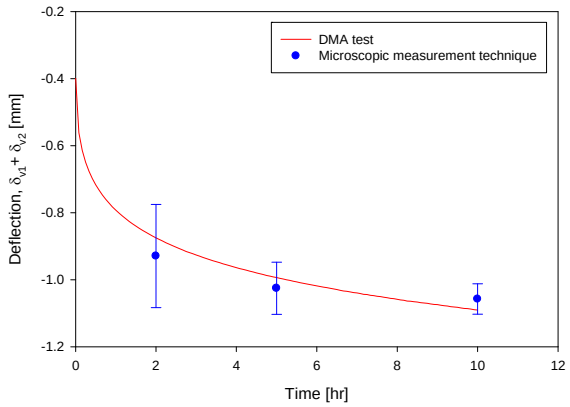

Figure 5-42 Comparison of the deflection between microscopic measurement and DMA techniques.

The measured deflection values using the microscopic measurement technique are corrected with the corresponding values obtained from DMA tests. The calculated correction factors are then applied to the measured values, as described in the following section.

The tests conducted on PC/ABS bars inside a DMA also provide the compliance of the sample under creep loading at 65 °C. The obtained compliance will be used in the numerical analysis of the following section.

5.6.2.2.2.3 Numerical Analysis and Comparison with Experiments

The coupling coefficients attributed to the interaction between the viscous component of structural mechanics and heat conduction and moisture diffusion are C_{ST} and $C_{S\mu}$, respectively. These coefficients were estimated by applying a MATLAB® optimization algorithm for curve fitting the experimental results. As the experiment is performed under an hygrothermal condition of 65 °C/50% RH, the parameters related to that condition are used for the numerical parameters; *i.e.*, $D = 6.51\ e^{-11}$ m^2/s and $m_\infty = 0.13\%$. The compliance of the material was obtained by applying the time-moisture superposition principle on the compliance curve obtained for samples that were tested in a dry condition at 65 °C inside the DMA furnace (Figure 5-42).

Since there are two elements of Kelvin-Voigt model in the viscoelastic behaviour considered for the 2D analysis, C_{ST} and $C_{S\mu}$ have each two values associated with each element: C_{ST1} and $C_{S\mu1}$ related to element 1 and C_{ST2} and $C_{S\mu2}$ linked to element 2. It was assumed that C_{ST2} and $C_{S\mu2}$ are fractions of C_{ST1} and $C_{S\mu1}$; *i.e.*, $C_{ST2} = m\ C_{ST1}$ and $C_{S\mu2} = n\ C_{S\mu1}$ where $0 \leq m \leq 1$ and $0 \leq n \leq 1$. Therefore, the optimization method finds four variables: C_{ST1}, $C_{S\mu1}$, m, and n, as tabulated in Table 5-3.

Table 5-3 The values of the coupling coefficients obtained from MATLAB® optimization method.

C_{ST1} $[m/(K.s)]$	$C_{S\mu1}$ $[s/m]$	m	n
3.60×10^{-14}	4.11×10^{-14}	0.5	5.0×10^{-5}

The deflection values obtained from the analysis are compared with the experimental values in Figure 5-43. The experimental values are corrected using the correction factors obtained in section 5.6.2.2.2.2.

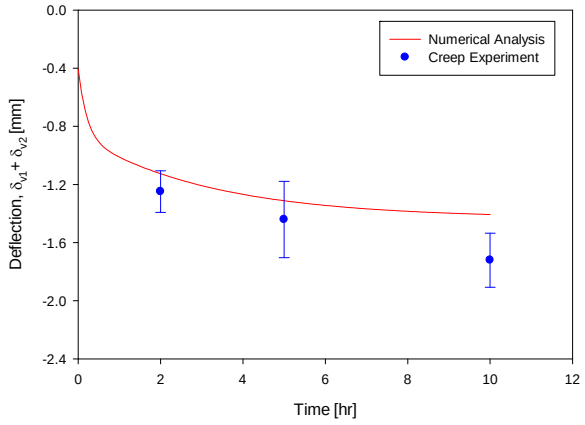

Figure 5-43 The deflection of PC/ABS obtained from a coupled MDT 2D analysis and creep experiments.

There is a maximum error of 22% between the numerical and experimental results. This error can be attributed to the error existing in the 2D analysis of bending of the bar compared to a 3D analysis (discussed previously). This is explored later in the model verification section (section 5.6.4.3).

Also, the moisture uptake of the samples after each creep loading was measured and the results are compared with the numerical results in Figure 5-44.

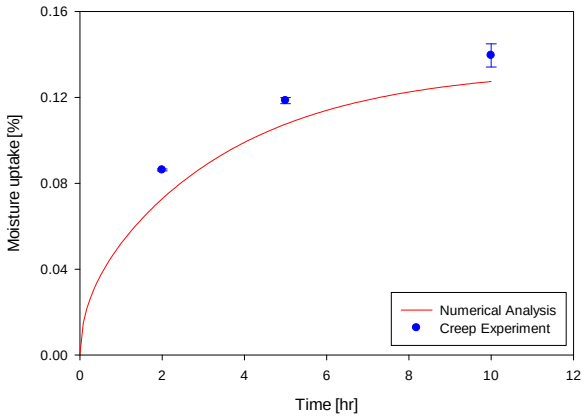

Figure 5-44 The moisture uptake of PC/ABS samples following creep loading.

The difference between the numerical and experimental mass uptake reaches at a maximum value of 19%, which may be mostly related to the error in 2D diffusion analysis.

5.6.3 The Effects of Physical Aging

As explained in section 1.2, there are four physical mechanisms involved in the modeling of coupled moisture diffusion and physical aging in plastic plates: structural mechanics, moisture diffusion, heat conduction, and physical aging. It is assumed that physical aging affects two mechanisms: structural mechanics and moisture diffusion.

5.6.3.1 The Effects on Structural Mechanics

It was described earlier that the structural relaxation in the material caused by the physical aging phenomenon influences the material's stiffness. It was observed in the stress relaxation experiments in Chapter 4 that the longer the PC/ABS blend is aged, the structural relaxation effects on the material's modulus become more pronounced. It was seen that the effect of physical aging is manifested as the shifting of modulus curves along the time axes to longer times (Figure 4-15 in Chapter 4). In those experiments, the samples were sequentially aged and then loaded under stress relaxation modes to measure the modulus of the material. The obtained experimental modulus was curve fitted using KWW model and Prony series. The obtained Prony series together with the shift factors can be used for modeling PC/ABS plates assuming that it follows the rheological model of generalized Maxwell model.

It was also shown previously in this chapter (section 5.5.1.2.1) that the compliance of the PC/ABS blend corresponding to the experimentally measured modulus can be obtained using a numerical analysis. The obtained Prony series for compliance as well as the shift factors can also be employed for modeling PC/ABS plates assuming that it follows the generalized Kelvin-Voigt model.

It should be pointed out that the volumetric change due to physical aging was not directly considered in the governing equations (Equations (5-31) to (5-33) and (5-36) to (5-38)). Although the effects of physical aging on material's volume at long aging times is known (experimental results of volume relaxation in section 4.1.2), incorporating its effect will add further to the complexity of the equations.

5.6.3.2 The Effects on Moisture Diffusion

In the mass uptake experiments discussed in section 4.1.4, it was seen that the structural relaxation during physical aging influences the moisture diffusion of PC/ABS samples that were hygrothermally aged in the four hygrothermal conditions. The effect was pronounced as an anomalous overshoot in the moisture uptake curves. This anomalous behaviour can be modeled by considering a time varying boundary condition. The concept of using time varying boundary condition was proposed by Long and Richman [169] and was later extended to Prony series forms by Cai and Weitsman [170]. In the model of Cai and Weitsman [170], the boundary condition was raised exponentially with time until it reached a plateau. A similar concept of using a time varying boundary condition was applied in this study to model the anomalous overshoot behaviour with the difference that a decaying function was used for boundary condition as follows:

$$C(t) = C_\infty + \frac{A}{1 + \exp\left(\frac{t - t_o}{B}\right)} \tag{5-74}$$

where C_∞ represents the equilibrium concentration; and A, B, and t_o designate the fitting parameters used to fit $C(t)$ to the experimental data.

A 2D analysis of moisture diffusion was performed on a PC/ABS bar having dimensions 25×3 *mm* to model the moisture uptake of the sample. The boundary condition was modeled in the form of Equation (5-74). The four parameters of Equation (5-74) should be determined in such a way that the numerical moisture uptake gets as close as possible to the corresponding experimental value. To achieve this, MATLAB® optimization method was employed with the four parameters of Equation (5-74); *i.e.*, C_∞, A, B, and t_o, as the variables. The coefficient of diffusion, D, was also considered as a fifth variable so that the best curve fit is acquired. The target function was set to be the 2D analysis performed in COMSOL Multiphysics®. The purpose was to obtain the five variables that can best fit the numerical moisture uptake to the experimental values obtained in the mass uptake experiments performed at the hygrothermal conditions (section 4.1.4). Among the four hygrothermal conditions considered for experiments of section 4.1.4, two conditions had the highest degree of overshoot (Table 5-4): 65 °C/50% RH and 50 °C/93% RH. Therefore, the modeling was conducted for these

two conditions and the five variables together with the corresponding coefficient of determination, R^2, were calculated, as tabulated in Table 5-4.

Table 5-4 The variables of time varying boundary condition for modeling overshoot behaviour.

Condition	C_∞	A	$B\ [s]$	$t_o\ [s]$	$D\ [m^2/s]$	R^2
65 °C/50% RH	7.05×10^{-4}	2.93×10^{-4}	2.47×10^{5}	1.63×10^{6}	1.09×10^{-11}	0.98
50 °C/93% RH	3.98×10^{-3}	4.54×10^{-4}	7.94×10^{4}	1.07×10^{6}	5.61×10^{-12}	0.99

The five variables presented in Table 5-4 were used to model the overshoot behaviour in the mass uptake curves for PC/ABS samples under two conditions of 65 °C/50% RH and 50 °C/93% RH in Figures 5-45 (a) and 5-45 (b), respectively.

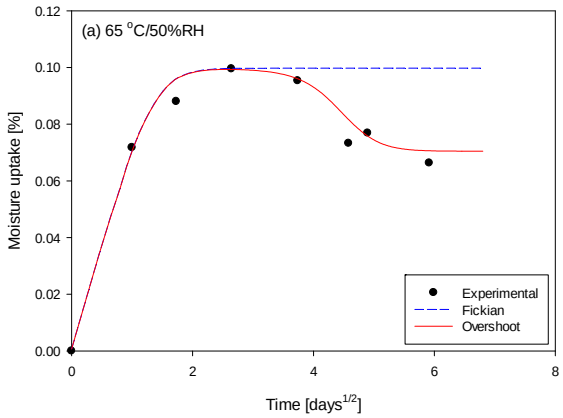

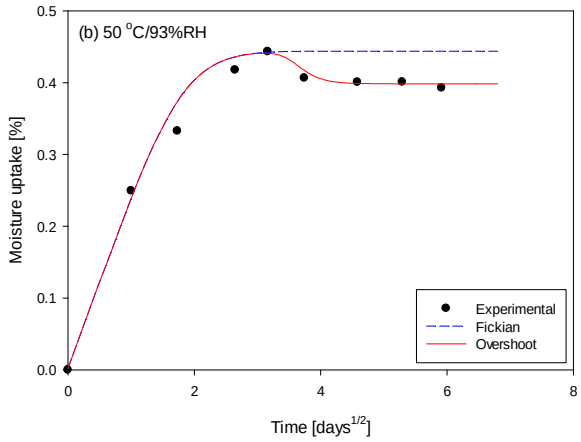

Figure 5-45 Moisture uptake curves obtained from overshoot numerical models for conditions of (a) 65°C/50%RH and (b) 50°C/93%RH.

The overshoot curve illustrated in Figure 5-45 show how the curve is differentiated from the Fickian curve (also depicted in the figure). As discussed earlier in section 4.1.4.4, the difference is attributed to the effect of structural relaxation on the moisture uptake of the PC/ABS samples as desorption of some of the moisture which has already diffused into the material system.

5.6.4 Model Verification Using Thin Housing Component

In previous sections (sections 5.5 and 5.6), different models were developed for both uncoupled and coupled physics. Material characterization experiments were performed (Chapters 3 and 4) and the coupling coefficients were obtained by comparing the results of numerical analyses with experimental results. The developed model for coupled physics is now employed to model the behaviour of PC/ABS blend of an actual part used in service. The backside case of a cell phone housing, which is made of 75/25% PC/ABS polymer blend, is considered for model verification (Figure 5-46).

Figure 5-46 Different views of the backside case of a cell phone housing.

It is seen in Figure 5-46 that the case is thinner than the PC/ABS bars used in experiments discussed in Chapters 3 and 4.

In this section, the major parameter of interest is the deflection of the part, which is a key engineering physical parameter used in the design of components. The following sections describe the experimental work on these plastic cases as well as the corresponding modeling work which follows by a comparison between the experimental results and numerical analyses.

5.6.4.1 Experiments

The first set of experiments includes applying a mechanical load on the samples of the cell phone housing as the part is subjected to moisture diffusion and heat conduction. The specimens of the cell phone housing are stored inside a desiccator for 48 hours and then are exposed to creep loading conditions in a three-point bending mode. The tests are performed inside an environmental chamber at the hygrothermal condition of 65 °C/50% RH. A constant load of 8.48 *N* was applied on the samples for 2, 5, and 10 hours, respectively. Two replicates were used for each time measurement. A typical sample mounted in the creep clamp is depicted in Figure 5-47.

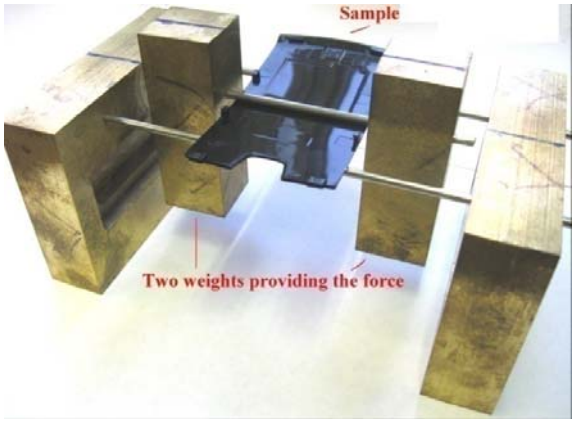

Figure 5-47 A typical sample of cell phone housing under the three-point bending mode.

Following each creep test, the maximum deflection of the case was determined by attaching the deformed sample to a flat reference plate and the distance between the deformed sample and the reference plate was measured using a stereo microscope.

In order to obtain the compliance of the material, the coefficient of diffusion, and the equilibrium moisture uptake; two different material characterization tests were performed. Since the average thickness of the cell phone housing is about 1.4 *mm*, PC/ABS bars of similar thickness were used for material characterization tests. First, the compliance of the specimens was determined for simultaneous physical aging and creep loading at 65 °C for 2 hours inside a DMA. These tests were similar to those described in section 5.6.2.2.2.2 with two differences: the thickness of the samples was 1.6 *mm* and the applied load was 2.19 *N*. Similar tests were also performed inside an environmental chamber at 65 °C/50% RH. The deflection of the samples following creep loading was then measured using a stereo microscope.

Next, PC/ABS bars with nominal dimensions 76.2×25.4×1.6 *mm* were exposed to the hygrothermal condition of 65 °C/50% RH to determine the equilibrium moisture uptake and the coefficient of diffusion of moisture into these thin samples using the mass uptake behaviour. The obtained parameters as well as the other parameters used for modeling are presented in the following section.

5.6.4.2 Modeling

The creep tests conducted on thin PC/ABS bars using the DMA resulted in the compliance of the PC/ABS bars in creep loading. The obtained experimental data is fitted to a Prony series in the form

of Equation (5-52). The compliance curve is then shifted using the hygrothermal shift factor determined in section 4.2.2.2 to obtain a new Prony series. The coefficients of the Prony series related to the shifted compliance; *i.e.*, D_e, D_1, and D_2 are listed in Table 5-5.

The coefficient of diffusion, D, as well as the equilibrium moisture uptake, m_∞, was obtained from the moisture uptake experiments of the thin PC/ABS bars. D and m_∞ together with the other parameters that were used in the modeling are also tabulated in Table 5-5.

Table 5-5 The model parameters of PC/ABS blend used for model verification.

Parameter	Value	Parameter	Value
Structural Mechanics			
D_e [$1/GPa$]	0.443	τ_1 [s]	5690
D_1 [$1/GPa$]	0.484	τ_2 [s]	341
D_2 [$1/GPa$]	0.041		
Moisture Diffusion			
ρ [kg/m^3]	1171	m_∞ [%]	0.12
D [m^2/s]	1.55×10^{-11}		
Heat Conduction			
c [$J/(kg.K)$]	1200	λ_T [$W/(m.K)$]	0.19
Coupling Coefficients			
α_T^e [$1/K$]	0.14×10^{-6}	$C_{T\mu}$ [$kg/(m.s.K$]	2.08×10^{-9}
α_T^{an1} [$1/K$]	0.13×10^{-6}	C_{TY} [$J/(kg.K)$]	79.7
α_T^{an2} [$1/K$]	0.02×10^{-6}	C_{ST1} [$m/(K.s)$]	3.60×10^{-14}
α_d^e	4.92×10^{-4}	C_{ST2} [$m/(K.s)$]	1.80×10^{-14}
α_d^{an1}	4.72×10^{-4}	$C_{S\mu1}$ [s/m]	4.11×10^{-14}
α_d^{an2}	0.64×10^{-4}	$C_{S\mu2}$ [s/m]	2.06×10^{-18}
K_μ [$kg.s/m^3$]	2.61×10^{-11}		

The parameters listed in Table 5-5 are used in a 3D analysis of the thin PC/ABS bars (thickness of 1.6 *mm*). The obtained numerical results are compared with experimental creep results in the next section. The comparison will demonstrate how a 3D analysis can improve the results compared to a 2D analysis. A similar 3D analysis was also performed on the cell phone housing case. Figure 5-48 shows the meshed model of the case with the boundary conditions. The case is meshed using tetrahedral elements. Because of the part symmetry, only half of the case was modeled.

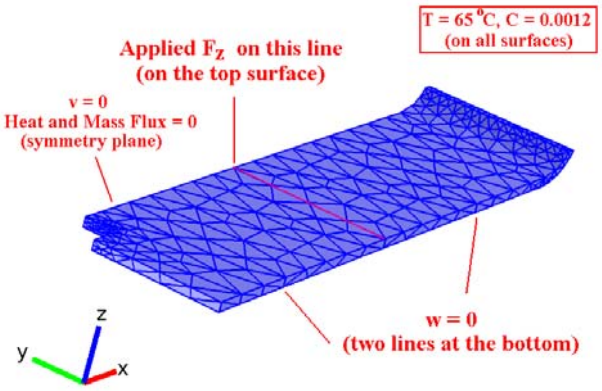

Figure 5-48 The 3D model of the cell phone housing case.

5.6.4.3 Results and Discussion

A 3D analysis was performed on a thin PC/ABS bar and the results were compared with the corresponding creep results. Figure 5-49 illustrates maximum value of viscoelastic deflection obtained from the numerical analysis. The deflection measured using the stereo microscope is also depicted in Figure 5-49.

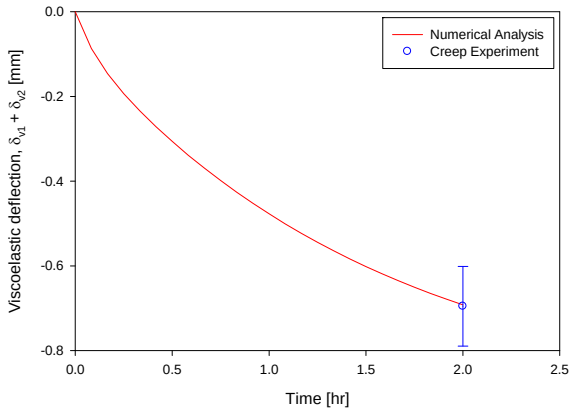

Figure 5-49 Maximum deflection of the thin bar obtained from 3D numerical analysis and creep experiments.

There is a good agreement between the experimental and numerical value of deflection depicted in Figure 5-49. This shows that the developed model works better for the 3D analysis of a thin PC/ABS bar as compared to the 2D analysis performed in section 5.6.2.2.2.3 (Figure 5-43).

The viscoelastic deflection of the case obtained from the numerical analysis following creep loading at 65 °C/50% RH is shown as function of loading time in Figure 5-50. The deflection shown in the figure is the summation of the deflection of the point where the load is applied and the end points of the case with respect to the undeformed state. For comparison, Figure 5-50 also includes the numerical analysis result for a case where the physics are modeled as uncoupled by setting all the coupling coefficients equal to zero. The experimental values of deflection are also plotted in Figure 5-50.

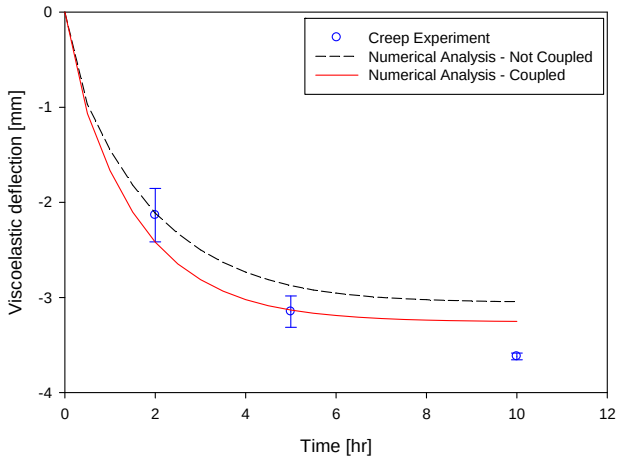

Figure 5-50 Maximum deflection of the housing case after creep loading at 65 °C/50% RH.

As seen in Figure 5-50, the consideration of coupling coefficients in the analysis improved the predictions by increasing the coefficient of determination (R^2) from 0.61 for the uncoupled case to 0.78 for the coupled case. It would be a larger challenge to determine the effect of each coupling coefficient on the deflection. This would require a thorough parametric analysis by accounting for the physical meaning of each coupling coefficient. The analysis is beyond the scope of this work. The discrepancies that exist between the numerical and experimental results in Figure 5-50 can also be reduced by the refinements suggested for future work in the following chapter. Nevertheless, the present model has demonstrated its capability in predicting deflection due to moisture diffusion and physical aging effects.

5.7 Concluding Remarks

In this chapter, the numerical modeling of the coupled physics was presented. The physics of structural mechanics, moisture diffusion, and heat conduction were separately modeled using PDEs and then the coupled physics were modeled. The effect of physical aging on the two mechanisms of structural mechanics and moisture diffusion were incorporated. The coupling coefficients between different physics were estimated by curve fitting the experimental data. Eventually, the comparison between the numerical and experimental results of three-point bending creep of both thin PC/ABS bars as well as cell-phone housing cases verified the model developed in this study.

Chapter 6
Conclusions

This chapter summarizes the results of the experiments conducted for material characterization, the model development procedure, and the model verification. It also presents some suggestions for future work.

6.1 Summary and Conclusions

The present study has focused on hygrothermal aging of glassy polymers with specific interest in moisture diffusion and physical aging phenomena. These two mechanisms have been known to cause changes in the thermophysical and mechanical properties of the material. These two processes, however, have opposite effects on the material structure and thus, on mechanical response. The coupling between the effects of moisture diffusion and physical aging complicates the prediction of the material's behaviour and this becomes more challenging when other external factors in engineering service are considered: structural loading and heat conduction.

In this work, the thermophysical and mechanical properties of a PC/ABS polymer blend subjected to coupled processes of moisture diffusion and physical aging was investigated. To achieve this, several experiments were performed on the material and the effects of the hygrothermal aging on the material's behaviour were explored. The experiments can be categorized into two main parts: thermophysical properties and mechanical properties. The results of these experiments can be summarized as follows:

1. The dual T_g's of the PC/ABS blend were assigned using two thermal analysis techniques; *i.e.*, TMA and DMA. In the TMA, the tests were performed at several heating rates under two modes of expansion and dilatometry. It was found that the lower heating rates (< 5 °C/min) can better capture both of the T_g's and therefore, the heating rate of 0.5 °C/min was selected for the physical aging tests. The T_g's of the blend were also determined using the three-point bending mode of the DMA. The obtained T_g's can be compared with those determined from the TMA as well as the DSC, which is available in the literature. It was concluded that the T_g's determined by the TMA are greater than those obtained from the other two methods. The obtained T_g's are used for selection of the aging temperature for

physical aging experiments because it is required in this study that the physical aging experiments be performed at the glassy region of the polymer material and therefore, the aging temperature is chosen below the T_g's of the blend.

2. The volume relaxation of the PC/ABS blend was studied by doing physical aging tests at the aging temperature of 80 °C. These tests were performed using the dilatometry mode of the TMA and covered the aging times in the range of 0.5 hr to 1008 hr. The experimental data were also fitted to the KWW model. This enabled us to find the volume relaxation at equilibrium. The obtained parameters, however, has to be corrected by performing tests at higher aging times.

3. The modulated DSC tests were performed on PC/ABS specimens before and after hygrothermal aging at different hygrothermal conditions. The statistical analysis of the specific heat capacity of the samples before and after hygrothermal aging revealed that the specific heat capacity is not significantly affected by the moisture uptake. This is while temperature influences the specific heat capacity and hence, a temperature-dependant linear relation was proposed for the specific heat capacity of the PC/ABS polymer blend. This relation can be used in the numerical analysis of heat conduction in blend specimens.

4. Moisture uptake behaviour of the PC/ABS blend was investigated by studying the mass uptake curves from the tests conducted on the test bars under five hygrothermal conditions. The moisture diffusion behaviour was found to be Fickian for the condition of immersed in distilled water at room temperature while anomalous behaviour with an overshoot was observed for the tests at conditions with temperatures of 50 °C and 65 °C and relative humidity of 50% and 93%. The coefficient of diffusion was obtained for the four hygrothermal conditions and the value was corrected for the edge effects. The equilibrium moisture uptake as well as the time to reach equilibrium was also determined and the effects of the aging temperature and relative humidity on these parameters were statically analyzed. It was found that the effects are coupled and complicated. The equilibrium moisture uptake values agreed reasonably well with theoretical results for PC. It was concluded that at the beginning of the moisture uptake tests, the moisture diffusion is the prominent physics but the physical aging becomes more influential as the test progresses. The physical aging mechanism, however, overcomes the moisture diffusion process in terms of affecting the material moisture uptake behaviour and consequently

desorbed some of the moisture which has already diffused into the material. The net effect is, therefore, manifested as an overshoot in the moisture uptake curve.

5. Stress relaxation tests were performed to study the effects of coupled moisture diffusion and physical aging mechanisms on the modulus of the PC/ABS samples. This was accomplished by comparing the test results of thermally and hygrothermally aged specimens with those of un-aged samples. It was seen that although the modulus of the material is decreased by the absorbed moisture but the net result is an increase in the modulus when compared to the un-aged sample. This suggests that the effect of physical aging is more prevalent on the modulus of the PC/ABS samples that are hygrothermally aged for up to 168 hours. The stress relaxation tests were performed in two regimes of aging time: short term and long term. The results of the stress relaxation tests can also be used for numerical modeling of structural mechanics in the PC/ABS blend.

6. The first set of coupling coefficients that exist in the coupled processes of structural mechanics, moisture diffusion, and heat conduction is defined to include the elastic coefficients of thermal and hygroscopic expansion. The elastic coefficient of thermal expansion can be extracted from the experimental results performed using the TMA. This coefficient is determined for both glassy and rubbery regions of the components of the PC/ABS at both expansion and dilatometry modes. The coefficient of hygroscopic expansion was obtained by an already established method using the TMA and TGA machines. The elastic coefficient of hygroscopic expansion was determined for samples that were hygrothermally aged at different conditions but no clear effect was observed on the coefficient. An average coefficient of hygroscopic expansion was proposed to be incorporated in the numerical modeling of the coupled processes.

The numerical modeling of the processes involved in the coupled moisture diffusion and physical aging processes in plastic specimens was also investigated in this study. First, the governing equations with a brief explanation of their derivation were presented and then the numerical modeling was developed for uncoupled as well as coupled processes, as follows:

1. The first uncoupled physics was structural mechanics, which was modeled considering two types of material behaviour: linear elastic and linear viscoelastic. The analyses were performed using the PDE mode of COMSOL Multiphysics® on a 2D pipe under internal pressure. For linear elastic behaviour, the analysis was conducted for the two modes of

plane stress and plane strain and it was shown that the results match with those of similar analyses run using the built-in module of COMSOL Multiphysics®. For the viscoelastic behaviour, two rheological models of generalized Maxwell and Kelvin-Voigt with two branches were considered. A transient analysis was performed on a 2D pipe under both creep and stress relaxation loading conditions in plane strain and plane stress modes. A comparison between the obtained results with those from similar analyses in ABAQUS® showed that the viscoelastic modeling has also been developed correctly.

2. Moisture diffusion in the PC/ABS material was modeled in both 1D and 2D cases. Mesh refinement was used as a method to reduce the error produced due to the low value of the coefficient of diffusion. In both cases, the results of numerical analyses were compared with the analytical solutions and the comparison showed that the analysis represented the mechanism very well.

3. A comparison between the numerical analysis performed using the PDE module and heat transfer module in COMSOL Multiphysics® showed that the PDE model of heat conduction works well for a PC/ABS bar. It was also shown that a 2D analysis can replace a 3D analysis for heat conduction without producing significant error. Moreover, an average value of specific heat capacity was proposed to be used instead of temperature-dependant relation.

4. The coupled models of structural mechanics, moisture diffusion, and heat conduction were analyzed on a pressurized pipe using the PDE module of COMSOL Multiphysics® while linear elastic behaviour was assumed for the pipe's material. There was a good agreement between the results of the analyses with those of the parametric study of Rambert *et al.* [46], which suggests that the developed model is capable of analyzing the triple coupled physics for linear elastic behaviour.

5. In order to conduct an analysis for the three coupled physics of structural mechanics, moisture diffusion, and heat conduction with the material having linear viscoelastic behaviour, the coupling coefficients needed to be determined. This was achieved by employing an optimization method using both software packages of COMSOL Multiphysics® and MATLAB®. The coupling coefficients $C_{T\mu}$ and C_{TY}, which relate moisture diffusion and heat conduction, as well as K_{μ} were estimated by comparing the results of numerical analyses with the results of moisture uptake experiments. The

optimization algorithm obtained the coupling coefficients so that the numerical results got as close as possible to the corresponding experimental results. Similarly, C_{ST} and $C_{S\mu}$, which are related to the interaction of structural mechanics with heat conduction and moisture diffusion, were determined by employing an optimization method to compare the numerical and experimental results. The experiments were performed by applying creep loading on a PC/ABS bar in both dry and humid environments. The obtained coefficients provided the numerical results that were closest to the experimental results.

6. The effects of physical aging on the structural mechanics and moisture diffusion were also studied. The influence of physical aging on structural mechanics was considered by the time/aging-time shift factors. The effects of physical aging on moisture diffusion were manifested as an overshoot in the moisture uptake curves. This was modeled by applying a time varying boundary condition with a decaying function. The parameters of the function were found for two conditions of 65 °C/50% RH and 50 °C/93% RH so that the numerical results were fitted with 0.98% coefficient of determination.

7. The complete quadruple coupled physical model was validated by creep experiments performed on thin PC/ABS bars and the backside case of a cell phone housing made of PC/ABS. The specimens were subjected to a three-point bending loading condition. A transient numerical analysis was conducted on a 3D model for both the PC/ABS bar and the cell phone housing. Maximum displacement of the bar obtained from the 3D numerical analysis had an exact agreement with the experimental results of creep loading for 2 hours. Similar comparison was made for the creep loading of the cell phone housing exposed to hygrothermal condition of 65 °C/50% RH for 10 hours. There was a reasonable agreement between the displacement obtained from the numerical analysis and that measured in the creep experiment.

In general, the current study led to a number of scientific contributions in both aspects of experimental and modeling work. The hygrothermal aging of PC/ABS polymer blend was investigated by doing mass uptake experiments as well as stress relaxation tests. The competing effects of physical aging and moisture diffusion on the material behaviour were studied using the experimental results. Moreover, the volume relaxation of the blend at 80 °C was studied and other thermophysical properties including glass transition temperature, specific heat capacity, and coefficients of thermal and hygroscopic expansion were determined. In the numerical work, the

coupled physics of structural mechanics, moisture diffusion, heat conduction, and physical aging were modeled in thin PC/ABS blends. In the developed model the material has linear viscoelastic behaviour. A strategy was also proposed for estimating the coupling coefficients between different physics in the model. The main scientific contributions of the current work can therefore be summarized as follows:

1. a modification of Fickian diffusion in the coupled PDEs to simulate the anomalous overshoot behaviour,
2. a model capable of simulating the viscoelastic behaviour of a polymer blend including the effect of moisture diffusion and physical aging, and
3. a model capable of simulating the coupled physical aging, moisture diffusion, heat transfer, and structural mechanics in a viscoelastic polymer blend.

A list of publications resulted from the present study is provided in Appendix D.

6.2 Recommendations for Future Work

The model developed in this study is capable of simulating the behaviour of a viscoelastic polymer blend subjected to coupled physics of structural mechanics, moisture diffusion, heat conduction, and physical aging. This was achieved by doing both experimental characterization tests and numerical simulation. Although the predictions are good, it is proposed that the model can be made more robust with the following recommendations:

1. The volume relaxation of the blend was investigated using physical aging experiments conducted at 80 °C in the TMA for the aging times up to 1008 hours. However, the maximum aging time in these experiments, 1008 hours, was not sufficient for determination of volume relaxation at equilibrium. Longer aging time experiments, on the other hand, may not be practically conducted in the TMA because of experimental limitations such as running out of purge gas in the tank for such long times. However, the volume relaxation data for longer aging times can be obtained using another technique. It was proposed by some authors [14, 171-176] that there is a linear relation between the volume and enthalpy relaxation of a polymer material. This relation, denoted by a term referred to as apparent bulk modulus, can be determined by conducting enthalpy relaxation tests with similar procedure to that performed by TMA. The enthalpy relaxation tests can be done using a DSC. The relation of the volume and enthalpy relaxation can lead to

determination of the apparent bulk modulus for PC/ABS polymer blend. Once the apparent bulk modulus is calculated, the volume relaxation can be obtained for longer aging times by conducting enthalpy relaxation tests at those high aging times and then calculate the volume relaxation of the material given the enthalpy relaxation and apparent bulk modulus. The advantage of doing enthalpy relaxation tests in a DSC compared to similar tests in a TMA is that it is possible to age the material outside of the DSC and inside an oven and therefore, it does not have the limitations that exist for volume relaxation measurements.

2. The coefficient of thermal expansion was measured for un-aged PC/ABS samples. The effects of hygrothermal aging in different hygrothermal conditions on the CTE can be studied by doing tests on hygrothermally aged specimens.

3. The coefficient of diffusion as well as the equilibrium moisture uptake was determined for the moisture diffusion into the polymer blend at 4 hygrothermal conditions. This can be obtained for other hygrothermal conditions for more accurate numerical analyses.

4. Stress relaxation tests can be performed for both thermally and hygrothermally aged specimens at other aging temperatures. Therefore, it will be possible to apply a time/temperature shift factor on the modulus curves. The obtained data can be used in the numerical modeling and for wider temperature range. Moreover, the PC/ABS samples can be exposed to hygrothermal conditions until saturation and then tested in the stress relaxation mode.

5. In the developed numerical model, the sample temperature was not necessarily constant throughout the analysis time. This is while the characterization experiments were performed at hygrothermal conditions which were constant in time. The aging experiments, however, can be conducted at variable temperatures. These tests, which are referred to as non-isothermal aging tests, have been done by some authors such as Guo *et al.* [28]. By determining the material properties at non-isothermal conditions, the analysis will lead to better results for the coupled physics.

6. The mechanical tests in this study were applied in the three-point bending mode. Similar experiments can be performed for other loading conditions such as tensile and compressive loads.

7. The current study investigates the behaviour of a typical thermoplastic material subjected to coupled processes of moisture diffusion and physical aging. This can be extended to other types of polymer materials such as thermosets, which have also various industrial applications exposed to hygrothermal aging.

References

[1] Comyn, J., 1983, "Durability of Structural Adhesives," Applied Science, London.

[2] McBrierty, V. J., Martin, S. J., and Karasz, F. E., 1999, "Understanding Hydrated Polymers: The Perspective of NMR," Journal of Molecular Liquids, **80**(2-3) pp. 179-205.

[3] Pryde, C. A., and Hellman, M. Y., 1980, "Solid State Hydrolysis of Bisphenol-A Polycarbonate - 1. Effect of Phenolic End Groups," Journal of Applied Polymer Science, **25**(11) pp. 2573-2587.

[4] Golovoy, A., and Zinbo, M., 1989, "Water Sorption and Hydrolytic Stability of Polycarbonates," Polymer Engineering and Science, **29**(24) pp. 1733-1737.

[5] Bair, H. E., Falcone, D. R., Hellman, M. Y., 1981, "Hydrolysis of Polycarbonate to Yield BPA," Journal of Applied Polymer Science, **26**(6) pp. 1777-1786.

[6] Ghorbel, I., Thominette, F., Spiteri, P., 1995, "Hydrolytic Aging of Polycarbonate. I. Physical Aspects," Journal of Applied Polymer Science, **55**(1) pp. 163-171.

[7] Ghorbel, I., Akele, N., Thominette, F., 1995, "Hydrolytic Aging of Polycarbonate. II. Hydrolysis Kinetics, Effect of Static Stresses," Journal of Applied Polymer Science, **55**(1) pp. 173-179.

[8] Gallucci, R. R., 2009, "Polycarbonate Hydrolysis," 67th Annual Technical Conference of the Society of Plastic's Engineers 2009, Anonymous Society of Plastics Engineers, Brookfield, CT, USA, **2,** pp. 903-7.

[9] Wong, E. H., Rajoo, R., Koh, S. W., 2002, "The Mechanics and Impact of Hygroscopic Swelling of Polymeric Materials in Electronic Packaging," Journal of Electronic Packaging, Transactions of the ASME, **124**(2) pp. 122-126.

[10] Ishisaka, A., and Kawagoe, M., 2004, "Examination of the Time-Water Content Superposition on the Dynamic Viscoelasticity of Moistened Polyamide 6 and Epoxy," Journal of Applied Polymer Science, **93**(2) pp. 560-567.

[11] Hutchinson, J. M., 1995, "Physical Aging of Polymers," Progress in Polymer Science (Oxford), **20**(4) pp. 703-760.

[12] Callister, W.D., 2006, "Materials science and engineering: an introduction," John Wiley & Sons, Hoboken, NJ.

[13] Klopffer, M. H., and Flaconneche, B., 2001, "Transport Properties of Gases in Polymers: Bibliographic Review; Transport De Molecule Gazeuses Dans Les Polymeres: Revue Bibliograpique," Oil and Gas Science and Technology, **56**(3) pp. 223-244.

[14] Adachi, K., and Kotaka, T., 1982, "Volume and Enthalpy Relaxation in Polystyrene," Polymer Journal, **14**(12) pp. 959-970.

[15] Weitsman, Y., 1979, "Interfacial Stresses in Viscoelastic Adhesive-Layers due to Moisture Sorption," International Journal of Solids and Structures, **15**(9) pp. 701-713.

[16] Weitsman, Y., 1987, "Stress Assisted Diffusion in Elastic and Viscoelastic Materials," Journal of the Mechanics and Physics of Solids, **35**(1) pp. 73-93.

[17] Aifantis, E. C., 1976, "Diffusion of a Perfect Fluid in a Linear Elastic Stress Field," Mechanics Research Communications, **3**(4) pp. 245-50.

[18] Aifantis, E. C., and Gerberich, W. W., 1977, "Gaseous Diffusion in a Stressed-Thermoelastic Solid. I. The Thermomechanical Formulation," Acta Mechanica, **28**(1-4) pp. 1-24.

[19] Aifantis, E. C., and Gerberich, W. W., 1978, "Diffusion of a Gas in a Linear Elastic Solid," Acta Mechanica, **29**(1-4) pp. 169-184.

[20] Aifantis, E. C., 1980, "On the Problem of Diffusion in Solids," Acta Mechanica, **37**(3-4) pp. 265-96.

[21] Cox, R. W., and Cohen, D. S., 1989, "A Mathematical Model for Stress-Driven Diffusion in Polymers," Journal of Polymer Science, Part B (Polymer Physics), **27**(3) pp. 589-602.

[22] Cox, R. W., 1991, "Stress-Assisted Diffusion. A Free Boundary Problem," SIAM Journal on Applied Mathematics, **51**(6) pp. 1522-1537.

[23] Treloar, L. R. G., 1953, "The Absorption of Water by Cellulose, and its Dependence on Applied Stress," Transactions of the Faraday Society, **49** pp. 816-823.

[24] Baum, J. S., and Schultz, J. M., 1981, "Rapid Measurements of Elastic Modulus and Density in Polypropylene Sheet during Aging," Journal of Applied Polymer Science, **26**(5) pp. 1579-1584.

[25] Hu, H., and Sun, C. T., 2000, "The Characterization of Physical Aging in Polymeric Composites," Composites Science and Technology, **60**(14) pp. 2693-2698.

[26] Zhu, W. H., Gan, S. L., and Toh, C. L., 2004, "Mechanical properties of molding compounds (MCs) under different moisture conditions and in a wide temperature range," Thermal and Mechanical Simulation and Experiments in Microelectronics and Microsystems - EuroSimE 2004, IEEE, Piscataway, NJ, USA, pp. 593-8.

[27] Larobina, D., Lavorgna, M., Mensitieri, G., 2007, "Water diffusion in glassy polymers and their silica hybrids: an analysis of state of water molecules and of the effect of tensile stress," Selected

Contributions from the 3rd International Conference on "Times of Polymers and Composites (TOP)", Anonymous Wiley-VCH, Weinheim, Germany, pp. 11-20.

[28] Guo, Y., Wang, N., Bradshaw, R. D., 2009, "Modeling Mechanical Aging Shift Factors in Glassy Polymers during Nonisothermal Physical Aging. I. Experiments and KAHR-a_{te} Model Prediction," Journal of Polymer Science, Part B: Polymer Physics, **47**(3) pp. 340-52.

[29] Sih, G. C., Shih, M. T., and Chou, S. C., 1980, "Transient Hygrothermal Stresses in Composites: Coupling of Moisture and Heat with Temperature Varying Diffusivity," International Journal of Engineering Science, **18**(1) pp. 19-42.

[30] Hayes, C. K., and Cohen, D. S., 1992, "The Evolution of Steep Fronts in Non-Fickian Polymer-Penetrant Systems," Journal of Polymer Science, Part B: Polymer Physics, **30**(2) pp. 145-161.

[31] Cohen, D. S., and White Jr., A. B., 1991, "Sharp Fronts due to Diffusion and Viscoelastic Relaxation in Polymers," SIAM Journal on Applied Mathematics, **51**(2) pp. 472-483.

[32] Vijalapura, P. K., and Govindjee, S., 2003, "Numerical Simulation of Coupled-Stress Case II Diffusion in One Dimension," Journal of Polymer Science, Part B (Polymer Physics), **41**(18) pp. 2091-108.

[33] Holalkere, V., Mirano, S., Kuo, A., 1997, "Evaluation of plastic package delamination via reliability testing and fracture mechanics approach," Proceedings of the 1997 47th IEEE Electronic Components & Technology Conference, May 18, 1997 - May 21, San Jose, CA, USA, pp. 430-435.

[34] Teh, L. K., Teo, M., Anto, E., 2005, "Moisture-Induced Failures of Adhesive Flip Chip Interconnects," IEEE Transactions on Components and Packaging Technologies, **28**(3) pp. 506-16.

[35] Abdel Wahab, M. M., Ashcroft, I. A., Crocombe, A. D., 2001, "Diffusion of Moisture in Adhesively Bonded Joints," Journal of Adhesion, **77**(1) pp. 43-80.

[36] Abdel Wahab, M. M., Crocombe, A. D., Beevers, A., 2002, "Coupled Stress-Diffusion Analysis for Durability Study in Adhesively Bonded Joints," International Journal of Adhesion and Adhesives, **22**(1) pp. 61-73.

[37] Wong, E. H., Koh, S. W., Lee, K. H., 2002, "Advanced moisture diffusion modeling and characterisation for electronic packaging," Electronic Components and Technology Conference, 52nd Proceeding, pp. 1297-1303.

[38] Yu, Y. -T., and Pochiraju, K., 2003, "Three-Dimensional Simulation of Moisture Diffusion in Polymer Composite Materials," Polymer-Plastics Technology and Engineering, **42**(5) pp. 737-56.

[39] Shirangi, H., Auersperg, J., Koyuncu, M., 2008, "Characterization of dual-stage moisture diffusion, residual moisture content and hygroscopic swelling of epoxy molding compounds," EuroSimE 2008 International Conference on Thermal, Mechanical and Multi-Physics; Simulation and Experiments in Microelectronics and Micro-Systems, IEEE, Piscataway, NJ, USA, pp. 455-62.

[40] Lin, T. Y., and Tay, A. A. O., 1997, "Mechanics of interfacial delamination under hygrothermal stresses during reflow soldering," Proceedings of the 1997 1st Electronic Packaging Technology Conference, EPTC, October 8, 1997 - October 10, IEEE, Singapore, Singapore, pp. 163-169.

[41] Yi, S., and Sze, K. Y., 1998, "Finite Element Analysis of Moisture Distribution and Hygrothermal Stresses in TSOP IC Packages," Finite Elements in Analysis and Design, **30**(1) pp. 65-79.

[42] Chang, K. -C., Yeh, M. -K., and Chiang, K. -N., 2004, "Hygrothermal Stress Analysis of a Plastic Ball Grid Array Package during Solder Reflow," Proceedings of the Institution of Mechanical Engineers, Part C (Journal of Mechanical Engineering Science), **218** pp. 957-70.

[43] Lahoti, S. P., Kallolimath, S. C., and Zhou, J., 2005, "Finite element analysis of thermo-hygro-mechanical failure of a flip chip package," 6th International Conference on Electronics Packaging Technology, IEEE, Piscataway, NJ, USA, pp. 330-5.

[44] Dudek, R., Walter, H., Auersperg, J., 2007, "Numerical analysis for thermo-mechanical reliability of polymers in electronic packaging," Polytronic 2007 - 6th International IEEE Conference on Polymers and Adhesives in Microelectronics and Photonics, January 15, 2007 - January 18, Inst. of Elec. and Elec. Eng. Computer Society, Tokyo, Japan, pp. 220-227.

[45] Fan, X., and Zhao, J. -H., 2011, "Moisture diffusion and integrated stress analysis in encapsulated microelectronics devices," Thermal, Mechanical and Multi-Physics Simulation and Experiments in Microelectronics and Microsystems (EuroSimE 2011), 12th International Conference, pp. 1/8-8/8.

[46] Rambert, G., Grandidier, J. -C., Cangemi, L., 2003, "A Modelling of the Coupled Thermodiffuso-Elastic Linear Behaviour. Application to Explosive Decompression of Polymers," Oil and Gas Science and Technology, **58**(5) pp. 571-591.

[47] Rambert, G., Jugla, G., Grandidier, J. -C., 2006, "A Modelling of the Direct Couplings between Heat Transfer, Mass Transport, Chemical Reactions and Mechanical Behaviour. Numerical Implementation to Explosive Decompression," Composites Part A: Applied Science and Manufacturing, **37**(4) pp. 571-584.

[48] Rambert, G., and Grandidier, J. -C., 2005, "An Approach to the Coupled Behaviour of Polymers Subjected to a Thermo-Mechanical Loading in a Gaseous Environment," European Journal of Mechanics, A/Solids, **24**(1) pp. 151-68.

[49] Rambert, G., Grandidier, J. -.C, and Aifantis, E. C., 2007, "On the Direct Interactions between Heat Transfer, Mass Transport and Chemical Processes within Gradient Elasticity," European Journal of Mechanics, A/Solids, **26**(1) pp. 68-87.

[50] Jugla, G., Jochum, C., and Grandidier, J. -.C, 2007, "Chemical-Thermal and Mechanical Coupling Model for the Cure of a Thermosetting Matrix: Application to FEM Simulation," Key Engineering Materials, **334-335** pp. 225-8.

[51] Valancon, C., Roy, A., and Grandidier, J. -C., 2006, "Modelling of Coupling between Mechanics and Water Diffusion in Bonded Assemblies," Oil and Gas Science and Technology, **61**(6) pp. 759-764.

[52] Roy, S., and Reddy, J. N., 1988, "Finite Element Analysis of Adhesively Bonded Composite Joints with Moisture Diffusion and Delayed Failure," Computers and Structures, **29**(6) pp. 1011-1031.

[53] Roy, S., 1999, "Modeling of Anomalous Moisture Diffusion in Polymer Composites: A Finite Element Approach," Journal of Composite Materials, **33**(14) pp. 1318-1343.

[54] Marques, S. P. C., and Creus, G. J., 1994, "Geometrically Nonlinear Finite Element Analysis of Viscoelastic Composite Materials Under Mechanical and Hygrothermal Loads," Computers and Structures, **53**(2) pp. 449-456.

[55] Ashcroft, I. A., Abdel Wahab, M. M., and Crocombe, A. D., 2003, "Predicting Degradation in Bonded Composite Joints using a Semi-Coupled Finite-Element Method," Mechanics of Advanced Materials and Structures, **10**(3) pp. 227-248.

[56] Loh, W. K., Crocombe, A. D., Abdel Wahab, M. M. A., 2005, "Modelling Anomalous Moisture Uptake, Swelling and Thermal Characteristics of a Rubber Toughened Epoxy Adhesive," International Journal of Adhesion and Adhesives, **25**(1) pp. 1-12.

[57] Schapery, R. A., 1969, "On the Characterization of Nonlinear Viscoelastic Materials," Polymer Engineering & Science, **9**(4) pp. 295-310.

[58] Lai, J., and Bakker, A., 1996, "3-D Schapery Representation for Non-Linear Viscoelasticity and Finite Element Implementation," Computational Mechanics, **18**(3) pp. 182-191.

[59] Oliveira, B. F., and Creus, G. J., 2000, "Viscoelastic Failure Analysis of Composite Plates and Shells," Composite Structures, **49**(4) pp. 369-384.

[60] Oliveira, B. F., and Creus, G. J., 2004, "An Analytical-Numerical Framework for the Study of Ageing in Fibre Reinforced Polymer Composites," Composite Structures, **65**(3-4) pp. 443-57.

[61] Govindjee, S., and Simo, J. C., 1993, "Coupled Stress Diffusion. Case II," Journal of the Mechanics and Physics of Solids, **41**(5) pp. 863-887.

[62] Nigam, I., Nigam, D., and Mathur, G. N., 2005, "Effect of Rubber Content of ABS on Properties of PC/ABS Blends. I. Rheological, Mechanical, and Thermal Properties," Polymer-Plastics Technology and Engineering, **44**(5) pp. 815-32.

[63] Tan, Z. Y., Xu, X. F., Sun, S. L., 2006, "Influence of Rubber Content in ABS in Wide Range on the Mechanical Properties and Morphology of PC/ABS Blends with Different Composition," Polymer Engineering and Science, **46**(10) pp. 1476-84.

[64] ASTM D 1238. Standard Test Method for Melt Flow Rates of Thermoplastics by Extrusion Plastometer, 1991.

[65] Gabbott, P., 2007, "Principles and applications of thermal analysis," Blackwell Publication, Ames, Iowa.

[66] Brazier, D. W., and Nickel, G. H., 1978, "Application of TMA for Rapid Evaluation of Low-Temperature Properties of Elastomer Vulcanizates," Thermochimica Acta, **26**(1-3) pp. 399-413.

[67] Neag, C. M., 1991, "Materials Characterization by Thermomechanical Analysis," ASTM STP 1136, A. T. Riga and C. M. Neag, Eds, Philadelphia, PA, pp. 3.

[68] Henderson, J. B., and Emmerich, W. -D., 1991, "Polymer Characterization using Thermomechanical Analysis," Journal of Thermal Analysis, **37**(8) pp. 1825-1831.

[69] Greco, R., and Sorrentino, A., 1994, "Polycarbonate/ABS Blends: A Literature Review," Advances in Polymer Technology, **13**(4) pp. 249-258.

[70] Tang, J. K. Y., and Lee-Sullivan, P., 2008, "Observations of Physical Aging in a Polycarbonate and Acrylonitrile- Butadiene-Styrene Blend," Journal of Applied Polymer Science, **110**(1) pp. 97-108.

[71] Haghighi Yazdi, M., and Lee-Sullivan, P., 2009, "Determination of Dual Glass Transition Temperatures of a PC/ABS Blend using Two TMA Modes," Journal of Thermal Analysis and Calorimetry, **96**(1) pp. 7-14.

[72] Schwartz, A., 1978, "Glass transition temperatures of polymer materials, measured by thermomechanical analysis-influence of rates of heating and cooling," Fifth Scandinavian Symposium on Thermal Analysis, Anonymous UK, **13,** pp. 489-97.

[73] TMA 2940 Thermomechanical Analyzer Operator's Manual, TA Instruments, 1991.

[74] Wiedemann, H.G., Widmann, G., and Bayer, G., 1994, "Assignment of the Glass Transition," ASTM STP 1249, R. J. Seyler, Ed., Philadelphia, PA, pp. 174.

[75] ASTM E 1545-05. Standard Test Method for Assignment of Glass Transition Temperature by Thermomechanical Analysis, 2006.

[76] ASTM E 2113-04. Standard Test Method for Length Change Calibration of Thermomechanical Analyzers, 2004.

[77] ASTM E 1363-03. Standard Test Method for Temperature Calibration of Thermomechanical Analyzers, 2003.

[78] Earnest, C. M., 1994, "Assignment of the Glass Transition," ASTM STP 1249, R. J. Seyler, Ed., Philadelphia, PA, pp. 75.

[79] ASTM D 5023-07. Standard Test Method for Plastics: Dynamic Mechanical Properties: In Flexure (Three-Point Bending), 2007.

[80] Guo, Y., and Bradshaw, R. D., 2007, "Isothermal Physical Aging Characterization of Polyether-Ether-Ketone (PEEK) and Polyphenylene Sulfide (PPS) Films by Creep and Stress," Mechanics of Time-Dependent Materials, **11**(1) pp. 61-89.

[81] Lee-Sullivan, P., and Dykeman, D., 2000, "Guidelines for Performing Storage Modulus Measurements using the TA Instruments DMA 2980 Three-Point Bend Mode. I. Amplitude Effects," Polymer Testing, **19**(2) pp. 155-164.

[82] Gaur, U., Shu, H. -C., Mehta, A., 1981, "Heat Capacity and Other Thermodynamic Properties of Linear Macromolecules. I. Selenium," Journal of Physical and Chemical Reference Data, **10**(1) pp. 89-117.

[83] Gaur, U., and Wunderlich, B., 1981, "Heat Capacity and Other Thermodynamic Properties of Linear Macromolecules. II. Polyethylene," Journal of Physical and Chemical Reference Data, **10**(1) pp. 119-52.

[84] Gaur, U., and Wunderlich, B., 1981, "Heat Capacity and Other Thermodynamic Properties of Linear Macromolecules. III. Polyoxides," Journal of Physical and Chemical Reference Data, **10**(4) pp. 1001-49.

[85] Gaur, U., and Wunderlich, B., 1981, "Heat Capacity and Other Thermodynamic Properties of Linear Macromolecules. IV. Polypropylene," Journal of Physical and Chemical Reference Data, **10**(4) pp. 1051-64.

[86] Gaur, U., and Wunderlich, B., 1982, "Heat Capacity and Other Thermodynamic Properties of Linear Macromolecules. V. Polystyrene," Journal of Physical and Chemical Reference Data, **11**(2) pp. 313-25.

[87] Gaur, U., Lau, S., Wunderlich, B. B., 1982, "Heat Capacity and Other Thermodynamic Properties of Linear Macromolecules. VI. Acrylic Polymers," Journal of Physical and Chemical Reference Data, **11**(4) pp. 1065-89.

[88] Gaur, U., Lau, S. -F., Wunderlich, B. B., 1983, "Heat Capacity and Other Thermodynamic Properties of Linear Macromolecules. VIII. Polyesters and Polyamides," Journal of Physical and Chemical Reference Data, **12**(1) pp. 65-89.

[89] Cheng, S. Z. D., and Wunderlich, B., 1986, "Heat Capacities and Entropies of Liquid, High-Melting-Point Polymers Containing Phenylene Groups (PEEK, PC, and PET)," Journal of Polymer Science, Part B (Polymer Physics), **24**(8) pp. 1755-65.

[90] Varma-Nair, M., Cheng, J., Jin, Y., 1991, "Thermal Properties of Polysilylenes," Macromolecules, **24**(19) pp. 5442-5450.

[91] Jin, Y., Cheng, J., Varma-Nair, M., 1992, "Thermodynamic Characterization of C60 by Differential Scanning Calorimetry," Journal of Physical Chemistry, **96**(12) pp. 5151-6.

[92] Http://athas.prz.edu.pl/.

[93] ASTM D 570-98. Standard Test Method for Water Absorption of Plastics, 2005.

[94] ASTM D 618-08. Standard Practice for Conditioning Plastics for Testing, 2008.

[95] Tang, J., 2007, "Physical Aging and Hygrothermal Response of Polycarbonateacrylonitrile-Butadiene-Styrene Polymer Blend," Master's Thesis, University of Waterloo, Waterloo, Ontario, Canada.

[96] Struik, L.C.E., 1978, "Physical aging in amorphous polymers and other materials," Elsevier Scientific Pub. Co., Amsterdam.

[97] Vleeshouwers, S., Jamieson, A. M., and Simha, R., 1989, "Effect of Physical Aging on Tensile Stress Relaxation and Tensile Creep of Cured EPON 828/epoxy Adhesives in the Linear Viscoelastic Region," Polymer Engineering and Science, **29**(10) pp. 662-670.

[98] Lee, A., and McKenna, G. B., 1997, "Anomalous Aging in Two-Phase Systems: Creep and Stress Relaxation Differences in Rubber-Toughened Epoxies," Journal of Polymer Science, Part B: Polymer Physics, **35**(8) pp. 1167-1174.

[99] O'Connell, P. A., and McKenna, G. B., 1997, "Large Deformation Response of Polycarbonate: Time-Temperature, Time-Aging Time, and Time-Strain Superposition," Polymer Engineering and Science, **37**(9) pp. 1485-1495.

[100] Gates, T. S., Brinson, L. C., Whitley, K. S., 2000, "Aging during elevated temperature stress relaxation of IM7/K3B composite," Time Dependent and Nonlinear Effects in Polymers and Composites, May 4, 1998 - May 5, ASTM, Atlanta, GA, USA, pp. 141-159.

[101] Veazie, D. R., and Gates, T. S., 2000, "Tensile and compressive creep of a thermoplastic polymer and the effects of physical aging on the composite time-dependent behavior," Time Dependent and Nonlinear Effects in Polymers and Composites, May 4, 1998 - May 5, ASTM, Atlanta, GA, USA, pp. 160-175.

[102] Nogueira, P., Ramirez, C., Torres, A., 2001, "Effect of Water Sorption on the Structure and Mechanical Properties of an Epoxy Resin System," Journal of Applied Polymer Science, **80**(1) pp. 71-80.

[103] LaPlante, G., and Lee-Sullivan, P., 2005, "Moisture Effects on FM300 Structural Film Adhesive: Stress Relaxation, Fracture Toughness, and Dynamic Mechanical Analysis," Journal of Applied Polymer Science, **95**(5) pp. 1285-94.

[104] Zhou, S. -M., Tashiro, K., Hongo, T., 2001, "Influence of Water on Structure and Mechanical Properties of Regenerated Cellulose Studied by an Organized Combination of Infrared Spectra, X-Ray Diffraction, and Dynamic Viscoelastic Data Measured as Functions of Temperature and Humidity," Macromolecules, **34**(5) pp. 1274-1280.

[105] Zhou, S. -M., Tashiro, K., and Ii, T., 2001, "Moisture Effect on Structure and Mechanical Property of Nylon 6 as Studied by the Time-Resolved and Simultaneous Measurements of FT-IR and Dynamic Viscoelasticity under the Controlled Humidity at Constant Scanning Rate," Polymer Journal, **33**(4) pp. 344-355.

[106] Zhou, S. -M., Tashiro, K., and Ii, T., 2001, "Confirmation of Universality of Time-Humidity Superposition Principle for various Water-Absorbable Polymers through Dynamic Viscoelastic Measurements Under Controlled Conditions of Relative Humidity and Temperature," Journal of Polymer Science Part B: Polymer Physics, **39**(14) pp. 1638-1650.

[107] Van Driel, W. D., Habets, P. J. J. H. A., Van Gils, M. A. J., 2005, "Characterization of interface strength as function of temperature and moisture conditions," 2005 6th International Conference on Electronics Packaging Technology, August 30, 2005 - September 2, Inst. of Elec. and Elec. Eng. Computer Society, Dameisha, Shenzhen, China, **2005,** pp. CIE-CEPS.

[108] Van Driel, W. D., Van Gils, M. A. J., and Zhang, G. Q., 2005, "Prediction of delamination in micro-electronic packages," 2005 6th International Conference on Electronics Packaging Technology,

August 30, 2005 - September 2, Inst. of Elec. and Elec. Eng. Computer Society, Dameisha, Shenzhen, China, **2005,** pp. CIE-CEPS.

[109] Phillips, J. C., 1997, "Stress Relaxation of Elongated Strips of Poly(Vinylidene Fluoride) in Ethyl Acetate Vapor," Polymer Engineering and Science, **37**(2) pp. 291-307.

[110] Ma, X., Jansen, K. M. B., and Ernst, L. J., 2006, "Moisture effects on the creep of thermosetting IC packaging polymers," 7th International Conference on Thermal, Mechanical and Multiphysics Simulation and Experiments in Micro-Electronics and Micro-Systems, EuroSimE 2006, April 24, 2006 - April 26, Inst. of Elec. and Elec. Eng. Computer Society, Como, Italy, **2006**.

[111] Leibler, L., and Sekimoto, K., 1993, "On the Sorption of Gases and Liquids in Glassy Polymers," Macromolecules, **26**(25) pp. 6937-6939.

[112] DMA 2980 Dynamic Mechanical Analyzer Operator's Manual, TA Instruments, 1997.

[113] Menard, K. P., 2008, "Dynamic mechanical analysis: a practical introduction," CRC Press, Boca Raton, FL.

[114] Wong, E. H., Chan, K. C., Rajoo, R., 2000, "The mechanics and impact of hygroscopic swelling of polymeric materials in electronic packaging," 50th Electronic Components and Technology Conference, IEEE, Piscataway, NJ, USA, pp. 576-80.

[115] Zhou, J., 2006, "Analytical and numerical bound analysis of hygroscopic swelling characterization," IEEE 56th Electronic Components and Technology Conference, May 30, 2006 - June 2, Institute of Electrical and Electronics Engineers Inc, San Diego, CA, United States, **2006,** pp. 734-739.

[116] Tong, Y. T., Chek, L. K., Yap, D., 2003, "Reliability Assessment and Hygroswelling Modeling of FCBGA with no-Flow Underfill," Microelectronics Reliability, **43**(5) pp. 741-9.

[117] Zhou, J., Tee, T. Y., Zhang, X., 2005, "Characterization and modeling of hygroscopic swelling and its impact on failures of a flip chip package with no-flow underfill," 7th Electronics Packaging Technology Conference, EPTC 2005, December 7, 2005 - December 9, Inst. of Elec. and Elec. Eng. Computer Society, Singapore, **2,** pp. 561-568.

[118] Zhou, J., 2008, "Transient Analysis on Hygroscopic Swelling Characterization using Sequentially Coupled Moisture Diffusion and Hygroscopic Stress Modeling Method," Microelectronics Reliability, **48**(6) pp. 805-10.

[119] Turi, E.A., 1981, "Thermal characterization of polymeric materials," Academic Press, New York.

[120] O'Neal, H. R., Welch, S., Rogers, J., 1995, "Comparison of T_g Values for a Graphite Epoxy Composite by Differential Scanning Calorimetry (DSC), Thermomechanical Analysis (TMA), and Dynamic Mechanical Analysis (DMA)," Journal of Advanced Materials, **26**(3) pp. 49-54.

[121] Cassel, B., and Twombly, B., 1991, "Materials Characterization by Thermomechanical Analysis," ASTM STP 1136, A. T. Riga and C. M. Neag, Eds., Philadelphia, PA, pp. 108.

[122] Hatakeyama, T., and Quinn, F.X., 1994, "Thermal analysis: fundamentals and applications to polymer science," Wiley, Chichester, England; New York.

[123] Mano, J. F., and Ribelles, J. L. G., 2004, "Influence of the Sample Mass on the Study of the Glass Transition and the Structural Relaxation by Differential Scanning Calorimetry," Journal of Non-Crystalline Solids, **337**(1) pp. 68-77.

[124] Ferrillo, R. G., and Achorn, P. J., 1997, "Comparison of Thermal Techniques for Glass Transition Assignment. II. Commercial Polymers," Journal of Applied Polymer Science, **64**(1) pp. 191-195.

[125] Sircar, A. K., Galaska, M. L., Rodrigues, S., 1999, "Glass Transition of Elastomers using Thermal Analysis Techniques," Rubber Chemistry and Technology, **72**(3) pp. 513-552.

[126] Cowie, J. M. G., and Ferguson, R., 1986, "The Ageing of Poly(Vinyl Methyl Ether) as Determined from Enthalpy Relaxation Measurements," Polymer Communications, **27**(9) pp. 258-60.

[127] Williams, G., and Watts, D. C., 1970, "Non-Symmetrical Dielectric Relaxation Behaviour Arising from a Simple Empirical Decay Function," Transactions of the Faraday Society, **66**(565) pp. 80-85.

[128] Narkis, M., Chaouat-Sibony, S., Nicolais, L., 1985, "Water Effects on Polycarbonate," Polymer Communications, **26**(11) pp. 339-42.

[129] Shen, C., and Springer, G. S., 1976, "Moisture Absorption and Desorption of Composite Materials," Journal of Composite Materials, **10**(1) pp. 2-20.

[130] Jost, W., 1969, "Diffusion in solids, liquids, gases," Academic Press, New York.

[131] Crank, J., and Park, G.S., 1968, "Diffusion in polymers," Academic Press, London.

[132] Flory, P.J., 1953, "Principles of polymer chemistry," Cornell University Press, Ithaca.

[133] Vrentas, J. S., and Vrentas, C. M., 1991, "Sorption in Glassy Polymers," Macromolecules, **24**(9) pp. 2404-2412.

[134] Doumenc, F., Bodiguel, H., and Guerrier, B., 2008, "Physical Aging of Glassy PMMA/Toluene Films: Influence of Drying/Swelling History," European Physical Journal E, **27**(1) pp. 3-11.

[135] Zoller, P., 1982, "A Study of the Pressure-Volume-Temperature Relationships of Four Related Amorphous Polymers: Polycarbonate, Polyarylate, Phenoxy, and Polysulfone," Journal of Polymer Science, Polymer Physics Edition, **20**(8) pp. 1453-64.

[136] Robertson, R. E., and Wilson, C. M., 1965, "Some Elastic Moduli Versus Temperature of Glassy Bisphenol-A Polycarbonate," Journal of Polymer Science -- Polymer Letters Part B, **3**(5) pp. 427-431.

[137] Bair, H. E., Johnson, G. E., and Merriweather, R., 1978, "Water Sorption of Polycarbonate and its Effect on the Polymer's Dielectric Behavior," **49**(10) pp. 4976-4984.

[138] O'Connell, P. A., and McKenna, G. B., 1999, "Arrhenius-Type Temperature Dependence of the Segmental Relaxation Below Tg," Journal of Chemical Physics, **110**(22) pp. 11054-60.

[139] Nick, B., and Suter, U. W., 2001, "Solubility of Water in Polymers-Atomistic Simulations," Computational and Theoretical Polymer Science, **11**(1) pp. 49-55.

[140] Dykeman, D., and Lee-Sullivan, P., 2003, "Mechanical Relaxations in Heat-Aged Polycarbonate. Part II: Statistical Analysis of Low-Molecular Weight Data," Polymer Engineering and Science, **43**(2) pp. 383-397.

[141] Montgomery, D.C., 2001, "Design and analysis of experiments," John Wiley, New York.

[142] Hancock, B. C., and Zografi, G., 1993, "The use of Solution Theories for Predicting Water Vapor Absorption by Amorphous Pharmaceutical Solids: A Test of the Flory-Huggins and Vrentas Models," Pharmaceutical Research, **10**(9) pp. 1262-1267.

[143] Akbar, S., and Zhang, T., 2008, "Moisture Diffusion in carbon/epoxy Composite and the Effect of Cyclic Hygrothermal Fluctuations: Characterization by Dynamic Mechanical Analysis (DMA) and Interlaminar Shear Strength (ILSS)," Journal of Adhesion, **84**(7) pp. 585-600.

[144] Katzman, H. A., Castaneda, R. M., and Han, S. L., 2008, "Moisture Diffusion in Composite Sandwich Structures," Composites Part A: Applied Science and Manufacturing, **39**(5) pp. 887-92.

[145] Soret, C., 1979, "Sur l'État d'Équilibre que Prend au Point de Vue de sa Concentration une Dissolution Saline Primitivement Homohéne Dont Deux Parties Sont Portées à des Températures Différentes," Archives Des Sciences Physiques Et Naturelles, **2** pp. 48-61.

[146] Platten, J. K., 2006, "The Soret Effect: A Review of Recent Experimental Results," Transactions of the ASME. Journal of Applied Mechanics, **73**(1) pp. 5-15.

[147] Crocombe, A. D., 1997, "Durability Modelling Concepts and Tools for the Cohesive Environmental Degradation of Bonded Structures," International Journal of Adhesion and Adhesives, **17**(3) pp. 229-238.

[148] Popineau, S., Rondeau-Mouro, C., Sulpice-Gaillet, C., 2005, "Free/bound Water Absorption in an Epoxy Adhesive," Polymer, **46**(24) pp. 10733-10740.

[149] Brewis, D. M., Comyn, J., and Tegg, J. L., 1980, "The Uptake of Water Vapour by an Epoxide Adhesive Formed from the Diglycidyl Ether of Bisphenol-A and Di-(1-Aminopropyl-3-Ethoxy) Ether," Polymer, **21**(2) pp. 134-138.

[150] Brewis, D. M., Comyn, J., and Shalash, R. J. A., 1982, "Effect of Moisture and Temperature on the Properties of an Epoxide-Polyamide Adhesive in Relation to its Performance in Lap Joints," International Journal of Adhesion and Adhesives, **2**(4) pp. 215-222.

[151] Wonders, A. G., and Paul, D. R., 1979, "Effect of CO2 Exposure History on Sorption and Transport in Polycarbonate," Journal of Membrane Science, **5** pp. 63-75.

[152] Jordan, S. M., Koros, W. J., and Fleming, G. K., 1987, "Effects of CO_2 Exposure on Pure and Mixed Gas Permeation Behavior: Comparison of Glassy Polycarobonate and Silicone Rubber," Journal of Membrane Science, **30**(2) pp. 191-212.

[153] Pekarski, P., Hampe, J., Bohm, I., 2000, "Effect of Aging and Conditioning on Diffusion and Sorption of Small Molecules in Polymer Glasses," Macromolecules, **33**(6) pp. 2192-2199.

[154] Akele, N., Thominette, F., Paris, D., 1996, "Physical Ageing and Water Sorption in Polycarbonate," Journal of Materials Science Letters, **15**(11) pp. 1001-1002.

[155] Matsuoka, S., 1992, "Relaxation phenomena in polymers," Hanser Publishers; Distributed in the USA and Canada by Oxford University Press, Munich ; New York; New York.

[156] Lee-Sullivan, P., Dykeman, D., and Shao, Q., 2003, "Mechanical Relaxations in Heat-Aged Polycarbonate. I. Comparison between Two Molecular Weights," Polymer Engineering and Science, **43**(2) pp. 369-82.

[157] Morland, L. W., and Lee, E. H., 1960, "Stress Analysis for Linear Viscoelastic Materials with Temperature Variation," Society of Rheology - Transactions, **4** pp. 233-263.

[158] Lemaître, J., and Chaboche, J., 1990, "Mechanics of solid materials," Cambridge University Press, Cambridge, pp. 556.

[159] Schiessel, H., Metzler, R., Blumen, A., 1995, "Generalized Viscoelastic Models: Their Fractional Equations with Solutions," Journal of Physics A (Mathematical and General), **28**(23) pp. 6567-84.

[160] Zimmerman, W.B.J., 2006, "Multiphysics modelling with finite element methods," London : World Scientific Pub., Hackensack, N.J.

[161] COMSOL Multiphysics User's Guide, COMSOL Multiphysics 4.0a Documentation.

[162] Taylor, R. L., Pister, K. S., and Goudreau, G. L., 1970, "Thermomechanical Analysis of Viscoelastic Solids," International Journal for Numerical Methods in Engineering, **2**(1) pp. 45-59.

[163] Madduri, S., Infantolino, W., and Sammakia, B. G., 2010, "3D Thermal-Diffusion Analysis on a Moisture Loaded Epoxy Sample," COMSOL Conference Boston 2010.

[164] Janek, J., Korte, C., and Lidiard, A. B., 2002, "Thermodiffusion in ionic solids - model experiments and theory," 4th International Meeting on Thermodiffusion (IMT4), Anonymous Springer-Verlag, Berlin, Germany, pp. 146-83.

[165] Davarzani, H., Marcoux, M., Costeseque, P., 2010, "Experimental Measurement of the Effective Diffusion and Thermodiffusion Coefficients for Binary Gas Mixture in Porous Media," Chemical Engineering Science, **65**(18) pp. 5092-104.

[166] Benjelloun-Dabaghi, Z., and Benali, A., 2001, "Mathematical Modelling of the Permeation of Gases in Polymers," Oil and Gas Science and Technology, **56**(3) pp. 295-303.

[167] Scheichl, R., Klopffer, M. -H., Benjelloun-Dabaghi, Z., 2005, "Permeation of Gases in Polymers: Parameter Identification and Nonlinear Regression Analysis," Journal of Membrane Science, **254**(1-2) pp. 275-93.

[168] User's Guide, MATLAB R2010b, MathWorks, USA.

[169] Long, F. A., and Richman, D., 1960, "Concentration Gradients for Diffusion of Vapors in Glassy Polymers and their Relation to Time Dependent Diffusion Phenomena," Journal of the American Chemical Society, **82**(3) pp. 513-519.

[170] Cai, L. -W., and Weitsman, Y., 1994, "Non-Fickian Moisture Diffusion in Polymeric Composites," Journal of Composite Materials, **28**(2) pp. 130-154.

[171] Oleinik, E. F., 1986, "Glassy Polymers as Matrices for Advanced Composites," Polymer Journal, **19**(1) pp. 105-117.

[172] Simon, S. L., Plazek, D. J., Sobieski, J. W., 1997, "Physical Aging of a Polyetherimide: Volume Recovery and its Comparison to Creep and Enthalpy Measurements," Journal of Polymer Science Part B: Polymer Physics, **35**(6) pp. 929-936.

[173] Slobodian, P., Lengálová, A., and Sáha, P., 2003, "Volume and Enthalpy Relaxation in a-PMMA after Temperature Up-Jumps," Journal of Thermal Analysis and Calorimetry, **71**(2) pp. 387-393.

[174] Slobodian, P., Říha, P., Lengálová, A., 2004, "Enthalpy and Volume Relaxation of PMMA, PC, and a-Se: Evaluation of Aging Bulk Moduli," Journal of Non-Crystalline Solids, **344**(3) pp. 148-157.

[175] Slobodian, P., Vernel, J., Pelíšek, V., 2006, "Aging Bulk Modulus obtained from Enthalpy and Volume Relaxations of a-PMMA and its Blends with PEO," Mechanics of Time-Dependent Materials, **10**(1) pp. 1-15.

[176] Slobodian, P., Říha, P., Rychwalski, R. W., 2006, "The Relation between Relaxed Enthalpy and Volume during Physical Aging of Amorphous Polymers and Selenium," European Polymer Journal, **42**(10) pp. 2824-2837.

Appendix A

Governing Equations — Viscoelastic Material

Generalized Kelvin-Voigt Model:

$$\begin{cases} \varepsilon_x = \dfrac{\partial u}{\partial x} \\ \varepsilon_y = \dfrac{\partial \mathrm{v}}{\partial y} \\ \varepsilon_z = \varepsilon_z^e + \varepsilon_z^{an_1} + \varepsilon_z^{an_2} \\ \varepsilon_{xy} = \dfrac{1}{2}\left(\dfrac{\partial u}{\partial y} + \dfrac{\partial \mathrm{v}}{\partial x}\right) \end{cases} \tag{A-1}$$

$$\begin{cases} \varepsilon_x^e = \varepsilon_x - \varepsilon_x^{an_1} - \varepsilon_x^{an_2} \\ \varepsilon_y^e = \varepsilon_y - \varepsilon_y^{an_1} - \varepsilon_y^{an_2} \\ \begin{cases} \varepsilon_z^e = \dfrac{\frac{2}{3}G - K}{\frac{4}{3}G + K}\left(\varepsilon_x^e + \varepsilon_y^e\right) \quad , & if\ plane\ stress \\ \varepsilon_z^e = 0 \quad , if\ plane\ strain \end{cases} \\ \varepsilon_{xy}^e = \varepsilon_{xy} - \varepsilon_{xy}^{an_1} - \varepsilon_{xy}^{an_2} \end{cases} \tag{A-2}$$

$$\begin{cases} e_x^e = \varepsilon_x^e - \dfrac{\varepsilon_{vol}^e}{3} \\ e_y^e = \varepsilon_y^e - \dfrac{\varepsilon_{vol}^e}{3} \\ e_z^e = \varepsilon_z^e - \dfrac{\varepsilon_{vol}^e}{3} \\ \varepsilon_{vol}^e = \varepsilon_x^e + \varepsilon_y^e + \varepsilon_z^e \end{cases} \tag{A-3}$$

$$\begin{cases} \sigma_x = 2Ge_x^e + K\varepsilon_{vol}^e \\ \sigma_y = 2Ge_y^e + K\varepsilon_{vol}^e \\ \sigma_z = 2Ge_z^e + K\varepsilon_{vol}^e \\ \sigma_{xy} = 2Ge_{xy}^e \end{cases} \tag{A-4}$$

$$\begin{cases} \sigma_x^{an_i} = \left(\frac{4}{3}G_i + K_i\right)\varepsilon_x^{an_i} + \left(K_i - \frac{2}{3}G_i\right)(\varepsilon_y^{an_i} + \varepsilon_z^{an_i}) \\ \sigma_y^{an_i} = \left(\frac{4}{3}G_i + K_i\right)\varepsilon_y^{an_i} + \left(K_i - \frac{2}{3}G_i\right)(\varepsilon_x^{an_i} + \varepsilon_z^{an_i}) \\ \sigma_z^{an_i} = \left(\frac{4}{3}G_i + K_i\right)\varepsilon_z^{an_i} + \left(K_i - \frac{2}{3}G_i\right)(\varepsilon_x^{an_i} + \varepsilon_y^{an_i}) \\ \sigma_{xy}^{an_i} = 2G_i\varepsilon_{xy}^{an_i} \quad , \quad i = 1{,}2\ (no\ summation\ convention) \end{cases} \tag{A-5}$$

$$\begin{cases} \sigma_x^{v_i} = \frac{\eta_i}{(1+\nu)(1-2\nu)}\left[(1-\nu)\dot{\varepsilon}_x^{an_i} + \nu\left(\dot{\varepsilon}_y^{an_i} + \dot{\varepsilon}_z^{an_i}\right)\right] \\ \sigma_y^{v_i} = \frac{\eta_i}{(1+\nu)(1-2\nu)}\left[(1-\nu)\dot{\varepsilon}_y^{an_i} + \nu\left(\dot{\varepsilon}_x^{an_i} + \dot{\varepsilon}_z^{an_i}\right)\right] \\ \sigma_z^{v_i} = \frac{\eta_i}{(1+\nu)(1-2\nu)}\left[(1-\nu)\dot{\varepsilon}_z^{an_i} + \nu\left(\dot{\varepsilon}_x^{an_i} + \dot{\varepsilon}_y^{an_i}\right)\right] \\ \sigma_{xy}^{v_i} = 2G_i\tau_i\dot{\varepsilon}_{xy}^{v_i} \quad , \quad i = 1{,}2\ (no\ summation\ convention) \end{cases} \tag{A-6}$$

Generalized Maxwell Model:

$$\begin{cases} \varepsilon_x = \dfrac{\partial u}{\partial x} \\ \varepsilon_y = \dfrac{\partial v}{\partial y} \\ \begin{cases} \varepsilon_z = \dfrac{-\lambda\left(\varepsilon_x + \varepsilon_y\right) + \sigma_{qz}}{\lambda + 2G} \quad , \ if\ plane\ stress \\ \varepsilon_z = 0 \quad , \ if\ plane\ strain \end{cases} \\ \varepsilon_{xy} = \dfrac{1}{2}\left(\dfrac{\partial u}{\partial y} + \dfrac{\partial v}{\partial x}\right) \end{cases} \tag{A-7}$$

$$\begin{cases} e_x = \varepsilon_x - \dfrac{\varepsilon_{vol}}{3} \\ e_y = \varepsilon_y - \dfrac{\varepsilon_{vol}}{3} \\ e_z = \varepsilon_z - \dfrac{\varepsilon_{vol}}{3} \\ \varepsilon_{vol} = \varepsilon_x + \varepsilon_y + \varepsilon_z \end{cases} \tag{A-8}$$

$$\begin{cases} \sigma_x = 2Ge_x + K\varepsilon_{vol} + \sigma_{qx} \\ \sigma_y = 2Ge_y + K\varepsilon_{vol} + \sigma_{qy} \\ \sigma_z = 2Ge_z + K\varepsilon_{vol} + \sigma_{qz} \\ \sigma_{xy} = 2G\varepsilon_{xy} + \sigma_{qxy} \end{cases} \tag{A-9}$$

$$\begin{cases} q^e_{x_i} = q_{x_i} - \dfrac{q_{x_i} + q_{y_i} + q_{z_i}}{3} \\ q^e_{y_i} = q_{y_i} - \dfrac{q_{x_i} + q_{y_i} + q_{z_i}}{3} \\ q^e_{z_i} = q_{z_i} - \dfrac{q_{x_i} + q_{y_i} + q_{z_i}}{3} \\ i = 1{,}2 \ (no\ summation\ convention) \end{cases} \tag{A-10}$$

$$\begin{cases} \sigma_{q_x} = 2G_i q^e_{x_i} + K_i\left(q_{x_i} + q_{y_i} + q_{z_i}\right) \\ \sigma_{q_y} = 2G_i q^e_{y_i} + K_i\left(q_{x_i} + q_{y_i} + q_{z_i}\right) \\ \sigma_{q_z} = 2G_i q^e_{z_i} + K_i\left(q_{x_i} + q_{y_i} + q_{z_i}\right) \\ \sigma_{q_{xy}} = 2G_i q^e_{xy_i} \quad , \quad i = 1{,}2 \ (summation\ convention) \end{cases} \tag{A-11}$$

$$\begin{cases} \dot{q}_{x_i} + \dfrac{1}{\tau_i} q_{x_i} = \dot{\varepsilon}_x \\ \dot{q}_{y_i} + \dfrac{1}{\tau_i} q_{y_i} = \dot{\varepsilon}_y \\ \dot{q}_{z_i} + \dfrac{1}{\tau_i} q_{z_i} = \dot{\varepsilon}_z \\ \dot{q}_{xy_i} + \dfrac{1}{\tau_i} q_{xy_i} = \dot{\varepsilon}_{xy} \\ i = 1{,}2 \ (no\ summation\ convention) \end{cases} \tag{A-12}$$

Appendix B
Convective Heat Transfer Coefficient

This Appendix deals with the calculation of the convective heat transfer coefficient, which is used in the modeling of heat conduction inside the PC/ABS material. The convective heat transfer coefficient, h_c, is employed in the definition of the Nusselt number. The Nusselt number, a dimensionless number, is the ratio of convective to conductive heat transfer across the boundary within a fluid, and is defined as follows:

$$Nu = \frac{h_c L_c}{\lambda_T} \tag{B-1}$$

where λ_T denotes the thermal conductivity of the fluid and L_c represents the characteristic dimension.

The Nusselt number can also be expressed in terms of other dimensionless numbers. In forced convection, which is the case for mass uptake of PC/ABS bars inside the environmental chamber, the Nusselt number for a turbulent flow over a flat plate, is defined as:

$$Nu = 0.036\, Pr^{1/3}\, Re^{0.8} \tag{B-2}$$

where *Pr* and *Re* designate the two dimensionless numbers of Prandtl number and Reynolds number, respectively. The Prandtl number is equal to 0.71 for air at around 60 °C and Reynolds number is:

$$Re = \frac{\mathrm{v} L_c}{\nu_f} \tag{B-3}$$

where v and ν_f are velocity and kinematic viscosity of fluid, respectively.

The kinematic viscosity of air at 60 °C is 18.90×10^{-6} m^2/s and assuming that the air velocity inside the environmental chamber is around 1 m/s, the Reynolds number for the PC/ABS bars used in mass uptake experiments (section 3.3.1.4) with characteristic length of 0.076 *mm* becomes 4021.2.

By replacing the Prandtl and Reynolds numbers in Equation (B-2), the Nusselt number becomes 24.6. By inserting the Nusselt number and the value of λ_T equal to 0.0285 $W/m.K$ for air at 60 °C in Equation (B-1), the convective heat transfer coefficient becomes 9.2 W/m^2K.

Appendix C

Corresponding Figures from [46]

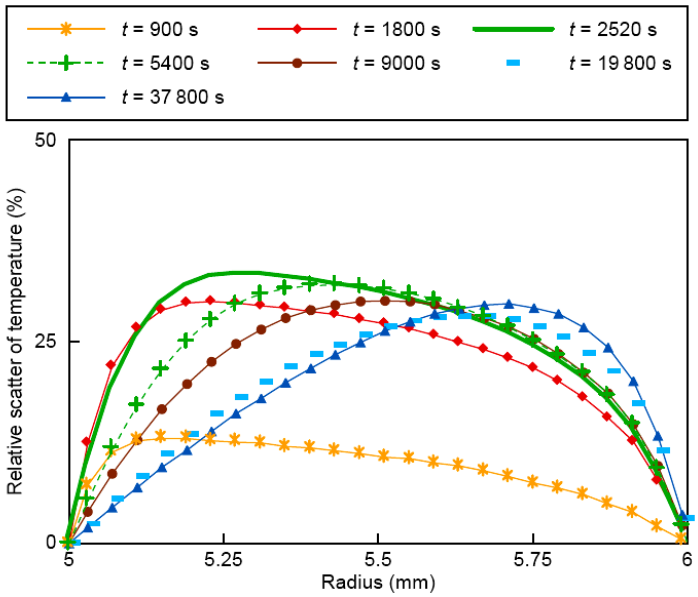

Figure C1 Spatial distribution of the relative scatter of temperature ($[T\text{-}T_1]/|T_1|$), for the coupled case (T) compared with the uncoupled case (T_1) for k_μ=2.104 $kg.s/m^3$ at different time [46] **(corresponding to Figure 5-26 on page 125)**

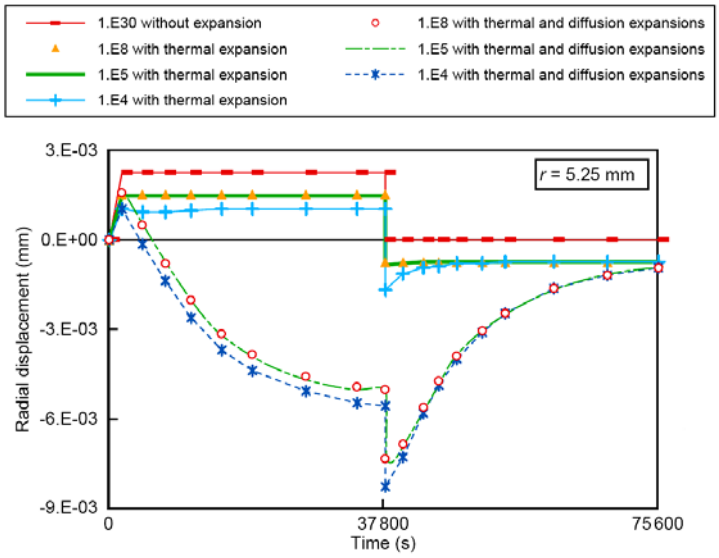

Figure C2 Effect of expansion coefficients on radial displacement [46] **(corresponding to Figure 5-27 on page 126)**

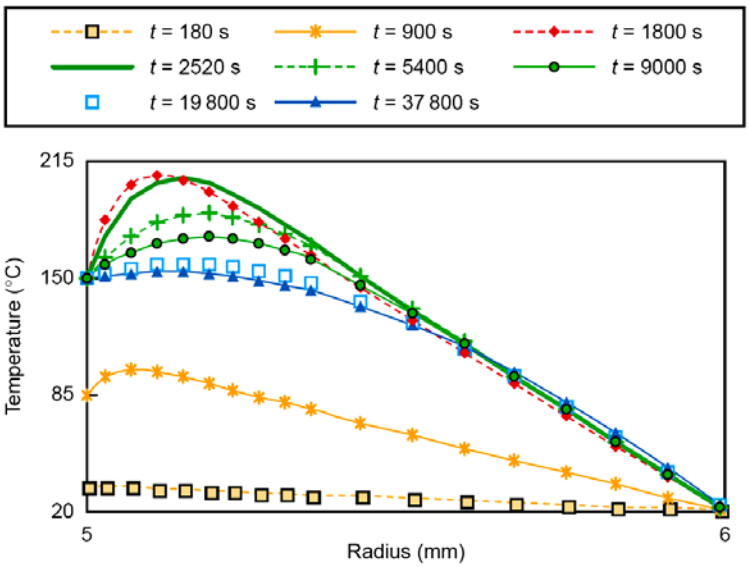

Figure C3 Effect of a small $C_{T\mu}$ vgalue: 10^{-2} *kg*/(*m.s.K*) on temperature [46] (corresponding to Figure 5-28 on page 127)

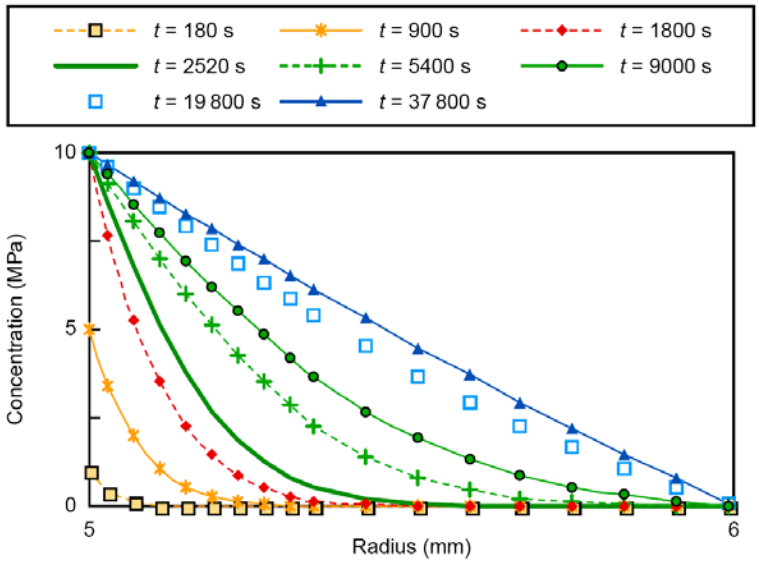

Figure C4 Effect of a small $C_{T\mu}$ value: 10^{-2} *kg*/(*m.s.K*) on concentration [46] **(corresponding to Figure 5-29 on page 127)**

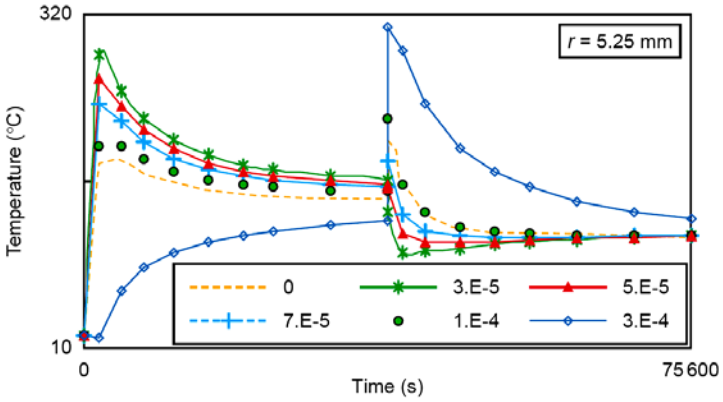

Figure C5 Effects of $C_{T\mu}$ and C_{TY} on the thermal problem for $K_m = 10^4$ $kg.s/m^3$, $C_{T\mu} = 1$ $kg/(m.s.K)$ and various C_{TY} [46] (corresponding to Figure 5-30 on page 128)

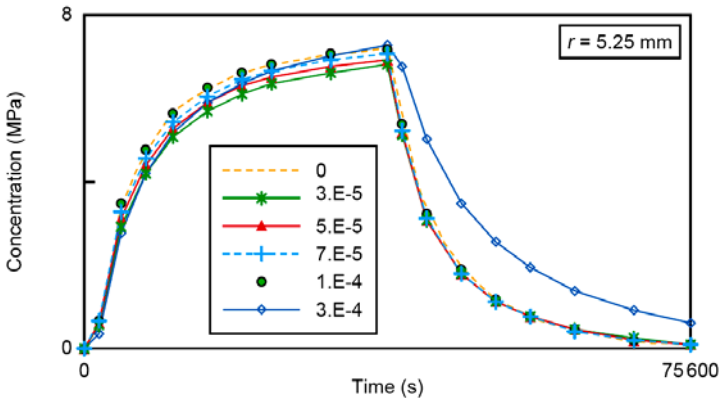

Figure C6 Effects of $C_{T\mu}$ and C_{TY} on the diffusion problem for $K_\mu = 10^4$ $kg.s/m^3$, $C_{T\mu} = 1$ $kg/(m.s.K)$ and various C_{TY} [46] (corresponding to Figure 5-31 on page 128)

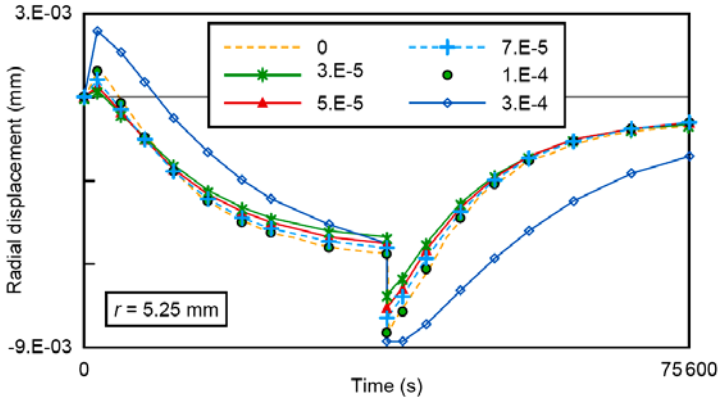

Figure C7 Effects of $C_{T\mu}$ and C_{TY} on the mechanical problem for $K_\mu = 10^4$ $kg.s/m^3$, $C_{T\mu} = 1$ $kg/(m.s.K)$ and various C_{TY} [46] (corresponding to Figure 5-32 on page 128)

Appendix D
List of Publications

Journal Publications

1. Haghighi-Yazdi, M. and Lee-Sullivan, P., "Determination of Dual Glass Transition Temperatures of a PC/ABS Blend Using Two TMA Modes," Journal of Thermal Analysis and Calorimetry, Vol. 96 (1), 2009, pp. 7-14.
2. Haghighi-Yazdi, M., Tang, J. K. Y., and Lee-Sullivan, P., "Hygrothermal Aging of a Polycarbonate/Acrylonitrile-Butadiene-Styrene Polymer Blend," accepted for publication (with minor revision) in Polymer Degradation and Stability, 2011.
3. Haghighi-Yazdi, M. and Lee-Sullivan, P., "Stress Relaxation of a Polycarbonate Blend after Hygrothermal Aging," submitted to the Mechanics of Time-Dependant Materials, 2011.

Manuscripts in Preparation

1. Haghighi-Yazdi, M. and Lee-Sullivan, P., "Numerical Modeling of Moisture Diffusion Coupled with Physical Aging in Thin Plastic Plates," in preparation, 2011.
2. Haghighi-Yazdi, M. and Lee-Sullivan, P., "Determination of Specific Heat Capacity for a Polycarbonate Blend Exposed to Hygrothermal Aging," in preparation, 2011.

Conference Proceedings and Presentations

1. Haghighi Yazdi, M. and Lee-Sullivan, P., "Glass Transition Studies of PC/ABS Blend Using Two Thermomechanical Analyzer Modes," 18th CTAS Annual Workshop and Exhibition, Mississauga, Ontario, Canada, May 13-14, 2008.
2. Haghighi-Yazdi, M. and Lee-Sullivan, P., "Two-dimensional Analysis of Triple Coupled Physics of Structural Mechanics, Diffusion and Heat Transfer in a Gas Pipe," Proceedings of the COMSOL Conference, Boston, MA, USA, October 8-10, 2009.
3. Haghighi-Yazdi, M. and Lee-Sullivan, P., "The Effect of Hygrothermal Aging on Specific Heat Capacity of PC/ABS Polymer Blend," The 22nd Canadian Materials Science Conference, Waterloo, ON, Canada, June 9-11, 2010.
4. Haghighi-Yazdi, M. and Lee-Sullivan, P., "Modeling Stress Relaxation Behaviour of a Hygrothermally Aged PC/ABS Polymer Blend," accepted for publication in the Proceedings

of the ASME 2010 International Mechanical Engineering Congress and Exposition, IMECE2010, Vancouver, BC, Canada, November 12-18, 2010.

5. Haghighi-Yazdi, M. and Lee-Sullivan, P., "Hygrothermal Aging of a Plastic for Thin-walled Housings," RIM Research Day, Waterloo, ON, Canada, December 13, 2010.